1999

The Laser Optogalvanic Effect in Radio Frequency Plasma: Applications in Analytical Chemistry.

Xuan Yao
Louisiana State University and Agricultural & Mechanical College

INFORMATION TO USERS

This manuscript has been reproduced from the microfilm master. UMI films the text directly from the original or copy submitted. Thus, some thesis and dissertation copies are in typewriter face, while others may be from any type of computer printer.

The quality of this reproduction is dependent upon the quality of the copy submitted. Broken or indistinct print, colored or poor quality illustrations and photographs, print bleedthrough, substandard margins, and improper alignment can adversely affect reproduction.

In the unlikely event that the author did not send UMI a complete manuscript and there are missing pages, these will be noted. Also, if unauthorized copyright material had to be removed, a note will indicate the deletion.

Oversize materials (e.g., maps, drawings, charts) are reproduced by sectioning the original, beginning at the upper left-hand corner and continuing from left to right in equal sections with small overlaps. Each original is also photographed in one exposure and is included in reduced form at the back of the book.

Photographs included in the original manuscript have been reproduced xerographically in this copy. Higher quality 6" x 9" black and white photographic prints are available for any photographs or illustrations appearing in this copy for an additional charge. Contact UMI directly to order.

UMI®

Bell & Howell Information and Learning
300 North Zeeb Road, Ann Arbor, MI 48106-1346 USA
800-521-0600

THE LASER OPTOGALVANIC EFFECT IN RADIO FREQUENCY PLASMA: APPLICATIONS IN ANALYTICAL CHEMISTRY

A Dissertation

Submitted to the Graduate Faculty of the
Louisiana State University and
Agricultural and Mechanical College
in partial fulfillment of the
requirements for the degree of
Doctor of Philosophy

in

The Department of Chemistry

by
Xuan Yao
B.S., Central-South University of Technology, Changsha, China, 1982
M.S., Central-South University of Technology, Changsha, China, 1984
May, 1999

ACKNOWLEDGEMENTS

The author wishes to thank Dr. Sean P. McGlynn for his scientific guidance and professional advice. Without his invaluable devotion and encouragement this research work would not have been possible.

The author acknowledges with gratitude the guidance and help of other professors in his graduate committee, Dr. S. F. Watkins, Dr. S. A. Soper, Dr. R. Hammer, Dr. K. Valsaraj and Dr. Jianhua Chen.

The author is also grateful to Dr. D. Kumar, Dr. K. Rupnik, Mr. B. Zinn and Dr. A. Vrancic for their help in equipment operation and maintenance, data acquisition and signal processing. Acknowledgement is also extended to Ms. M. Edwards for her help and Ms. D. Wood for useful discussion.

Financial assistance in support of this research by the Department of Energy and the Louisiana State University is gratefully acknowledged.

TABLE OF CONTENTS

LIST OF TABLES

LIST OF FIGURES

ABBREVIATIONS

OGE	Optogalvanic Effect
LOGE	Laser Optogalvanic Effect
LOGS	Laser Optogalvanic Spectroscopy
DC	Direct Current
RF	Radio Frequency
RFLOGS	Radio Frequency Laser Optogalvanic Spectroscopy
PA	Photoacoustic
IRC	Ionization Rate Change
VUV	Vacuum Ultra Violet
ICP	Inductively Coupled Plasma
CCP	Capacitively Coupled Plasma
DCP	Direct-Current Plasma
MIP	Microwave-Induced Plasma
SICP	sealed inductively-coupled plasma
ICP-AES	Inductively Coupled Plasma-Atomic Emission Spectroscopy
ICP-MS	Inductively Coupled Plasma-Mass Spectroscopy
ICP-AAS	Inductively Coupled Plasma-Atomic Absorption Spectroscopy

ABSTRACT

The laser optogalvanic effect (LOGE) is the change of electrical impedance of a plasma produced by resonant absorption of laser radiation. Selected excitations can be used to detect specific species by tuning the laser to an appropriate wavelength.

For optimum utilization of LOGE as a detection tool, one must understand the temporal profile of the LOGE signal in terms of the various processes occurring in the plasma. In this work, the characteristics of the LOGE signal and the potential applications of laser optogalvanic spectroscopy (LOGS) have been investigated.

First, by analyzing the LOGE signal profiles of the neon excitations $1s_{2,4}\rightarrow 2p_{1,3}$, we studied the effect of radiation trapping and collisional energy transfer on the generation of LOGE signals. The kinetics of the signal generation has been discussed quantitatively. The ionization rate change (IRC) signal profile has been modeled qualitatively. The dominant transient features were found to be associated with trapping of the $1s_2$ state. The temperature of the radio frequency (RF) plasma is ~1000K.

Second, the influence of the distance traveled by the acoustic pulse on the signal profiles has been investigated. It was found that the acoustic wave launched by non-radiative $2p_k\rightarrow 1s_j$ and $1s_{3,5}\rightarrow {}^1S_0$ deexcitations travels at the speed of sound. On the other hand, the acoustic wave launched by non-radiative $1s_{2,4}\rightarrow {}^1S_0$ deexcitations of trapped $1s_{2,4}$ states produces an instantaneous LOGE signal. A model of the photoacoustic (PA) signal formation has been constructed and used to predict the PA signal profiles successfully.

Third, we have studied the capability of LOGS to detect and analyze iodine in an RF plasma. It is shown, by careful selection of the operating conditions, that the signals of iodine atoms and molecules can be distinguished by separating the IRC/PA components. Both air and nitrogen can be used as the filler/carrier gas in the plasma. The detection limit of iodine in nitrogen is approximately one order of magnitude better than that in air. The response of signal intensity to sample concentration is linear in the range of $0.1\mu g/cm^3 - 2.5\mu g/cm^3$. The detection limit achieved in our experiments is $\sim 10^{-7}\mu g/cm^3$ for both iodine atoms and molecules.

CHAPTER 1: INTRODUCTION

1.1 Plasmas and Optogalvanic Effect

1.1.1 Background Information

Plasmas created by electrical discharges in gases have a variety of important applications. For example, they are used in (i) high-power, short wavelength lasers, (ii) high-power, high-speed switching, (iii) efficient lighting systems, (iv) microelectronic etching and plasma-enhanced chemical vapor deposition (e.g., diamond, silicon oxide, etc.), (v) sensitive analytical instrumentation (e.g., inductively coupled plasma), and (vi) sensitive pollution monitoring and control devices.

Despite extensive investigation, the characteristics of plasmas are not very well understood. Plasmas are complex mixtures of species (atoms, ions, radicals, etc) in various stages of excitation/ionization. Under steady state conditions, a dynamic equilibrium prevails in the plasma between collision processes and photon-flux absorption or emission processes. The complexity of plasma and poor knowledge about the plasma rates and cross-sections precludes quantitative modelling even for the simplest of plasma applications. The experimental characterization of high frequency plasmas (frequency $\geq$ 1MHz) is beset by additional complications. The conventional plasma probe techniques, for example, are rendered useless by the plasma distortions produced by the capacitive and inductive loading effects of the probe. And, since the other diagnostic techniques (i.e., optical absorption, emission, scattering, etc) provide only limited or incomplete information about the plasma, it remains largely uncharacterized. Consequently, many critical applications of RF plasma proceed mostly on a trial-and-error basis.

Both direct current (DC) and radio frequency (RF) discharges may be used to generate the plasma. While DC discharges are simple to generate, they are, unfortunately, characterized by non-uniform plasmas (discrete discharge regions) and suffer the risk of electrode contamination by reactive gases or species present in the discharge. The RF discharge, on the other hand, has the advantages of spatial uniformity (except for a sheath in the vicinity of the electrodes), "contactless" nature (i.e., need not have metal electrodes inside the discharge tube), and background noise levels that are not critically dependent on either the gas pressure or gas type.[1]

The temporal profiles of LOGE signals, which contain considerable mechanistic information, are crucial to the understanding of the various mechanisms involved in the generation of these signals. Unfortunately, the temporal profiles of LOGE signals are very complex and very sensitive to discharge conditions (e.g., discharge configuration, electrical input power, RF source characteristics, laser intensity, region of the plasma excited by the laser, etc.) and, presumably for those reasons, the existing LOGE models are either wrong or incomplete.

1.1.2 A Brief Description of This Work

The primary purpose of this work is to investigate the characteristics of LOGE signals and the potential applications of laser optogalvanic spectroscopy (LOGS). This goal has been achieved: the temporal profiles of the LOGE signals have been fully interpreted in terms of the various processes in the plasma that gives rise to such signals.

The main body of this dissertation is composed of three chapters (Chapter 2-4), which are base on three journal articles (published or accepted):

Chapter 2: An analysis of the LOGE signal profiles of the neon excitations $1s_{2,4} \rightarrow 2p_{1,3}$ has enabled us to generate a model that accounts for the effects of radiation trapping and collisional energy transfer on the generation of LOGE signals as well the effects of different lower and upper states on the polarity and intensity of the LOGE profiles. We have also studied the kinetics of signal generation and have been able to produce a primitive modelling of the PA and IRC signal profiles. The population of the different $1s_j$ states has also been studied and the temperatures of low RF power neon plasma have been measured.

The reason for selection of the two pairs of transitions, $1s_{2,4} \rightarrow 2p_{1,3}$ is to compare the LOGE profiles excited from the same lower state to two different higher states and those excited from two different lower states to the same higher state. The $1s_2$ and $1s_4$ states were chosen as the lower states because they are both radiatively trapped and, as a result, the effects of such trapping on LOGE signals should be emphasized. The $2p_1$ and $2p_3$ states were selected as the upper states because they have only two optically-allowed decay pathways (i.e., $2p_{1,3} \rightarrow 1s_2$ and $2p_{1,3} \rightarrow 1s_4$) and, therefore, they permit a more facile ingress to details of the collisional energy transfer between them and their neighbouring $2p$ states.

It is found in this work that (1) The lower $1s_j$ states are the sole determinants of signal polarity. The dominant transient features, IRC2 and PA1, are associated with trapping of $1s_2$ states; (2) For a given upper $2p_k$ state, the LOGE signals for excitations from the $1s_4$ state are much stronger than those from the $1s_2$ state. This is attributed to higher $1s_4$ populations: the data suggest that the relative populations are $N(1s_4)/N(1s_2) \approx 10$ and that the plasma temperature is $T \approx 10^3$ K; (3) The signatures of the various

transient components (+/-) are interpreted on the basis of $1s_j$ population changes; (4) IRC profiles are readily modeled as a resultant of Penning and trapped-photon ionizations. The modeling of PA profiles, however, is dependent on a crucial difference between the acoustic events associated with radiationless degradation of the $1s_{3,5}$ states and radiationless degradation of the radiatively-trapped $1s_2$ state.

Chapter 3: The influence of the distance traveled by the acoustic pulse on the signal profiles has been investigated by varying the distance between the point of laser excitation and the plasma proper. The delay of the acoustic wave launched by either non-radiative $2p_k \rightarrow 1s_j$ or $1s_{3,5} \rightarrow {}^1S_0$ deexcitations relative to the delay of the acoustic wave launched by non-radiative $1s_{2,4} \rightarrow {}^1S_0$ deexcitations was determined and analysed. A model of PA signal formation was constructed and used to predict PA profiles. Unlike the excitations studied in chapter 2, the $1s_3$ and $1s_5$ metastable states are emphasized in this chapter because they are the primary non-ionic, excited metastable state plasma components that maintain the plasma by collisional Penning ionization.

It has been concluded that the radiatively trapped $1s_2$ and $1s_4$ states produce an acoustic signal that differs from these produced by all other (i.e., non-radiatively trapped) states: a movement of the acoustic wave from the site of laser excitation to regions of high ion density is not required for a radiatively trapped state because such states permeate the entire plasma volume at an effective speed approaching that of light. It is also found that the $1s_2 \rightarrow {}^1S_0$ deexcitation is acoustically more effective than the $1s_4 \rightarrow {}^1S_0$ deexcitation. Modelling of the acoustic components has shown that the different time characteristics of the metastable ($1s_{3,5}$) and trapped ($1s_{2,4}$) states are crucial to a correct prediction of the shape of the acoustic transients.

Chapter 4: The feasibility of a laser optogalvanic analysis for iodine in an RF plasma was studied. We were successful in separating and identifying the atomic and molecular iodine LOGE signals by careful selection of the operating conditions (e.g., RF power, filler gas or carrier gas pressures, and discharge tube geometry).

In this work both air and nitrogen were found to be good filler/carrier gases for LOGE iodine detection. The LOGE can be used to detect trace I atoms and I_2 molecules in both static and flowing conditions. By careful selection of the operating conditions (e.g., RF power, filler gas or carrier gas pressures, discharge tube geometry), a pure atomic iodine signal excited at 16912 cm^{-1} constitutes the IRC LOGE profile and a pure molecular iodine signal excited at 16980 cm^{-1} constitutes the PA LOGE profile. The response of signal intensity-sample concentration is linear in a wide range. The detection limits achieved in our experiments are ~$10^{-7}\mu g/cm^3$ for both iodine atoms and molecules. We believe that optimization of the equipment and the experimental conditions can improve the detection limit by 2 to 3 orders of magnitude.

The reasons for the choice of iodine as a test analyte were based on the following considerations:

(1) Iodine is classed as a poison because it is a gastrointestinal irritant.[2] Iodine vapor is also irritating to the eyes, lungs and skin. The radioactive iodine (I^{129}) vapors which may be released from nuclear reactor wastes are extremely harmful. Consequently, the monitoring and analysis of both atomic and molecular iodine vapors (radioactive and non-radioactive) is important to a safe and healthy environment. Moreover, by detecting I^{129} concentration we can measure the radioactive decay rates of iodine and monitor mixed nuclear waste activity (i.e., know how "hot" the nuclear reactor is.).

(2) Iodine is a solid, melting at 113.6°C. The solid sublimes at temperatures well below the melting point[2] to give a significant vapor pressures (e.g., ~178 mTorr at 22°C). By changing the temperature of the cooling bath, we can easily control the partial pressure of the iodine vapor in the sealed sample tube and calculate the sample concentration. Therefore, it is a simple matter to study the LOGE signal characteristic at different sample concentration and to investigate the relationship between the sample concentration and LOGE signal intensity.

In addition to the research covered by the three publications mentioned above, we have also studied atomization sources for a LOG spectrometry system in a fourth publication.[3] Since I am not the primary author of this paper, I will not include it in this dissertation. However, I will give a detailed review of this work in section 1.5 of the present chapter (i.e., Chapter 1).

1.2 Plasma Processes

As we discussed earlier, plasma is a very complex state of matter that is controlled by many different events. The following are some plasma processes that are important to the optogalvanic effect.

1.2.1 Direct Photoionization

Direct photoionization processes can be represented by

$$M + h\nu = M^{+} + e^{-}$$

where $h\nu$ is a photon; and M^{+} is the excited state of the ground state plasma entity M (atom or molecule).

Direct photoionization is an instantaneous process that produces a "fast" IRC signal. The rise time of this process is the convolution of the rise times of laser pulse and

detection electronics circuit (and, therefore, coincident in the present instance with the laser pulse rise time of ~1 μs). But its decay time is largely controlled by the slow process of plasma re-equilibration. Plasma re-equilibration times are functions of the particular plasma, the characteristics of the particular laser excited levels of the plasma constituents and the impedance of the electrical power source which controls the stimulus for re-equilibration. If a local thermodynamic equilibrium is assumed, the plasma temperature can be used to determine the population distribution of the intermediate states that are available for laser excitation. Conversely, emission, absorption, or either of the two LOGE components may be used to estimate the plasma temperature.[4]

1.2.2 Metastable-Metastable or Penning Ionization

Metastable-metastable or Penning ionization is a process usually symbolized by

$$M^* + M^* \rightarrow M + M^+ + e^- \qquad \text{(metastable-metastable ionization)}$$

$$M + M^* \rightarrow M + M^+ + e^- \qquad \text{(Penning ionization)}$$

where M* is the metastable excited state of the ground state plasma entity M. This process dominates at low RF powers (a few Watts) and moderate pressures (a few Torr).[5,6] Any perturbation of the M* population will be followed by a slow collisionally-dominated re-equilibration process which may extend into the 10^1-10^2μs range. When Penning ionization is dominant, as in a 5 Torr neon RF discharge powered at 1W to be discussed later, depletion of the metastable M* level by non-ionizing laser excitation will produce a decrease of the ionization rate [5,6] and, hence, a negative IRC signal component. By the same token, given that collisions are the dominant

re-equilibration mode, the decay characteristics of the levels produced by laser excitation may also dictate a PA component.

1.2.3 Radiation Trapping

Radiation trapping is a process of sequential emission-reabsorption that is particularly important for high-extinction ground state absorption events in atoms (where, unlike molecules, there is no Stokes loss). For example, in an RF discharge in Neon at 5 Torr, the $1s_2$ and $1s_4$ states (Paschen notation) are so strongly trapped, that their effective lifetimes increase by a factor of $\sim 10^3$ (from ns to μs).[7] This process is illustrated in Fig. 1-1.

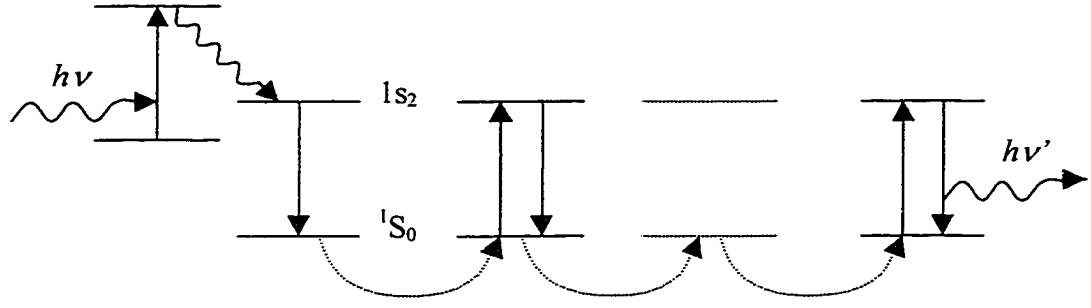

Fig. 1-1 Radiation trapping process

Since the $1s_2/1s_4 \rightarrow$ ground state photons lie in the VUV, they can readily photoionize M* or other excited levels and give rise to a delayed IRC component.

1.2.4 Acoustic Effects

When a part of the laser excitation energy is converted into an acoustic shock wave by non-radiative processes, whether collisionally induced or not, it disturbs the equilibrium distribution of positive ions. Such a disturbance represents a "flow" of

current and it will give rise to a LOGE signal induced by a PA shock wave. For example, it was shown in our previous work[8] that the pressure wave generated by the PA effect produced LOGE signals by an actual physical movement of the charged species in the "sensitive" region of the RF plasma. In a low-power iodine discharge, these "sensitive" regions are confined to the vicinity of the RF electrodes, and are attributable to positive ion sheaths. Thus, any perturbation of these positive ion sheaths by the PA wave should alter the discharge current and produce a LOGE signal. The polarity of this LOGE signal is inverted when the direction of the PA wave is reversed (as shown in Fig. 1-2). Therefore, the temporal component of LOGE profiles, recorded by many workers in both RF and dc discharges, may well be predominantly photoacoustic in nature.[8,9]

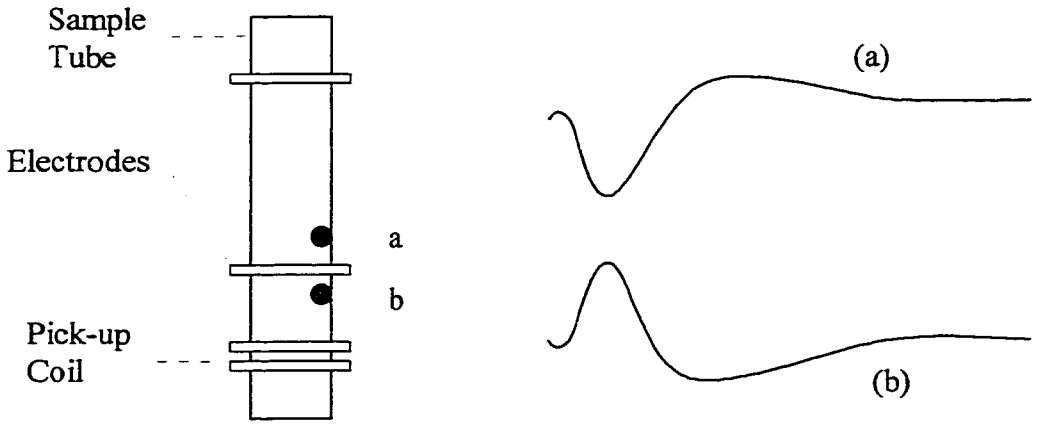

Fig. 1-2 Effect of the propagation direction of the photoacoustic wave on the polarity of the LOGE signal. (a) is the signal profile when the laser beam hits at point a and the acoustic wave moves downwards. (b) is the signal profile when the laser beam hits at point b and the acoustic wave moves upwards.

1.2.5 Collisional Transfer of Excitation Energy

A part of the laser excitation energy deposited in a given species may be lost by collision to other entities in the plasma. This collisional energy transfer can be very efficient if the energy gap between the "donor" and "acceptor" states is small. Since this type of energy transfer can occur between entities of the same species, and since the "donor" and "acceptor" states are likely to generate LOGE signals with their own distinctive characteristics, a detailed analysis of the LOGE signal profile can provide information concerning collisional transfers of excitation energy.

For example,[4] the $2p_9$ upper state in the excitation $1s_5 \rightarrow 2p_9$ has only one optically allowed decay pathway ($2p_9 \rightarrow 1s_5$). Thus, if there is no collisional energy transfer, the net result of this excitation should be a transient increase in the $2p_9$ population and a corresponding transient decrease of the $1s_5$ population. Since the fluorescence decay time of $2p_9$ is $\sim 10^{-2}\mu s$, these population changes will be restored to normalcy within $\sim 1\mu s$ (the duration of the laser pulse). This, however, is contrary to observation, a fact which, we believe, points to the occurrence of collisional energy transfer in the $2p_9$ upper state. Because the energy gap between the $2p_9$ and $2p_8$ states is very small (only $167.2cm^{-1}$), energy may be lost by collisional transfer from the $2p_9$ state to the $2p_8$ state. Thus, the LOGE characteristics associated with the excitation $1s_5 \rightarrow 2p_9$ will be determined, at least in part, by the decay characteristics of the $2p_8$ level. The LOGE signal profile of the excitation $1s_5 \rightarrow 2p_9$, then, should bear some similarity to the LOGE signal profile of the excitation $1s_5 \rightarrow 2p_8$. Fig. 1-3 shows the degree of match of the PA and IRC profiles of these two transitions on an expanded time scale.

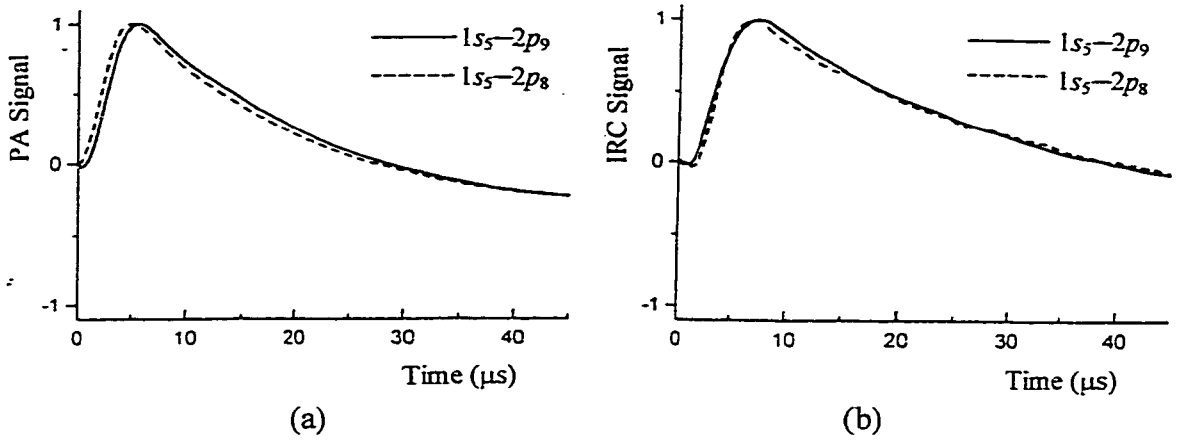

Fig. 1-3 Overlapped temporal profiles of the PA (a) and IRC (b) components of transitions $1s_5 \rightarrow 2p_9$ and $1s_5 \rightarrow 2p_8$ shown on an expanded time scale.

1.3 Models of the Optogalvanic Effect

The electrical impedance of a plasma depends on charge carrier density and mobility. Consequently, the two phenomenological models that had been proposed for the generation of the LOGE signal were:

(i) Direct or collision-assisted ionization rate changes (IRC) of the excited plasma atoms and molecules produced by laser excitation, which causes an increase or decrease of the electron-ion pair density and, hence, an increased or decreased conductivity.

(ii) An electron-temperature coupling model in which an increased electron kinetic energy, caused by laser energy deposition, produces an increase of discharge conductivity by enhancing the electron mobility.[10,11]

Mechanism (ii) was invoked in order to explain the generation of LOGE signals by low energy (e.g., vibrational) optical excitation to levels far below ionization threshold. Mechanism (ii), though apparently adequate in cases of unchopped IR irradiation of molecular discharges,[10] fails to explain many important features of the

LOGE signals,[12-14] such as the dependence of signal polarity on the site of laser excitation (See Fig. 1-2).

These correlative deficiencies are overcome if a photoacoustic (PA) effect is implicated in the production of LOGE signals by low-energy photons. While the production of LOGE signals via a PA intermediacy has been known for over a decade,[15] and several simultaneous PA and IRC studies have been carried out,[14,16,17] the true significance of this intermediacy was never fully appreciated. That is, an important aspect of the mechanism by which the PA wave generates the LOGE signal was not correctly understood. Heating and cooling, which accompany the PA wave, were incorrectly supposed to generate the LOGE signal via mechanism (ii) above. It is now known that this is incorrect.[8] The transient perturbation of the distribution of charged species by the pressure wave produces the transient PA-mediated LOGE signal directly. This assertion follows from the definition of an electric current as a flow of charges: any perturbation of the position of charges constitutes a current perturbation in the plasma.

1.4 Recent Developments

We have shown recently[4] that the pure IRC components of LOGE signals can be generated by direct, selective laser excitation from the ground state (or from an excited level which does not itself contribute significantly to the production of a PA component) to a level that is either in the continuum or so close to threshold that collisional ionization is guaranteed. Examples of such pure IRC signal production, all of which involve pre-threshold ionization, are available in xenon,[18] cesium,[19] and iodine[8]

discharges. The temporal profile of the LOGE signal (i.e., a pure IRC component in this case) matches that of the excitation laser pulse.

We have also shown[8,9,20] that LOGE signals generated via the photoacoustic (PA) effect need not involve thermal effects (mobility changes) or ionization rate changes in the final step of signal production. A simple perturbation of the distribution of positive ions (or other charged species) by the pressure wave which accompanies the photoacoustic effect can generate a PA component of the LOGE signal directly. As an example, the pressure wave induced-displacement of the positive sheath of I^+ ions in the vicinity of the electrodes in a low power RF discharge in iodine vapor generates a LOGE signal whose polarity reverses as the propagation direction of the pressure wave is reversed.[8] The pressure wave generates these LOGE signals by an actual physical movement of the positive ions in the sheath region (i.e., the "sensitive" region) of the discharge. This "sensitive" region may be confined to the vicinity of the electrodes (as in the case of a low power RF discharge in iodine) or it may be spread out over a wider discharge region (e.g., as in a low power RF discharge in neon).[9]

Thus, the LOGE signal can be generated by two distinct mechanisms. These are (a), ionization rate changes (IRC); and (b), displacement of charged species in the "sensitive" region of the discharge. Mechanism (b) is the photoacoustic (PA) component. Mechanism (ii), if it is at all operative, should have the same temporal profile as the PA component except that the polarity of a LOGE signal induced by mechanism (ii) should not be inverted when the direction of propagation of the PA wave is reversed. We conclude that, under our experimental conditions, mechanism (ii) is either inoperative or negligibly small.[9] Consequently, the temporal profile of a LOGE

signal consists, in general, of two physically distinct components: one attributable to ionization rate changes, the other to a photoacoustic effect.

In our recent work it was shown that the two LOGE signal components, IRC and PA, can be separated experimentally.[20,21] The method of separation is based on the fact that ionization alters the total concentration of charge carriers whereas acoustic effects do not; in the first case, this leads to frequency modulation and, in the latter case, to amplitude modulation of the resonance characteristics of the driver/plasma circuit. This technique has been discussed in our previous works.[4,21]

We have shown that, for small perturbations, the IRC and the PA components of a LOGE signal can be separated even when they exhibit temporal overlap. The primary requirement for separability is that the RF plasma be "tightly coupled" to the electrical excitation circuit. The impedance of the system is determined by its resistance, capacitance and inductance. The electrical resonance frequency of the system (f_0) is determined by its capacitance and inductance.* Consequently, laser induced changes in the effective inductance or capacitance of the plasma will shift the RF resonance frequency f_0.

As we discussed earlier, the photoacoustic wave is the physical movement of charged particles and, consequently, it does not produce any net changes of the electron or ion densities. Thus, while the photoacoustic wave may produce transient changes of plasma resistance it will not produce significant changes of either the inductance or the

* For series connection circuit, $f_0 = 1/(2\pi\sqrt{LC})$
For parallel connection circuit, $f_0 \approx 1/(2\pi\sqrt{LC})$, when the resistance is relatively much smaller than capacitance and inductance.

capacitance of the plasma. Therefore, small PA components will change the resonance amplitude, while leaving the resonance frequency more or less unchanged (See Fig. 1-4).

However, a transient increase in the ionization rate in the plasma will result in a transient increase in inductance or capacitance or both and, consequently, a transient change of f_0. Therefore, a net positive IRC component will shift the system resonance curve to one side (left or right, depending on the characteristics of the electrical circuit.), and a net negative IRC component will shift the system resonance curve to the other side (as shown in Fig. 1-4).

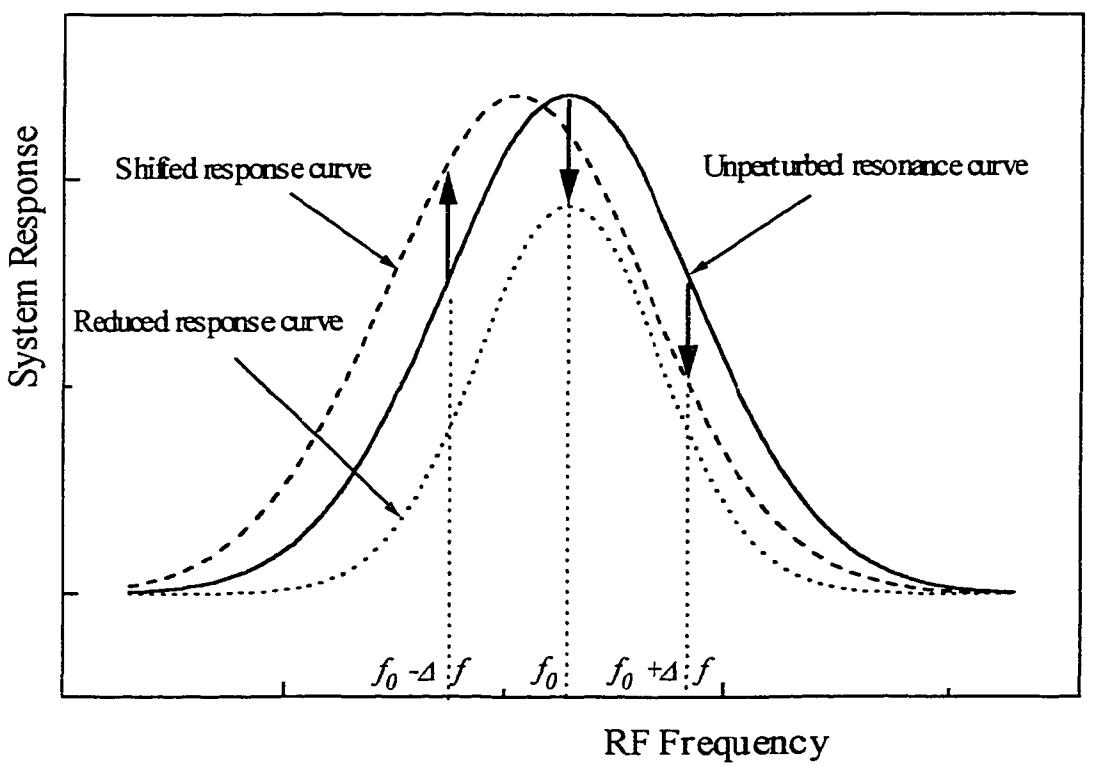

Fig. 1-4 The resonance response curve of the system. The solid curve is the unperturbed resonance curve. The dashed curve is the shifted response curve due to a laser-induced pure IRC effects. The dotted curve is the reduced response curve due to laser-induced pure PA effects. The shift shown are exaggerated.

Thus, a simple procedure, one which involves recording the temporal profiles of the LOGE signal at the system resonance frequency f_0 and off-resonance at $f_0 + \Delta f$ and $f_0 - \Delta f$ (where Δf is a small change in the system resonance frequency) may be used to separate the IRC and PA components.[21]

Let $Y(f_0)$, $Y(f_0 + \Delta f)$ and $Y(f_0 - \Delta f)$ be the temporal profiles of the LOGE signals when the system frequency is f_0, $f_0 + \Delta f$ and $f_0 - \Delta f$, respectively. Let Y(PA) and Y(IRC), respectively, be the PA and the IRC components of the observed LOGE signal. As detailed above, one may write

$$Y(f_0) = Y(PA) \tag{1}$$

and

$$Y(f_0 + \Delta f) = k\, Y(PA) + k'\, Y(IRC) \tag{2}$$

$$Y(f_0 - \Delta f) = k\, Y(PA) - k'\, Y(IRC) \tag{3}$$

or, equivalently

$$Y(PA) = Y(f_0) \tag{4}$$

$$Y(IRC) = (Y(f_0 + \Delta f) - Y(f_0 - \Delta f))/2k' \tag{5}$$

where k and k' are constants. Thus, by recording the temporal LOGE signal profiles at f_0, $f_0 + \Delta f$ and $f_0 - \Delta f$, one can calculate the temporal profile of the pure PA and pure IRC components of the LOGE signals using equations (4) and (5).

In a study of optogalvanic transients in a neon RF plasma using this separation technique,[21] we found out that: (1) The optogalvanic signals produced by $1s_j \rightarrow 2p_k$ excitations are functions of the laser-induced population redistribution among the $1s_j$ states. The $2p_k$ states merely serve as mediators of this redistribution. (2) The temporal profiles of LOGE signals in the intermediate range 2-20μs are largely controlled by

radiatively trapped $1s_2$ and $1s_4$ populations. The trapped $1s_2 \rightarrow {}^1S_0$ photons produce acoustic and ionization signals on a ~5μs scale; the trapped $1s_4 \rightarrow {}^1S_0$ photons produce acoustic and ionization signals on a ~20μs scale. (3) The $1s_3$ and $1s_5$ states are the primary non-ionic, excited metastable state plasma components and they maintain the plasma by collisional Penning ionization.

1.5 Application of Laser Optogalvanic Spectroscopy

The most significant series of events that occurred during the past two decades in the field of analytical atomic spectroscopy was the emergence of various atmospheric-pressure, flame-like plasma dissociation and excitation media, among them inductively coupled plasma (ICP), capacitively coupled plasma (CCP), direct-current plasma (DCP) and microwave-induced plasma (MIP). Of all these, ICP has been most widely used in analytical chemistry (e.g., ICP-AES, ICP-MS) because of its remarkable selectivity and sensitivity. However, like any other analytical technique, ICP spectrometry has its limitations (e.g., sample introduction, interferences, noise, etc).

With most pneumatic nebulizers, only 1-5% of the sample solution can be injected into the discharge and, if solid sampling techniques are used, the reproducibility of measurements deteriorates.[22] Stray light, matrix effects and spectral overlap are three groups of interferences in ICP-AES.[23] These interferences pose serious problems, and much work has been done in an attempt to minimize them.[24-30] The conventional ICP-AES techniques also suffer background noise arising from the nebulizer and from sample introduction techniques.[31] Although the SICP (sealed inductively coupled plasma) technique minimizes the low-frequency noise, the noise due to statistical variations of the RF power input and to heat release to the environment still exists. In addition, in all ICP instruments,

ICP is merely an ionization source and the species to be detected are determined by the detector. Different ICP techniques (such as ICP-AES, ICP-MS) can detect different species. However, with one single detector, ICP cannot be used for detection of atoms, molecular ions, molecules or radicals at the same time. In addition, ICP-AES and ICP-AAS can not be used for the direct determination of nonmetals, because nonmetal species are excited to a lesser extent than metal species, resulting in poor sensitivity for nonmetallic elements.[32]

Therefore, the need for an innovative diagnostic tool suitable for RF plasmas cannot be overemphasized. We have applied our recently developed laser optogalvanic technique as a weakly perturbative probe of RF plasmas, the intent being to extract information pertinent to some or all of the above applications. As mentioned earlier, under steady-state conditions (e.g., in dc discharges), there is a dynamic equilibrium between the plasma species, and a well-defined impedance is offered to the flow of current in the plasma. Laser excitation of a species in the discharge constitutes a net deposition of energy in that species and, consequently, the dynamic equilibrium is disturbed. This perturbation results in a change in the impedance of the discharge and a LOGE signal is generated. Selective laser excitations of different transitions in different plasma moieties can be used in order to determine such important plasma characteristics as decay branching ratios, collisional energy transfer rates, number densities, etc. A separation method can be used to analyse different components of the LOGE signal profile. This technique provides a unique ability to disentangle the overlapped photoacoustic and ionization components usually present in the optogalvanic signals generated by laser excitation of a RF plasma. Since both photoacoustic and photo-induced ionization-rate-change signals in plasmas are extremely sensitive, the

optogalvanic effect can be developed into a diagnostic tool of high specificity and wide applicability. We have successfully used such tools to interpret the complex temporal profiles of transient optogalvanic signals, to monitor collisional energy transfer processes, and to identify radiation trapping effects in such simple systems as rare gases and halogens. Thus, the potential for extremely selective, sensitive analytical technique, certainly exists.

Radio frequency laser optogalvanic spectroscopy (RFLOGS) is a new kind of spectrometry. It still uses plasma (ICP or CCP) as the source of excitation, atomization and ionization. However, it has an innovative sample introduction and detector system. Compared with conventional ICP-AES technique, the RFLOGS technique has many advantages:

(1) In the RFLOGS system, the plasma can be either inductively or capacitively coupled to the system. The plasma can operate at atmospheric or even lower pressures; it can also be in a continuous flow state or static (i.e., in sealed tube) state. Therefore, it demonstrates high flexibility and analytical merit. For example, one can use sealed, capacitively coupled plasma (SCCP) to analyze toxic and reactive gases; the required sample sizes can be very small; since no flow exists in the plasma, the contribution of flow variations to flicker noise is eliminated.

(2) In ICP-AES, ICP is used to excite atoms of the sample, and a photomultiplier is used to detect the resulting emission lines. Because any kind of photomultiplier exhibits dark current, even in the absence of illumination, there is always a background noise. The signal from the photomultiplier tube is also affected by shot noise and Johnson noise.[33] In addition, the typical photomultiplier shows linear response only in

restricted wavelength ranges. The RFLOGS system, however, works in a totally different way. In this system, when the plasma is irradiated by laser (or any other light source), an optogalvanic effect (LOGE) signal is generated. The LOGE signal is actually the change of the electrical impedance of plasma produced by resonant absorption of laser radiation by a plasma moiety.[34-36,12] This change is detected by a pick-up coil and treated by digital signal analysis. An external detector is not required in this system because the plasma, being an integral part of the detector circuit, acts as its own detector. This makes the system less complicated and more reliable. Since LOGE is extremely sensitive in nature, selective wavelength excitation (usually by a laser) can be used to detect specific species by tuning the laser to an appropriate wavelength.

(3) Optogalvanic detection has the characteristics of zero background, selective excitation from metastable states, and the ability to pick up the very weak signals of the photoacoustic and photo-ionization effects from non-emitting species. Therefore, the RFLOGS technique has very high sensitivity. Finally, the overlap of emission lines, which so often occurs in ICP spectroscopy, is not pertinent to LOGE spectroscopy because it is not the emission that is monitored. Thus, the inter-element interferences that are so bothersome in ICP-AES, are totally eliminated. The resolution of RFLOGS spectrometry, indeed, is comparable with, and in many instances, better than that of conventional ICP-AES.

Laser optogalvanic spectroscopy (LOGS) has long been recognized as a well-developed spectroscopic technique for various applications, such as laser wavelength calibration,[37] spectral analysis of atoms and molecules,[38] isotopic shift measurements of complex atoms,[39] and as an extremely sensitive detection tool.[40, 41] LOGS has been

used for direct detection of metal species at ultra-low concentrations in flames and electric discharges. LOGS has been developed as an ultra-sensitive diagnostic tool for on-line, real-time measurements of the concentration of volatile, toxic trace metals, radionuclides, and other gas-phase pollutants.

The LOGS technique is a gas phase technique. Thus, even for solid samples, the metal species must exist as airborne metal oxide and/or metallic particles or, better, as free, single atoms. These gas phase species can be produced by a variety of atomization sources, such as flames, planar glow discharges, hollow cathode discharges, RF discharges, and microwave discharges, all of which were discussed and evaluated in a recent work.[3]

The test on a planar-glow-discharge atomization source proved unsatisfactory.[3] The magnitude of the LOGS signal is sensitive to the distance between the laser beam and the cathode, because most of the voltage drop across the planar glow discharge occurs in the cathode fall region, which is only 2 mm thick. Thus, the laser beam position must be maintained within 0.01 mm to avoid any alteration of equipment sensitivity. While this position alignment requirement is feasible in the laboratory, it is difficult to either achieve or maintain in the field.

A hollow-cathode-discharge atomization source is preferable to a planar glow discharge because the electron density in a hollow cathode is much greater; therefore, the probability of producing a LOGS signal by laser-assisted electron impact ionization is increased.[3] When the system was running, metal particles (such as lead, cadmium and sodium) were introduced into the hollow cathode cell from an ultrasonic nebulizer.

Under proper conditions, the LOGS detectivity in a hollow cathode plasma can be highly sensitive.

A low-power-RF-discharge atomization source has the advantage of involving no combustible gases and no internal electrodes and, hence, is free of issues associated with the corrosion or oxidation of electrodes.[3] Therefore, this method is very useful for monitoring and detecting corrosive, toxic and radioactive species. In this work, iodine, sodium and cadmium samples were detected in both static and flowing conditions. The experimental results show that RFLOGS is a valuable laboratory technique for trace element analysis, especially for gaseous samples. However, without further improvement, it is not viable for continuous, on-line monitoring of metal species at near-atmospheric pressure because of the broad background noise and sample dilution.

The feasibility of quantitative LOGS detection of metal species aspirated into flames has also been studied.[3] Selected metals were introduced into the burner system as airborne, desolvated metal oxide particles from an ultrasonic nebulizer. It was found that the detection limit of the flame LOGS method is comparable to or better than that of the air ICP-AES method. Further optimization of the LOGS system can improve the limit of detection by 1-3 orders of magnitude. Therefore, a flame-based LOGS system can detect metal species at and below environmentally mandated concentrations, and at and below concentrations that can be monitored by other on-line, real-time technologies.

1.6 References

1. R. E. Muenchausen, R. D. May, and G. W. Hills, *Opt.Commun.* **48**, 317 (1984)
2. F. D. Snell and L. S. Ettre, *Encyclopedia of Industrial Chemical Analysis*, Interscience Publishers, New York, **14**, 584 (1971)

3. D.L. Monts, S. Abhilasha, S. Qian, D. Kumar, X. Yao and S.P. McGlynn, *J. Thermophysics & Heat Transfer,* **12**(1), 66 (1998)

4. D. Kumar, R. R. Zinn, T. D. Armstrong and S. P. McGlynn, *J. Phys. Chem.,* **99**, 7530 (1995)

5. G. A. Bickel and K.K Innes, *Appl. Opt.*, **24**, 3620 (1985)

6. A. Sasso, M. Ciocca and E. Arimondo, *J. Opt. Soc. Am.,* **B5**, 1484 (1988)

7. Y. Uetani and T. Fujimoto, *Opt. Commun.*, **49**, 258 (1988)

8. D. Kumar, P. L. Clancy, and S. P. McGlynn, *J.Chem. Phys.,* **90**, 4008 (1989)

9. D. Kumar and S. P. McGlynn, *J. Chem. Phys.,* **93**, 3899 (1990)

10. S. Mofatt and A. L. S. Smith, *J. Phys. D: Appl. Phys.,* **17**(59) (1984)

11. C. R. Webster and R. T. Menzies, *J. Chem. Phys.,* **78**, 2121 (1983)

12. R. A. Keller, B. E. Warner, E. F. Zalewski, P. Dyer, R. Engleman, Jr., and B.A. Palmer, *J. Phys. Colloq.* **C7**, 23 (1983)

13. R. A. Keller and E. F. Zalewski, *Appl. Opt.* **19**, 3301 (1980)

14. E. Arimondo, M. G. DiVito, K. Ernst and M. Inguscio, *Opt. Lett.,* **9**, 530 (1984)

15. C. T. Rettner, C. R. Webster and R. N. Zare, *J. Phys. Chem.,* **85**, 1105 (1981)

16. C. Hameau, E. Arimondo, J. Wascat, and P. Glorieux, *Opt.Commun.* **53**, 375 (1985)

17. A. Sasso and M. G. DiVito, *Opt. Commu.,* **66**, 270 (1980)

18. D. Kumar, L. Klasinc, P.L. Clancy and S.P. McGlynn, *Int. J. Quantum Chem.,* Quantum Chem. Symp., **19**, 403 (1986)

19. D. Kumar, P. L. Clancy, L. Klasinc and S.P. McGlynn, *Croat. Chem. Acta,* **66**, 217 (1993)

20. D. Kumar and S. P. McGlynn, *Chem. Phys. Lett.,*. **176**, 536 (1991)

21. D. Kumar, R. R. Zinn, and S. P. McGlynn, *J. Chem. Phys.,* **101**(3), 1959 (1994)

22. A. Montaser and D. W. Golightly, *Inductively Coupled Plasmas in Analytical Atomic Spectrometry,* p3, VCH Publishers, Inc., New York, (1987)

23. M. Thompson and J. N. Walsh, *A Handbook of Inductively Coupled Plasma Spectroscopy,* p25, Blackie & Son, Ltd., New York (1983)

24. S. S. Berman, J. W. McLaren and D. S. Russel, *Anal. Proc. Int. Winter Conf.,* Ed. R.M. Barnes, p586, Heyden, London (1981)

25. M. Thompson and J. N. Walsh, *A Handbook of Inductively Coupled Plasma Spectrometry,* p126, Blackie & Son, Ltd., New York (1983)

26. G. M. Hieftje and S. W. Downey, *ICP Info. Newslett.,* 7, 560, (1982)

27. W. J. Crooks, G. R. Choppin and A. Saoto, *Anal. Lett.,* **27**(14),2737 (1994)

28. J. Fucsko, S. H. Tan, H. La and M. K. Balazs, *Appl. Spec.,* **47**(2), 150 (1993)

29. M. Thompson and J. N. Walsh, *A Handbook of Inductively Coupled Plasma Spectrometry,* p29, Blackie & Son, Ltd., New York (1983)

30. R. K. Winge, V. A. Fassel, V. J. Peterson and W. A. Floyd, *Inductively Coupled Plasma-Atomic Emission Spectroscopy,* 1st ed., Elsevier, New York, (1985)

31. T. Jacksier, M. J. Jahl and R. M. Barnes, *Spectrochimica Acta,* Part B, **47**(12), (1992)

32. B. S. Sheppard, J. A. Caruso, K. A. Wolnik and F. L. Fricke, *Appl. Spectros.,* **44**(4) 712(1990)

33. A. Montaser and D. W. Golightly, *Inductively Coupled Plasmas in Analytical Atomic Spectrometry,* p103, VCH Publishers, Inc., New York, (1987)

34. B. Barbieri, N. Boverini and A. Sasso, *Rev. Mod. Phys.,* **62**,603(1990)

35. C. R. Webster and C. T. Rettner, *Laser Focus,* **19**, 41 (1983)

36. J. E. M. Goldsmith and J. E. Lawler, *Contemp. Phys.,* **22**, 235 (1981)

37. M. C. Su, S. R. Oritz and D. L. Monts, *Optics Communications,* **61**(4), 257 (1987)

38. J. Pfaff, M. H. Begemann and R. J. Saykally, *Molecular Physics,* **52**(3), 541(1984)

39. P. Pianarosa, Y. Demers and J. M. Gagne, *J. Opt. Soc. of Am. B,* **1**(5), 704(1984)

40. R. B. Green, *Analytical Applications of Lasers*, p75-105, Wiley, New York, 1986

41. O. Axner and H. Rubinsztein-Dunlop, *Spectrochimica Acta B*, **44** (9), 835(1989)

CHAPTER 2: OPTOGALVANIC TRANSIENTS IN THE $1S_{2,4} \rightarrow 2P_{1,3}$ EXCITATIONS OF RADIO FREQUENCY NEON PLASMA *

2.1 Introduction

Discharge plasmas, both direct current (DC) and radio frequency (RF), are used in analytical chemistry and materials engineering.[1] A number of specific techniques have been developed to probe and study them. The technique of interest here is the optogalvanic effect (OGE).[2-4] Although several phenomenological models attempt to explain various aspects of the OGE signal,[5-11] none is particularly satisfactory.

For example, the OGE signals associated with different electronic excitations of the plasma may have different signs/polarities: the Ne $1s_4 \rightarrow 2p_1$ excitation has a positive major peak whereas the same peak for the Ne $1s_2 \rightarrow 2p_1$ excitation is negative. The sign (or polarity) of this signal must bear on the proposed mechanisms of OGE signal formation. The following explanations of these polarity effects have been given:

--- R. Shuker et al.[12] attributed the sign changes to a population inversion.

--- T. Caesar and J. Heully[13] pointed out that inversion of the population of any $2p$ level relative to the $1s_2$ level does not occur under such conditions.

Minor changes have been made to the journal article in order to satisfy the format requirements of the Graduate School. Fig. 2-5, sections 2.4.3, and one part of section 2.2 are materials original for dissertation.

--- L. Yin and Y. Zhang suggested[14,15] that the inverted signal results from photoelectric effects produced by strong (internal) VUV radiation on the surface of the hollow cathode.

--- T. Fujimoto et al. made the most seminal suggestions.[16] They proposed that population re-distributions among the $1s_j$ levels (see Fig. 2-1) were responsible for the OGE signal and its sign and, in specific, that the $1s_{3,5}$ metastable-level populations actually determine the decay characteristics. They inferred that perturbations of the $2p_k$ populations had little or no effect on OGE signals. They also showed[17] that OGE signals were not linearly related to the electron density in the plasma.

While all these works are fundamental, many were done on DC plasma and a very important mechanism in generating OGE signals, the photoacoustic effect (PA), went completely undetected. As a result the mechanisms of OGE signal inversion remain unclear.

The laser optogalvanic effect (LOGE) signal is the impedance change produced in a plasma by laser irradiation. This signal contains two very different components:[18-19] one produced by ionization rate changes (IRC), the other by a change in the rate of radiationless energy dumping that leads to the photoacoustic (PA) effect. These two components, IRC and PA, can be separated experimentally.[19,20] The method of separation is based on the fact that ionization alters the total concentration of charge carriers whereas acoustic effects do not; in the first case, this leads to frequency modulation and, in the latter case, to amplitude modulation of the resonance

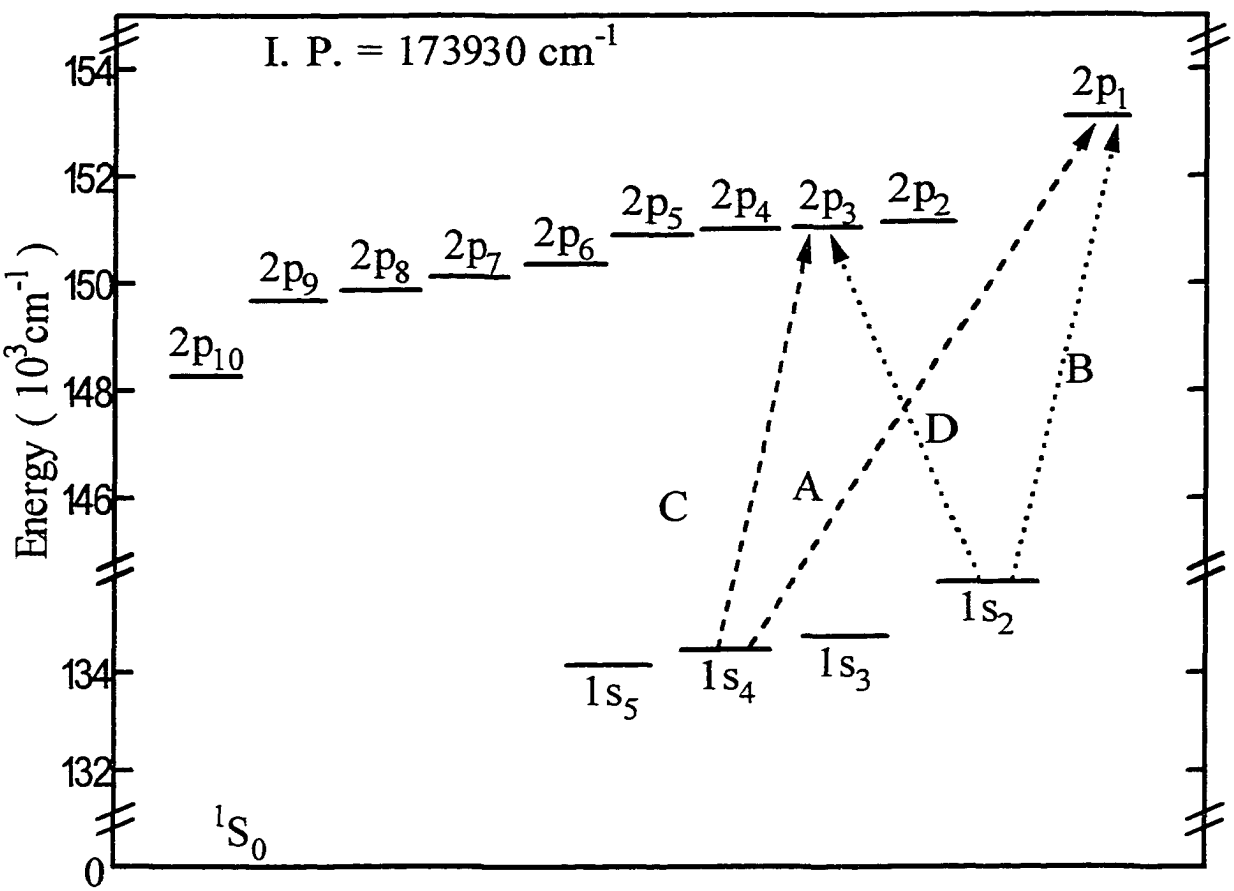

Fig. 2-1 Partial energy level diagram for neon. States are labelled in the Paschen notation. The arrows represent the excitations discussed in this work. The labels A, B, C, D relate these excitations to the signals of Fig's. 2-3, 2-4 and 2-5.

characteristics of the driver/plasma circuit. This topic has been discussed in detail by Kumar et al.[21, 22]

Kumar et al. applied their separation technique to the IRC and PA transients produced by laser excitation of a radio frequency discharge in neon.[21] Their results are best appreciated by reference to the energy level diagram for neon plasma shown in Fig. 2-1. The Ne ground state is denoted $^1S_0$. The states responsible for plasma maintenance are the four states arising from the 2p→3s excitation which, in Paschen notation,[23] are denoted $1s_2$, $1s_3$, $1s_4$ and $1s_5$. Of these, it is the two metastable states $1s_3$ and $1s_5$ that maintain the plasma. The $1s_2$ and $1s_4$ states produce $1s_2 \rightarrow {}^1S_0$ and $1s_4 \rightarrow {}^1S_0$ trapped radiative events, the intrinsic lifetimes for which, at minimal pressures, are of the order of 10^{-3} and 10^{-2} μs, respectively, but which, at the 5 Torr pressures used in this work, exhibit lifetimes of ~2 and 20 μs, respectively, because of resonant trapping.[10] The 2p→3p excited configuration produces the ten $2p_{1\text{-}10}$ states. Of these, the $2p_3$, $2p_5$ and $2p_7$ states, produced by $1s_2 \rightarrow 2p_3$, $1s_4 \rightarrow 2p_{3,7}$ and $1s_5 \rightarrow 2p_{5,7}$ laser excitations, were the terminal states in the experiments of Kumar et al.[21] Their results were:

1. The dominant event in both the IRC and PA transients appeared to be attributable to $1s_2 \rightarrow {}^1S_0$ trapped radiation. However, both of these dominant IRC and PA events were found to be more or less temporally coincident. In all previous work, PA events were found to be delayed[18-22] relative to the corresponding IRC events because the sound waves required a finite time to travel from the point of laser excitation to the plasma proper. No interpretation of this anomalous temporal coincidence was

given by Kumar et al.[21, 22]; and the propriety of the attribution of the dominant IRC and PA events to $1s_2 \rightarrow {}^1S_0$ trapping was questionable. One purpose of this work is to verify and interpret this coincidence, and to secure the $1s_2 \rightarrow {}^1S_0$ assignment.

2. The signature of all other peaks in the IRC and PA transients seemed to be opposite to that of the presumptive $1s_2 \rightarrow {}^1S_0$ trapped radiation peak. Why this should be so, or if in fact it was so, was not clear. One purpose of this work is to verify and explain these assertions.

3. All laser excitations initiating in $1s_4$ produced more intense IRC and PA signals than those initiating in $1s_2$, a fact attributed to much larger $1s_4$ populations: $n(1s_4) \cong 10^2 n(1s_2)$*. This work is also concerned with these observations.

4. The $2p_k$ states, apart from direct branching into the $1s_j$ states, appeared to exert little or no effect on the signals. That is not the case: excitations to the $2p_3$ state are more efficient than those to the $2p_1$ state with respect to signal production. This topic will be discussed.

Thus, the purpose of this work is to clarify and amend points 1 through 4 above. Towards that end, we have chosen the four transitions shown in Fig. 2-1. The reason for this choice is vested in the data of Table 2-1: the branching ratios for $2p_k \rightarrow 1s_j$ decay show that the immediate result of $1s_2$ or $1s_4$ excitation to either $2p_1$ or $2p_3$ is merely a redistribution of the $1s_2$ and $1s_4$ populations. No branching occurs into the metastable $1s_3$ or $1s_5$ states. Thus, the laser excitations of Fig. 2-1 merely produce disequilibrium $1s_2$ and $1s_4$ state populations.

* This result is now known to be in error. See page 46 for more recent results.

The laser wavelengths used in this work cannot lead to direct ionization. However, both the $1s_2 \rightarrow {}^1S_0$ and $1s_4 \rightarrow {}^1S_0$ trapped radiations, which are the eventual results of the laser excitations, can ionize the $1s_j$ states. Finally, the reequilibration of the $1s_4$ and $1s_2$ states will alter the metastable $1s_3$ and $1s_5$ state populations and produce a change of the Penning ionization rates for which the $1s_3$ and $1s_5$ states are dominantly responsible.

The same events that lead to ionization can also produce non-radiative energy dumping and, hence, acoustic effects.

Table 2-1 Selected Neon Transitions

Transition $2p_k \rightarrow 1s_j$	Energy (cm^{-1})	Transition Probability, A_{kj} ($10^7\ s^{-1}$)	Branching Ratio, f_{kj} %
$2p_1 \rightarrow 1s_2$	17082	6.820	98.7
$2p_1 \rightarrow 1s_4$	18517	0.090	1.3
$2p_3 \rightarrow 1s_2$	15029	0.029	0.5
$2p_3 \rightarrow 1s_4$	16458	6.030	99.5

2.2 Experiment

Fig. 2-2 represents the experimental arrangement. A commercial hollow cathode lamp with neon filler gas is used as the discharge tube. The Ne sample is housed at ~5 Torr in this lamp, which is ~6 inches in length and ~1 inch in diameter. Two electrodes, ~3 cm apart, are wound around the exterior of the lamp. RF power of ~0.5 W and

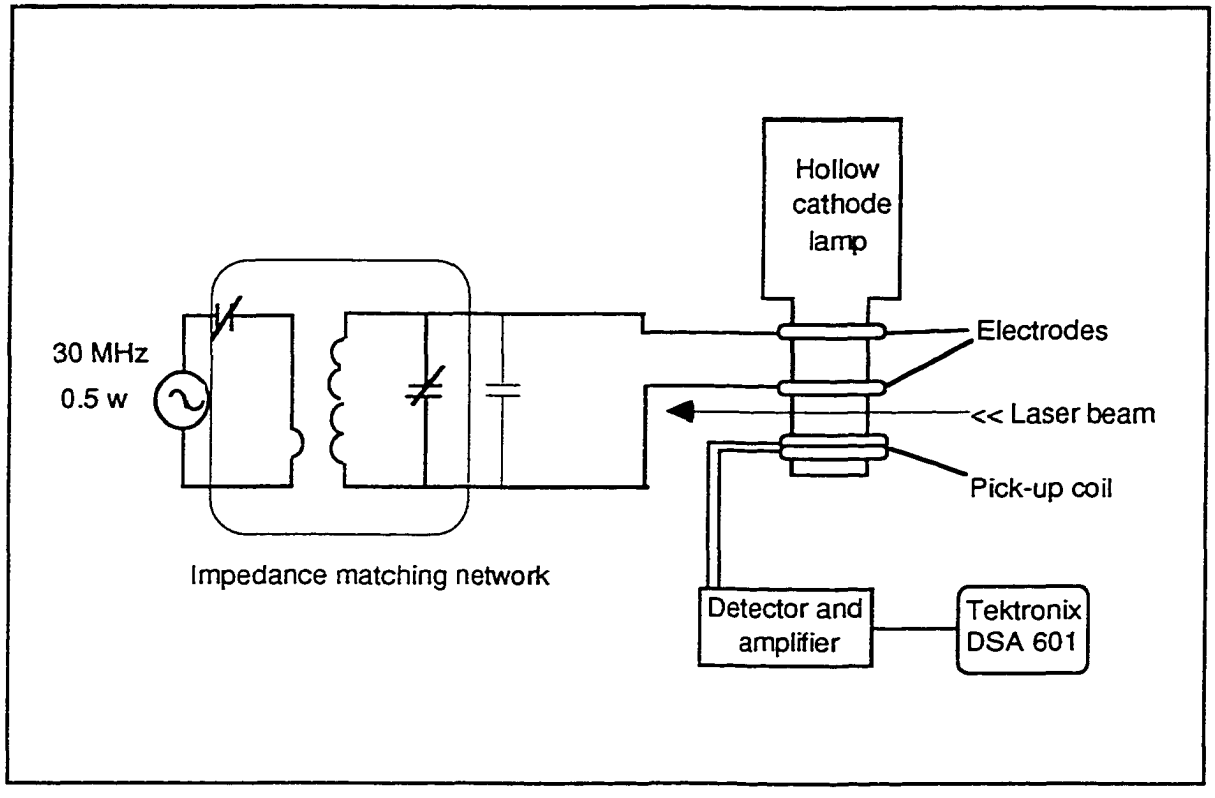

Fig. 2-2 Schematic of the experimental arrangement

~30 MHz is applied at high voltage and generates a stable, low-noise, capacitively coupled discharge. A resonantly tuned pick-up coil is also wrapped around the exterior of the cell, ~1 cm below the bottom electrode. A pulsed laser (CMX-4, ~1 μs half bandwidth, ~0.1 cm^{-1} resolution) beam whose wavelength is tuned to a desired Ne transition excites the plasma transversely at a point between the lower electrode and the pick-up coil. Thus, the distance from the site of excitation to the plasma proper is 1 to 2 cm. When the laser excites a Ne transition, the change of RF power is detected by the pick-up coil. This is the LOGE signal.

The operation of this system was discussed by Kumar et al.[20] The entire system of RF power supply, plasma tube and detector can be tuned to, or de-tuned from resonance by adjusting the RF frequency and/or the capacitors present in the pick-up and RF power circuits. In this work, tuning is facilitated by using a 1000Hz RF signal as the modulation and trigger source and doing pulse averaging (averaging number = 32). The system is first tuned to resonance and the transient temporal profiles of the OGE signals are recorded. The RF power is then detuned by Δf =0.1 MHz and the signals at $f = f_0 - \Delta f$ and $f = f_0 + \Delta f$ are recorded. The IRC and PA components can be derived from the following equations:

$$Y(PA) = Y(f_0)$$

$$Y(IRC) = (Y(f_0 + \Delta f) - Y(f_0 - \Delta f))/2k'$$

where Δf is a small change in the RF frequency; $Y(f_0)$, $(Y(f_0 + \Delta f)$ and $Y(f_0 - \Delta f)$ are temporal profiles of the OGE signal at frequencies f_0, $f_0 - \Delta f$ and $f_0 + \Delta f$; Y(PA) and Y(IRC) are the PA and IRC components; and k' is a constant.[20]

2.3 Results

2.3.1 The $1s_2 \rightarrow {}^1S_0$ Nature of the Dominant Peak

The dominant peak in the acoustic transients of Fig. 2-3 is the first peak, and it is denoted PA1. The dominant peak in the ionization transients of Fig. 2-4 is the second peak, and it is denoted IRC2. Comparison of Fig's. 2-3 and 2-4 suggests that these peaks are very similar. Indeed, when the modification of the left-hand side (LHS) of IRC2 by the oppositely signed IRC1 and the modification of the right-hand side (RHS) of PA1 by the oppositely signed PA2 are taken into account the two transient peaks, IRC2 and PA1 become virtually identical.

The mean lifetimes of the IRC2 and PA1 transients, as measured on the RHS of both peaks are given in Table 2-2. They all have a mean lifetime of ~2μs, which is characteristic of the $1s_2 \rightarrow {}^1S_0$ trapped radiative decay process under the conditions of this experiment.

Table 2-2 Experimental Data for the Ne Transitions

Transition	$1s_4 \rightarrow 2p_1$		$1s_2 \rightarrow 2p_1$		$1s_4 \rightarrow 2p_3$		$1s_2 \rightarrow 2p_3$	
Component	PA1	IRC2	PA1	IRC2	PA1	IRC2	PA1	IRC2
Intensity (V)	1.352	0.122	0.460	0.220	1.640	0.588	1.560	0.676
Relative Intensity (V)	1.352	0.122	0.026	0.013	2.642	1.048	0.823	0.362
Mean Lifetime (μs)*	2.6	1.2	2.6	1.6	2.4	1.5	2.7	1.6
Polarity	+	+	–	–	+	+	–	–

* The mean lifetime refers to the "major peak" (PA1 or IRC2). It was measured on the right hand shoulder of that peak at intensities between 1/3 and 2/3 of maximum.

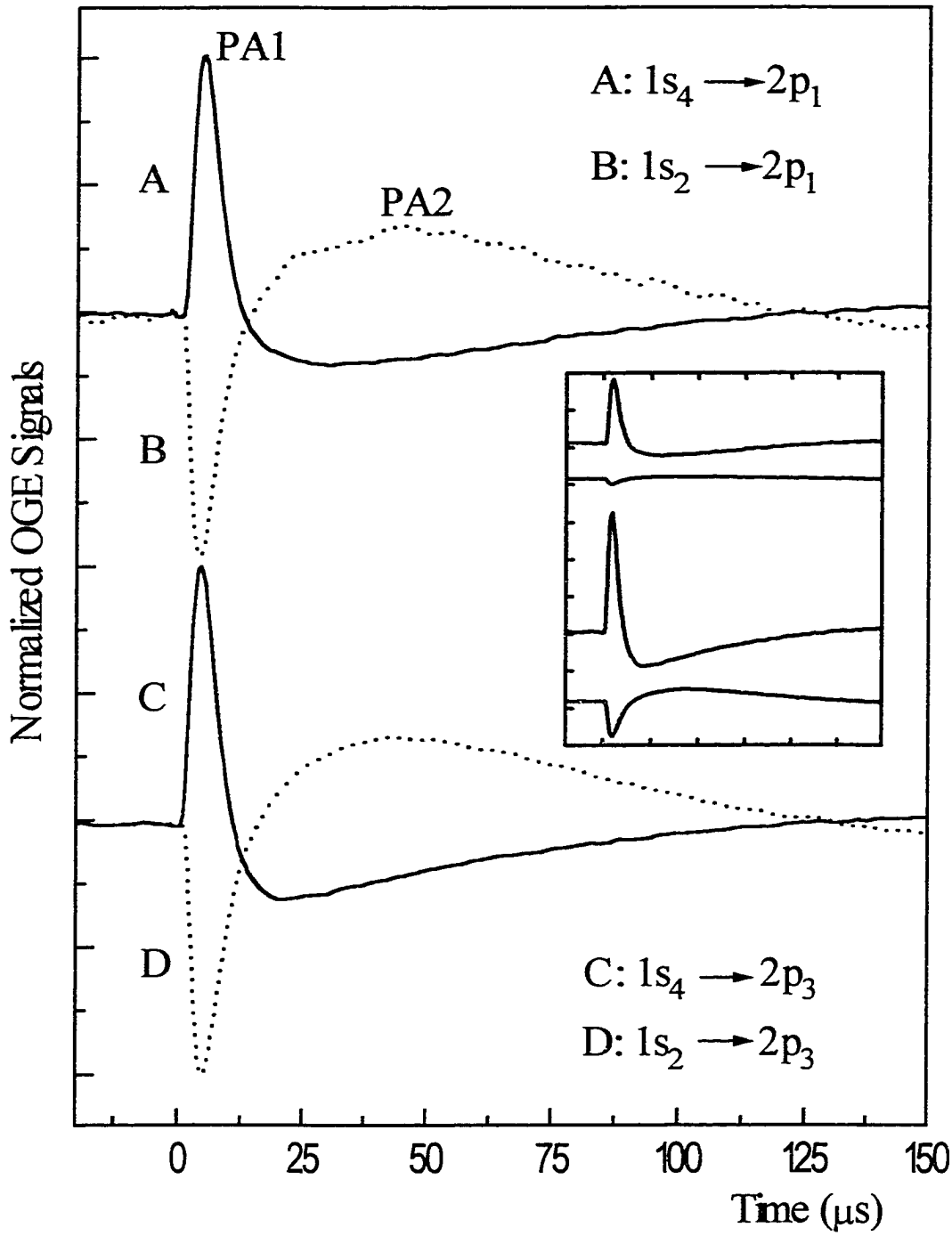

Fig. 2-3 The normalized PA components of the OGE signals for the $1s_{2,4} \rightarrow 2p_{1,3}$ excitations. Normalization is used to emphasize the symmetry of the signals. The unnormalized signals, in similar top-to-bottom order, are shown in the insert, in which the y and x axes are scaled 0.5V/div and 25μs/div, respectively. In addition, the zero voltage positions in the insert have been arbitrarily separated to avoid crowding.

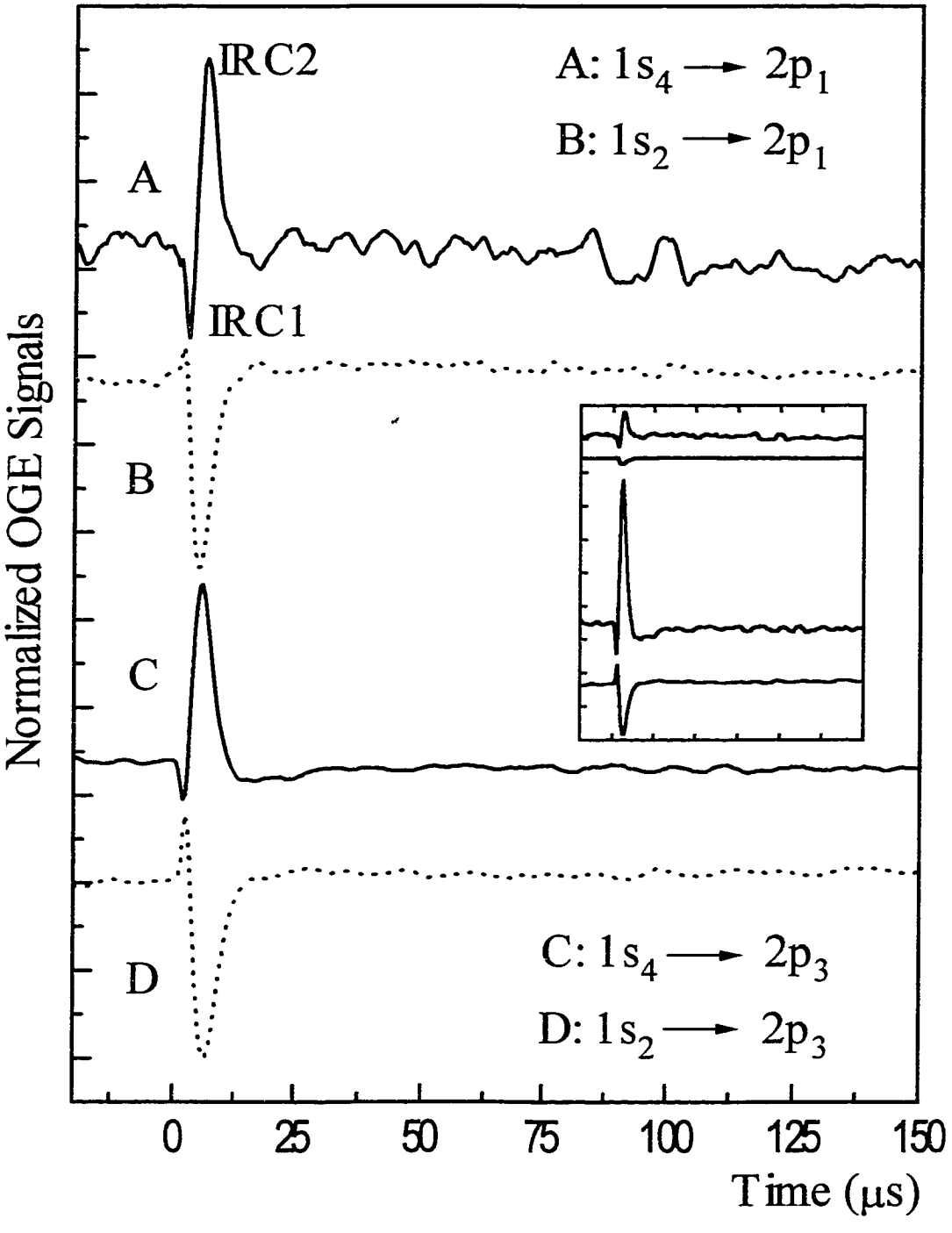

Fig. 2-4 The normalized IRC components of the OGE signals for the $1s_{2,4} \rightarrow 2p_{1,3}$ excitations. Normalization is used to emphasize the symmetry of the signals. The unnormalized signals, in similar top-to-bottom order, are shown in the insert, in which the y and x axes are scaled 0.13V/div and 25μs/div, respectively. In addition, the zero voltage positions in the insert have been arbitrarily separated to avoid crowding.

We conclude that the dominant IRC2 and PA1 features, which are modified to some extent by other interfering transients and by differences of instrumental response to the ionization and acoustic events, are identical in origin and caused by $1s_2 \rightarrow {}^1S_0$ trapped radiation.

2.3.2 Alternation of Signs

Inspection of Fig's. 2-3 and 2-4 shows, for a given excitation, that (i) the IRC2 and PA1 peaks always have the same signs; (ii) the IRC1 and PA2 peaks always have the same signs; and the signs in (ii) are always opposite to those in (i). Thus, positive/negative signatures for IRC2 and PA1 always correspond to negative/positive signatures for IRC1 and PA2.

2.3.3 The Relative Signal Intensity

The unnormalized PA components of the OGE signals are also shown in Fig. 2-3 (insert) and their intensities are given in Table 2-2. The signals obtained by excitation from the $1s_4$ state are always stronger than the signals obtained by excitation from $1s_2$. The same is true of the IRC components, as is shown in Fig. 2-4 (insert) and Table 2-2. Thus, the $1s_j$ initiating state determines both the signal polarity and the signal intensity.

The $2p_k$ states, however, are not without influence. It is clear from Fig. 2-3 and Table 2-2 that the PA signal associated with the $1s_2 \rightarrow 2p_3$ excitation is stronger than that associated with the $1s_2 \rightarrow 2p_1$ excitation; and that the PA signal of $1s_4 \rightarrow 2p_3$ is also stronger than that of $1s_4 \rightarrow 2p_1$. The unnormalized IRC profiles in Fig. 2-4 also confirm this result. However, while excitations to $2p_3$ are more efficient than those to $2p_1$ in terms of signal production, they do not affect the signs.

In order to emphasize the similarities of the dominant peaks of the PA and IRC signals, we have isolated them in Fig. 2-5. The average decay constant for the dominant PA peak is ~2 μs and that for the dominant IRC peak is ~1.5 μs. Since the decay constant for trapped $1s_2 \rightarrow {}^1S_0$ radiation under the conditions of our experiment should be ~2 μs, we feel confident that it is events initiated by this trapped radiation that produce the dominant peak. The dominant IRC peak is preceded by ~3 μs by another sharp peak of opposite phase, whereas the dominant PA peak appears to be singular, and followed at much longer time, ~20 μs, by a broad peak of opposite polarity.

No decay event was observed in the ~20 μs range. Consequently, one may assume that trapped radiation of $1s_4 \rightarrow {}^1S_0$ origin is unimportant. It is possible that a $1s_4 \rightarrow {}^1S_0$ event could contribute to the processes underlying the ~30 μs PA2 peak. However, because of the definitive absence of any ~20 μs event in the IRC signal, the presence of such events in the PA signal are unlikely.

2.4 Discussion

2.4.1 IRC Component

As shown in Fig. 2-4, the typical IRC OGE signal consists of two peaks of opposite polarity: a weak initial peak (IRC1) followed by a stronger (IRC2). This IRC signal is modeled in Fig. 2-6.

In the $1s_4 \rightarrow 2p_{1,3}$ excitations, laser depletion of the $1s_4$ state is followed immediately by reequilibration processes in which the $1s_3$ and $1s_5$ metastable states are depleted by collisional processes in the attempt to restore the $1s_4$ status quo. It is these metastable states that are responsible for plasma maintenance. Consequently, their

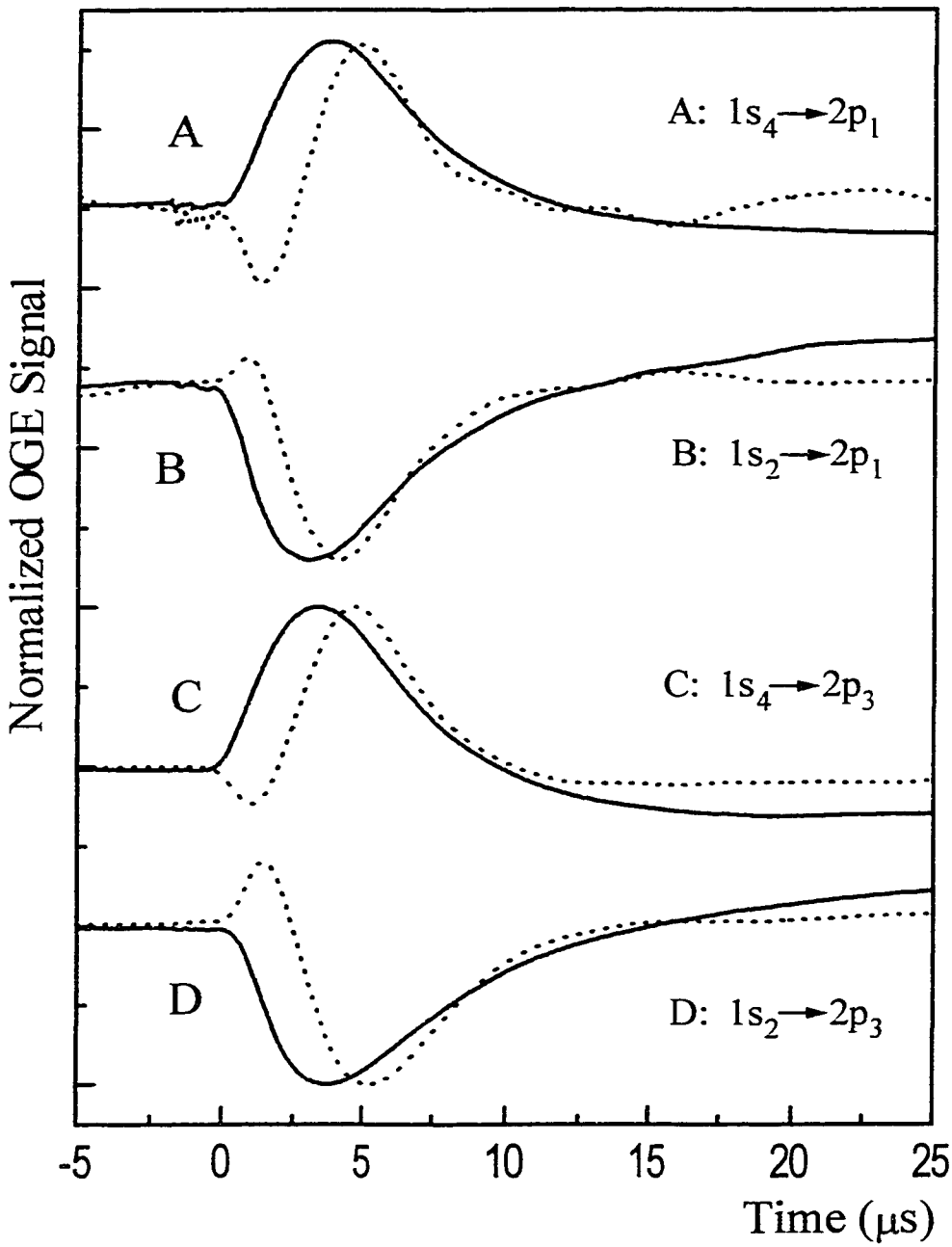

Fig. 2-5 Dominant peaks, magnified and normalized to illustrate similarities and differences.

PA component: ————————
IRC component: - - - - - - - - - - - - - - - - -

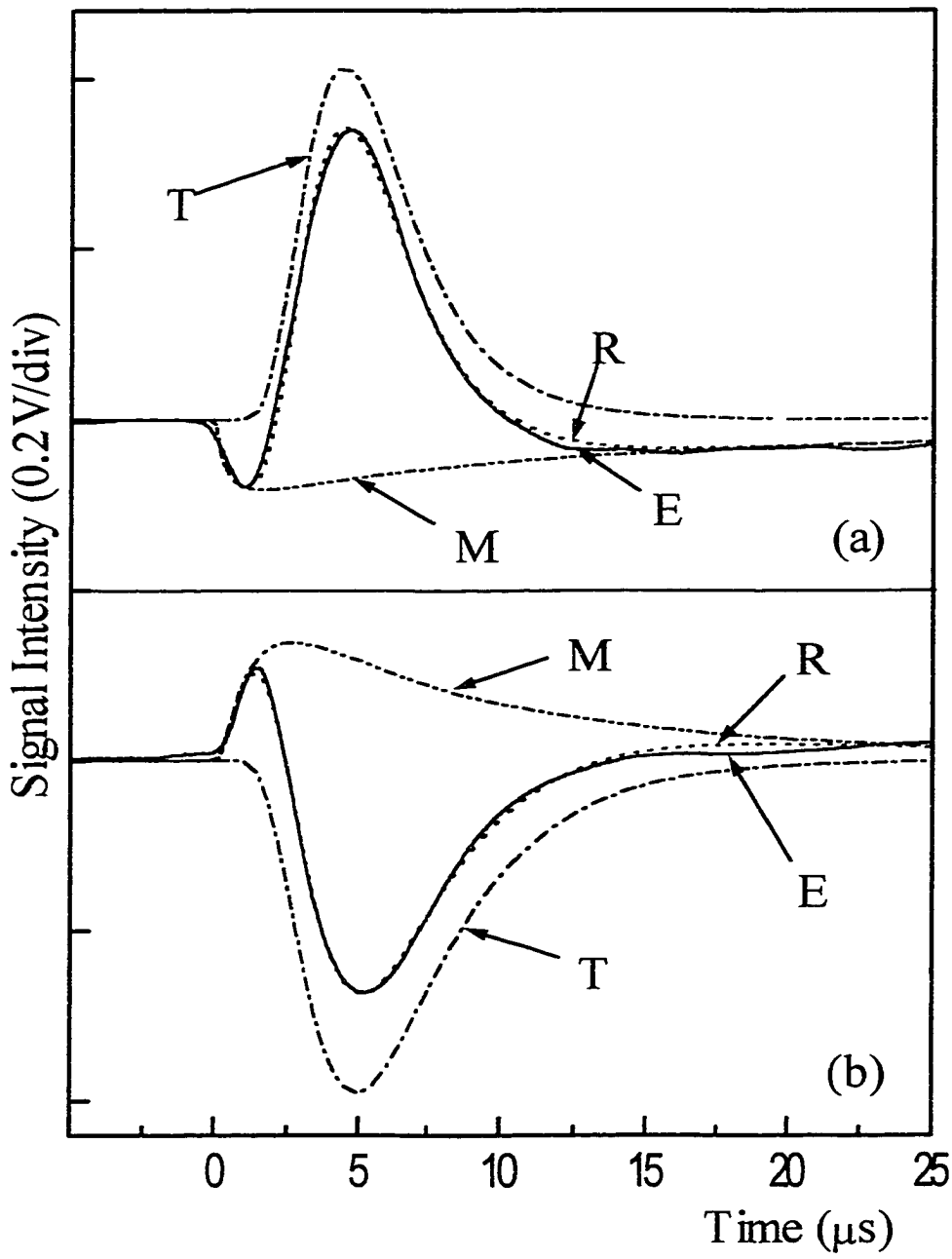

Fig. 2-6 Illustration of IRC signal formation produced by $1s_4 \rightarrow 2p_3$ (Fig. 2-6(a)) and $1s_2 \rightarrow 2p_3$ (Fig. 2-6(b)) excitations. Log-normal functions are used to model the Penning collisional ionization of metastable states (M) and the $1s_2 \rightarrow {}^1S_0$ trapped radiation ionization (T). Curve denotations are:

Penning ionization of metastable states (M): ——·——·——

Trapped radiation ionization (T): —— ————

Resultant of M and T (R): ----------

Experimental curve (E): ——————

depletion launches a negative signal (i.e., a diminution of ionization) that is synchronous with the laser pulse. It also follows that recovery will be slow because it involves the collisional adjustment of all populations to their equilibrium values. This signal component is modeled as the log-normal resolvent, curve M, in Fig. 2-6(a).

Part of the reequilibration process involves the $2p_3 \rightarrow 1s_2$ decay, leading to higher $1s_2$ populations and an increase of $1s_2 \rightarrow {}^1S_0$ trapped photons which should have a lifetime of ~2 μs and a high probability for ionizing the $1s_3$ and $1s_5$ metastable states. The resulting peak should be positive. Peak T of Fig. 2-6(a), with maximum at ~5 μs and a decay time of ~2 μs, is the log-normal model of this event. The superposition of these two processes, M and T, produces curve R, which is an excellent experimental fit (curve E).

The $1s_2 \rightarrow 2p_{1,3}$ can be modeled by the same method. When laser depletion of $1s_2$ occurs, the excited populations, because of relaxation to $1s_4$ and energetic proximity of $1s_4$ to the metastable $1s_3$ and $1s_5$ states, increase the metastable populations and, by arguments advanced earlier, increase the ion/electron populations. This produces a positive signal that should initiate synchronously with the laser pulse. On the other hand, the depletion of the $1s_2$ population now generates a sharp negative peak caused by a decrease of $1s_2 \rightarrow {}^1S_0$ trapped photons. The superposition of these two processes should produce the OGE signal profile of the excitations $1s_2 \rightarrow 2p_{1,3}$: a sharp positive peak at ~2 μs and a sharp negative peak at ~5 μs. Convolution produces an excellent fit to the observed signal, as shown in Fig. 2-6(b).

The rise time of the M band to its minimum (Fig. 2-6(a)) or maximum (Fig. 2-6(b)) should contain information on the collisional processes $1s_{3,5}+{}^1S_0 \rightarrow 1s_4$ and $1s_4+{}^1S_0 \rightarrow 1s_{3,5}$, respectively. Unfortunately, the rise time shown in Fig. 2-6 merely reflects that of the laser pulse, ~1 μs, used in this work and it will be necessary to employ excitation sources of 1ns or shorter pulse width in order to extract this sort of information. Such work, required in order to confirm the primacy of the $1s_4$ state in collisional energy transfer from and to the metastable states, is planned.

Thus, based on a rather simple model, both the signs and time structure of the IRC signals are fully explicable on the basis of a rather simple model.

2.4.2 PA Component

The PA OGE profiles also exhibit two peaks: a stronger sharp peak (PA1) and a weaker broad peak at longer times (PA2), as shown in Fig. 2-3.

The PA1 Event: PA1 is generated by $1s_2 \rightarrow {}^1S_0$ radiation trapping and is coincident with IRC2. This coincidence requires explanation. Acoustic transients should be delayed relative to the ionization event that arises from the same kinetic events. Ionization alters the charge carrier concentrations and, on the time scale of our experiments, produces an instantaneous change of the resonant circuit characteristics. Not so the acoustic events: while the energy dumping that initiates the compression wave is instantaneous with the ionization events, the compression wave must still travel from the locus of laser excitation to a region of high carrier concentration in the plasma, a region usually located somewhere between the two electrodes (See Fig. 2-2). The physical movement of these carriers by the sound wave alters the resonant circuit

characteristics and produces the PA transient. Thus, the PA transient should be delayed relative to the corresponding IRC transient by the travel time of the sound wave from the site of excitation to the site of high carrier concentrations (i.e., the ion sheaths). That is certainly not the case here. The interpretation of this novel coincidence resides in the peculiarities of trapped radiations.

An emissive event of intrinsic lifetime 1ns, on which trapping confers an effective lifetime of 1 μs, is basically a series of $\sim 10^3$ emission/absorption events or, equivalently, a series of $\sim 10^3$ random photon walks. Consequently, in a time of 1 μs, the excitation can readily fill a volume of $\sim 10^2$ m^3, which is considerably larger than the volume of the hollow cathode lamp of Fig. 2-2. That is, the trapped photons are uniformly dispersed over the entire Ne ensemble and, when $1s_2$ states undergo non-radiative energy dumping, some of them will do so where carrier concentrations are high and will produce PA events that coincide with the corresponding IRC event. Since some of the PA1 events may be initiated by energy dumping at some remove from the regions of high carrier density, some broadening of PA1 relative to IRC2 should occur on the LHS of PA1. It is in that sense that the slightly larger PA1 decay times of Table 2-2 are rationalized.

In the excitation $1s_2 \rightarrow 2p_{1,3}$, a decrease of trapped $1s_2 \rightarrow {}^1S_0$ photons occurs. Thus, a negative, sharp peak with a decay time constant of about 2 μs should be generated, as is the case (See Fig. 2-3). In the excitation $1s_4 \rightarrow 2p_{1,3}$, on the other hand, the population excited to the $2p_k$ states decays rapidly back to the $1s_2$ state and produces an increase of $1s_2 \rightarrow {}^1S_0$ trapped photons. Therefore a positive sharp peak is expected, and is observed (See Fig. 2-3).

The PA2 Event: This event initiates in the same set of kinetic occurrences that produce IRC1 but which, instead of ionization, end in non-radiative energy dumping. This is a localized set of events and registration of the compression wave requires movement of it to the plasma proper. That is, PA2 will be delayed relative to IRC1. Since the distance into the plasma is ~1 cm and the average delay of PA2 relative to IRC1 is ~30 μs, one computes a velocity of ~320 ms^{-1}, a correspondence to the velocity of sound in Ne at ~5 Torr, namely 330 ms^{-1}, which is largely coincidental but also corroborative of the model.

The only common feature in the IRC and PA transients is the rise and fall of trapped $1s_2 \rightarrow {}^1S_0$ photon densities. This commonality is associated here with the rapid diffusion of trapped photons throughout the tube volume, such that the shock wave is generated in the sensitive region of the plasma rather than solely at the locus of laser radiation incidence. On the other hand, the shock wave generated by the $1s_3$ and $1s_5$ population perturbations occurs at the point of laser incidence and requires 20 to 40 μs for travel to the sensitive region.

The modeling of the PA transients follows immediately. One merely takes event IRC2 and adds to it an oppositely-signed IRC1 transient that has been displaced to the right by ~30 μs. Adjustments of amplitudes and delay time provide a satisfactory match to the experimental PA transients and will be discussed in more detail in another paper.

2.4.3. General Transient Considerations

Despite all the similarities imputed above, it is quite evident that the PA and IRC signals are very different. The ~20 μs PA transient is absent in the IRC signal and the very fast IRC transient is absent in the PA signal. Indeed, the only common feature is

the "dominant peak" which originates in the rise and fall of trapped $1s_2 \rightarrow {}^1S_0$ trapped photon densities. We believe that this commonality is associated with the rapid diffusion of trapped photons throughout the tube volume, such that the shock wave is generated without much delay in the sensitive region of the plasma rather than solely at the locus of laser radiation incidence (in which case, dependent on distance, it might require 15 to 40 μs for the shock wave to travel to the sensitive region). On the other hand, the shock wave generated by $1s_3$ and $1s_5$ population perturbations at the point of laser incidence must travel to the sensitive region in order to register, causing this transient to be removed (i.e., be absent) at short times ($t < 5$ μs) from the PA transient and to be displaced (i.e., to appear) at longer times ($t > 20$ μs) in the same transient. Therefore, the fast IRC peak and the slow PA peak must always have identical polarities in any OGE transient. This prediction accords with experiment. In this way, the gross differences evident in Fig's 2-3 and 2-4 are readily interpreted.

The slight differences evident in Fig. 2-6 are explicable as interference of the $1s_2 \rightarrow {}^1S_0$ radiatively-trapped IRC component and the oppositely phased $1s_2$, $1s_4$ population perturbation IRC component, interferences that do not occur in the PA transient. Thus, we can rationalize all facets of Fig's 2-3, 2-4 and 2-5.

2.4.4 Kinetics

The transient signal intensity S_{jk} associated with excitation $1s_j \rightarrow 2p_k$ can be written

$$S_{jk} = \pm k\, N_j\, I_{jk}\, B_{jk}\, f \quad \ldots\ldots\ldots\ldots\ldots\ldots\ldots\ldots\ldots\ldots \quad (1)$$

where k is a constant that is different for the PA and IRC transients; N_j is the population

of the $1s_j$ state; I_{jk} is the photon density in the laser beam; B_{jk} is the transition probability of absorption; and f is a branching ratio. In these excitations that initiate in the $1s_2$ state, the interest resides in depopulation of this state, hence the negative sign and the attribution $f \equiv f_{k4}$ (i.e., the fraction of the $2p_k$ state that does not return to $1s_2$). In those excitations that initiate in the $1s_4$ state, the interest resides in the creation of an excess $1s_2$ population; hence, the positive sign and the attribution $f \equiv f_{k2}$. The quantities S_{jk} and I_{jk} are measured in this work. The quantity B_{jk} can be calculated from

$$B_{jk} = 6.01\lambda^3 g_k A_{kj} \quad \ldots\ldots\ldots\ldots\ldots\ldots \quad (2)$$

where λ is the wavelength of the transition $j \leftrightarrow k$, k being the index for the upper state; g represents degeneracies; and A_{kj} is the transition probability for the spontaneous $k \rightarrow j$ emission as defined by Wiese et al.[24]. Branching ratios, as calculated from the data compilation of Ben-Amar et al.[10], are given in Table 2-1.

One may now write the IRC1 signal ratio

$$S_{43}/S_{23} = -(I_{43}/I_{23})(N_4/N_2)(B_{43}/B_{23})(f_{32}/f_{34}) \quad \ldots\ldots\ldots\ldots \quad (3)$$

which, upon insertion of the experimental quantities, becomes $N_4/N_2 = 3.34$. The ratio S_{41}/S_{21} similarly yields $N_4/N_2 = 12.19$. This ratio of population densities differs considerably from the number 10^2 cited by Kumar et al.[15] If one now assumes that these states are in thermal equilibrium in the steady state plasma, one may estimate the plasma temperature as $800 < T(K) < 1700$, which is considerably different from that cited[11] for a DC hollow-cathode discharge, namely $1100 < T(K) < 3500$.

As pointed out, the transition intensities generated by excitations to the $2p_3$ state are always larger than those engendered by excitations to $2p_1$. We now inquire into this

result. The S_{43}/S_{41} ratio should be given by

$$S_{43}/S_{41} = (I_{43}/I_{41})\,(B_{43}/B_{41})\,(f_{32}/f_{12}) \quad \text{..... (4)}$$

which is independent of any population density and which, upon insertion of the values of I, B and f yields $S_{43}/S_{41} = 0.3$. By similar means, it is found that $S_{23}/S_{21} = 0.053$. That is, one predicts the exact opposite of the experimental findings, $S_{43}/S_{41} = 4.82$ and $S_{23}/S_{21} = 3.07$. That is, excitation into the $2p_3$ state is between 16 and 58 times more efficient than one would predict. No ready interpretation for the greater efficacy of excitations to the $2p_3$ state in producing both ionization and acoustic effects suggests itself. A reinvestigation of different I_{jk} and S_{jk} data sets indicates that the fault lies elsewhere. Consequently, we are inevitably led to suspect the A_{kj} data from which the B_{jk} and f_{kj} data are computed. On the other hand, as we discussed earlier, the $2p_3$ state is energetically close to the $2p_2$ (121 cm^{-1}) and $2p_4$ (59cm^{-1}) states whereas the $2p_1$ state is quite far removed ($\geq$1932cm^{-1}) from any other $2p_k$ states (See Fig. 2-1). Therefore, when we predict the LOGE signal profiles, we must consider not only the transition probabilities and branching ratios, but also other effects, such as collisional energy transfer between the $2p$ upper states. However, this is a question that is better left open, one which necessitates further work.

The acoustic data for the PA1 peak, when analyzed in the same way, lead essentially to the same conclusions for both N_4/N_2 and the ratios S_{43}/S_{41} and S_{23}/S_{21}. Consequently, one must conclude that the $2p_k \rightarrow 1s_j$ events play no differential role in producing either the IRC or the PA events. That is, non-radiative $2p_k \rightarrow 1s_j$ decay seems to play no role in producing the acoustic phenomena.

2.5 Conclusions

(1) The lower $1s_j$ states are the sole determinants of signal polarity. The dominant transient features, IRC2 and PA1, are associated with trapping of $1s_2$ states.

(2) For a given upper $2p_k$ state, the OGE signals for excitations from the $1s_4$ state are much stronger than those from the $1s_2$ state. This is attributed to higher $1s_4$ populations: the data suggest that the relative populations are $N(1s_4)/N(1s_2) \approx 10$ and that the plasma temperature is $T \approx 10^3$ K.

(3) The signatures of the various transient components (+/-) are interpreted on the basis of $1s_j$ population changes. No requirement for population inversion or laser action of the $2p_k$ states is needed.

(4) Excitations into the $2p_3$ state are more effective in signal production than excitations into the $2p_1$ state, which is contrary to prediction. No interpretation of this happenstance is available.

(5) Population changes of the $1s_3$ and $1s_5$ metastable states, which alter the rates of Penning ionizations, and $1s_{2,4} \rightarrow {}^1S_0$ radiation trapping, which leads to direct ionization of the $1s_{3,5}$ states, control the nature of the OGE signals. IRC profiles are readily modeled as a resultant of these Penning and trapped-photon ionizations.

(6) The PA profiles are also readily modeled. This modeling, however, is dependent on a crucial difference between the acoustic events associated with radiationless degradation of the $1s_{3,5}$ states and radiationless degradation of the radiatively-trapped $1s_2$ state. The former exhibits a delay of the acoustic transient, PA2 relative to IRC1, whereas, in the latter, PA1 and IRC2 are contemporaneous.

(7) Photon trapping leads to rapid uniformity of $1s_2$ excitation density throughout the plasma. This uniformity, it is asserted, is responsible for the un-delayed production of the PA1 acoustic transient.

2.6 References

1. V. A. Godyak, R. B. Piejak and B. M. Alexandrovich, *IEEE Trans. Plasma Sci.*, PS-19, 660 (1991)

2. B. Barbieri, N. Boverini and A. Sassa, *Rev. Mod. Phys.* , **62**, 603 (1990)

3. C. R. Webster and C. T. Rettner, *Laser Focus* , **19**, 41 (1983)

4. J. E. M. Goldsmith and J. E. Lawler, *Contemp. Phys.*, **22**, 235 (1981)

5. S. Mofatt and A. L. S. Smith, *J. Phys. D: Appl. Phys.*, **17**, 59 (1984)

6. R. S. Stewart, K. W. McKnight and K. I. Hamad, *J. Phys. D: Appl. Phys.* **23**, 832(1990)

7. J. E. Lawler, *Phys. Rev. A*, **22**, 1025 (1980)

8. D. K. Doughty and J. E. Lawler, *Phys. Rev. A*, **28**, 773 (1983)

9. D. M. Kane, *J. Appl. Phys.*, **56**, 1267 (1984)

10. A. Ben-Amar, G. Erez and R. Shuker, *J. Appl. Phys.*, **54**, 3688 (1983)

11. E. F. Zalewski, R. A. Keller and R. Engleman, Jr., *J. Chem. Phys.*, **70**(2), 1015 (1979)

12. R. Shuker, A. Ben-Amar and G. Erez, *Opt. Commun.*, **42**, 29 (1982)

13. T. Caesar and J. Heully, *Opt. Commun.*, **45**, 258 (1983)

14. L. Yin, *Acta Opt. Sin.*, **4**, 673 (1984)

15. Y. Zhang, L. Yin. Q. Hu, G. Zhang, C. Jin and F. Lin, *Chinese Phys. Lett.*, **2**(9), (1985)

16. T. Fujimoto, Y. Uetani, Y. Sato, C. Goto and K. Fukuda, *Opt. Commun.*, **47**(2), 111 (1983)

17. Y. Uetani and T. Fujimoto, *Opt. Commun.*, **49**, 258 (1984)

18. D. Kumar, P.L. Clancy and S. P. McGlynn, *J. Chem. Phys.*, **90**,4008(1989)

19. D. Kumar and S. P. McGlynn, *J. Chem. Phys.*, **93**, 3899 (1990)

20. D. Kumar and S. P. McGlynn, *Chem. Phys. Lett.*, **176**, 536 (1991)

21. D. Kumar, R.R. Zinn and S. P. McGlynn, *J. Chem. Phys.*, **101**(3), 1959(1994)

22. D. Kumar, R.R. Zinn, and S. P. McGlynn, *J. Phys. Chem.*, **99**, 7530 (1995)

23. F. Paschen, *Ann. der Phys.*, **60**(4), 405(1919)

24. W. L. Wiese, M. W. Smith, and B. M. Glennon, *Atomic Transition Probabilities*, vol. 1, U. S. Government Printing Office, Washington, D.C., 1966

CHAPTER 3: OPTOGALVANISM IN A NEON PLASMA*

3.1 Introduction

The signal of an optogalvanic effect (OGE) in a capacitively-coupled, low-temperature RF plasma consists of two components: one component attributable to a change in the rate of ionization (IRC) in the plasma,[2,3] the other to a physical movement of charged species by an acoustic disturbance.[2,4] The acoustic disturbance initiates in photon absorption followed by energy degradation into thermal modes, and is known as the photoacoustic (PA) component.[4,5] These two components can be separated and measured,[2] and they carry quite different information. For example, in an RF discharge in iodine vapor, one can arrange the conditions of plasma and laser excitations so that the IRC signal is induced only by atomic excitations and the PA signal only by molecular excitations.[6] One merely takes advantage of the greater efficiency of molecules for radiationless dumping of electronic excitation energy.

Ionization alters the charge carrier concentrations and, hence, the plasma impedance. Since the plasma is an integral part of a resonant circuit, this impedance alteration causes a change of the resonant frequency (i.e., a frequency modulation), a change which, on the μs time scale of these experiments, is instantaneous.[7] Not so, however, the photoacoustic effect. The acoustic disturbance must first travel to a region

* Reproduced by permission from the *International Journal of Quantum Chemistry.* Copyright 1998.

Minor changes have been made to the journal article in order to satisfy the format requirements of the Graduate School.

of large carrier concentrations, at which time the movement of these carriers by the decompression/compression pulse produces a detectable change of impedance. Thus, the acoustic effect is delayed by the time of travel from the site of laser excitation to the region of high carrier densities.[8] And, in addition, since carrier densities are unaffected by the acoustic wave, only a change of resonance amplitude (i.e., an amplitude modulation) occurs. Thus, the PA signal is delayed whereas the IRC signal is instantaneous and the two signals, PA and IRC, can be discriminated by AM/FM detectors.[2,5]

These interpretations, while generally quite successful, ran into some difficulty in the case of atomic discharges (e.g., Ne). We now believe that these difficulties can be resolved by noting the very different spatial characteristics of the energy dumping associated with prompt and trapped atomic deexcitations:

Both the energy dumping and ionization events associated with prompt deexcitation occur at the site of laser excitation, the IRC response being immediate and the PA response being delayed by the transit time of the acoustic disturbance to regions of high carrier concentrations. Thus, these two events, the IRC and PA signal registrations, will not be temporally coincident and, in addition, the PA signal will be considerably broadened by diffusion during transit. The two signals will also have identical signs (i.e., both positive or both negative).

The situation with trapped deexcitations will be much different. Trapped excitations spread throughout a volume at speeds approaching that of light. Thus, in the cases investigated here, in which trapping increases the decay time of certain excited states from nanoseconds to microseconds,[9] a simple random walk of photons can fill a

volume of $\sim 10^2$ m^3 with uniformly distributed trapped excitations. Consequently, the locus of excitation is no longer that at which either the ionization or the acoustic perturbation occurs. These events occur now throughout the entire volume and, since no travel is required of the acoustic wave, this having been taken care of by photon random walk, the ionization and acoustic signals should now be temporally coincident. They should also possess very similar shapes and identical signs. Consequently a very simple means of distinguishing prompt and trapped deexcitations might well be at hand.

This model is illustrated in Fig. 3-1 for a situation in which only one trapped state is operative. Prompt deexcitation produces an IRC signal, IRC1, which precedes the corresponding PA signal, PA2, by a time $\Delta t = \Delta d/\upsilon$, where υ is the velocity of sound and Δd is the distance the acoustic wave has to travel in order to encounter high carrier densities. Given the tube geometries used in this work, Δt may be as large as 0.1 ms. Consequently, the diffusion of the acoustic pulse may be extensive and it should be much broader than its IRC counterpart. Not so, however, the IRC and PA signals, IRC2 and PA1, that are produced by a trapped deexcitation: both of these should be temporally coincident and of similar shape.

The purpose of this work is to verify the proposed model and the assertions based on it.

To that end, we have used an RF discharge in neon gas at 5 Torr pressure as the plasma. The states of Ne (see Fig. 3-2) responsible for plasma maintenance are the $1s_3$ and $1s_5$ metastable states arising from the $...2p^5 3s$ configuration. The other two states arising from this same configuration, the $1s_2$ and $1s_4$ states, are trapped. As a result, their intrinsic lifetimes increase by $\sim 10^3$ and, at the pressures used in this work, they

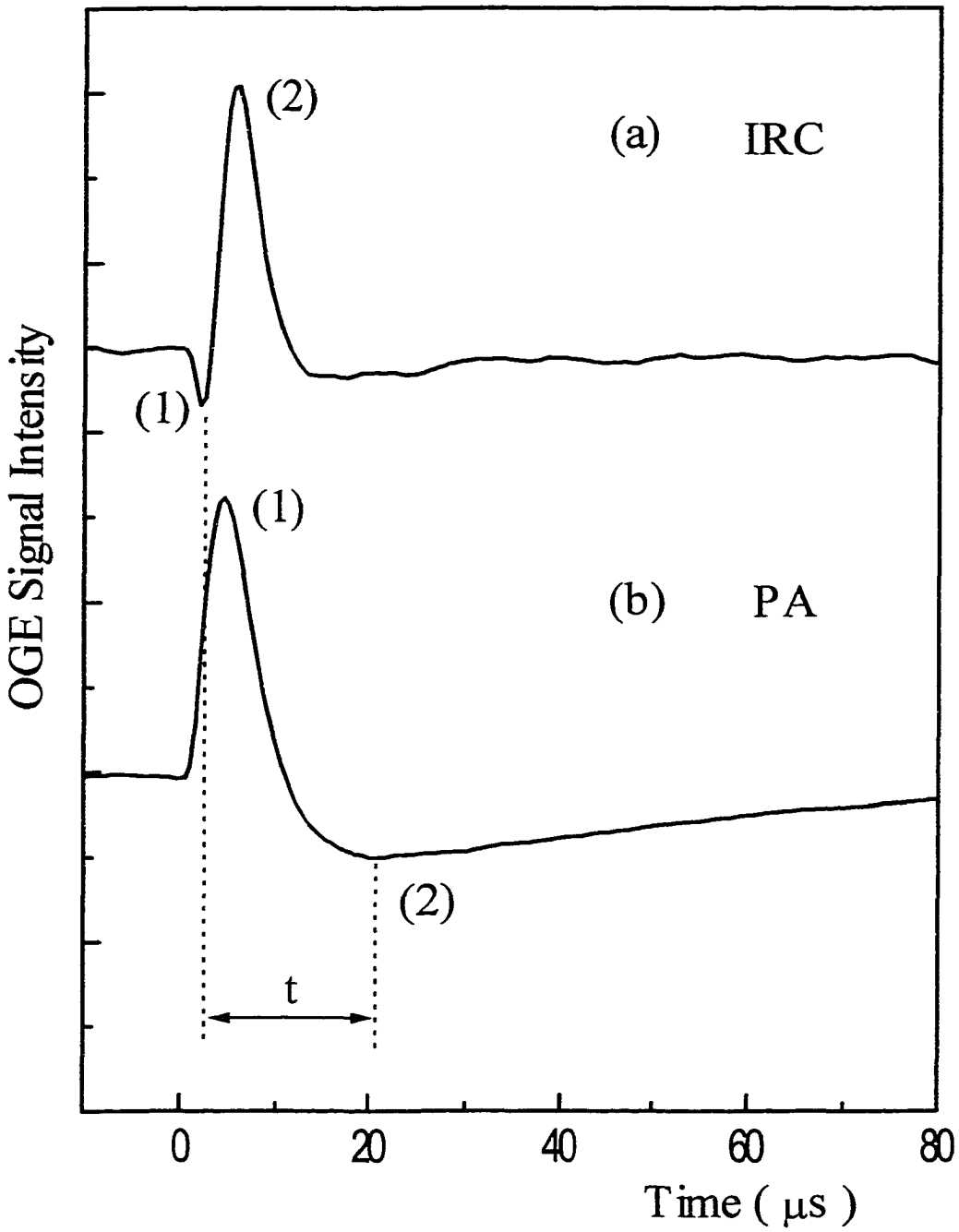

Fig. 3-1 IRC and PA signals illustrative of the model advanced in the text. Peaks are labelled sequentially and are referred to as IRC2, PA1, etc. IRC2 and PA1 are produced by the deexcitation of radiatively trapped states; IRC1 and PA2 are generated by population changes of non-radiatively-trapped states. The time Δt is that required for movement of an acoustic pulse from the site of excitation to a plasma region of high ion densities.

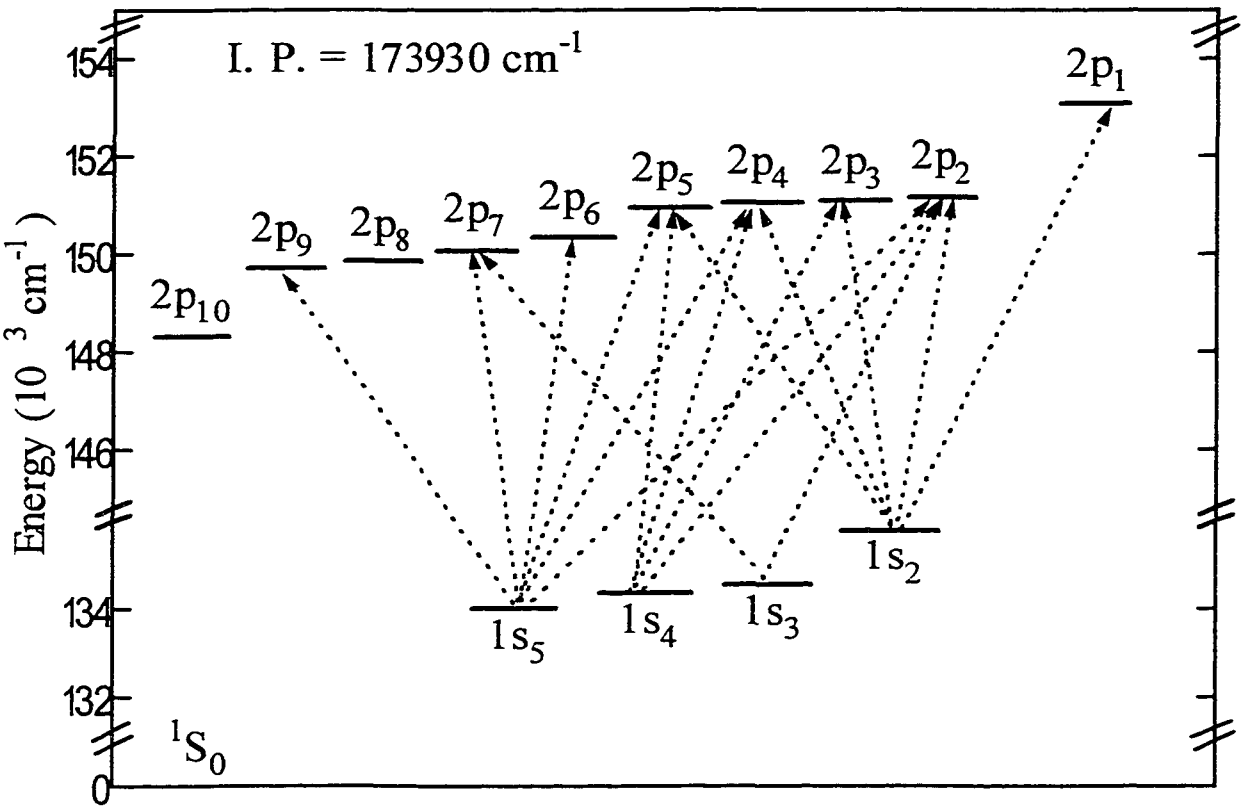

Fig. 3-2 Energies of the $1s_j$ and $2p_k$ states of neon. Energy states are labelled in the Paschen notation[1]. The arrows represent the excitations discussed in this work. The ground state is denoted $^1S_0$.

exhibit decay lifetimes of ~2 μs and ~20 μs, respectively.[9] The presence of two trapped radiative states does not impose any interpretative difficulty because limiting experiments can be so arranged that one of these, the $1s_2$ state, dominates. All laser excitations discussed here take place from some one of the four $1s$ states to some one of the 10 $2p$ states of Ne. The signs, whether positive or negative, of the IRC and PA signals can be understood in terms of population changes of the various $1s_j$ states produced by either their direct excitation or a re-populating of them by $2p_k \rightarrow 1s_j$ decay branching. This topic is discussed fully elsewhere[10] and will not be broached any further here.

3.2 Experiment

Fig. 3-3 is a schematic of the experiment. A commercial hollow cathode lamp with neon filler gas is used as the discharge tube. The Ne sample is housed at ~5 Torr in this lamp, which is ~10 cm in length and ~2 cm in diameter. The volume of the lamp is only 30 cm^3, and it can be filled entirely with trapped excitations at times much less than 1μs. Two electrodes, ~3 cm apart, are wound around the exterior of the lamp. RF power of ~0.5 W and ~30 MHz is applied at high voltage and generates a stable, low-noise, capacitively coupled plasma. A resonantly-tuned pick-up coil is also wrapped around the exterior of the cell and is situated between the two electrodes. A pulsed laser, whose wavelength is tuned to a desired Ne transition, excites the plasma transversely at a point below the lower electrode. When the laser excites a Ne transition, the change of RF power that it causes will be detected by the pick-up coil and an OGE signal will be generated. By moving the locus of laser excitation, one can study the influence of the distance that must be travelled by the acoustic pulse on the signal

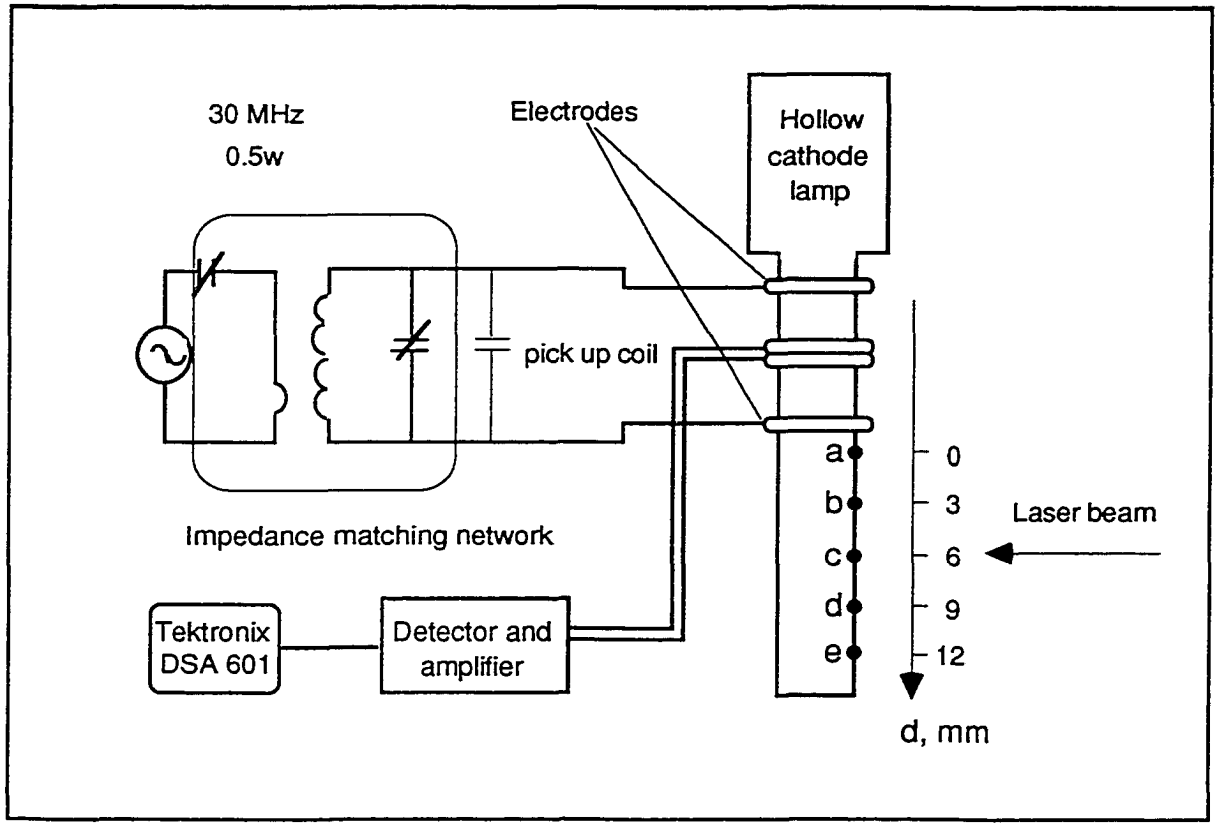

Fig. 3-3 Schematic of the experimental arrangement. A hollow cathode lamp is used as the plasma tube. The two electrodes are ~30 mm apart. The laser excites the plasma at five sites, each separated by 3 mm. The first site, site a, lies 1-2 mm below the lower electrode.

profiles and, thereby, measure sound velocity in the plasma. For each excitation, five data sets were obtained for both the IRC and PA signals, the laser being focused on positions d = 0, 3mm, 6mm, 9mm and 12mm.

Fifteen different neon excitations were investigated: $1s_5 \rightarrow 2p_{2,4,5,6,7,9}$, $1s_3 \rightarrow 2p_{2,7}$, $1s_2 \rightarrow 2p_{3,4,5}$ and $1s_4 \rightarrow 2p_{2,3,4,5}$. The wavelengths of those excitations ranged from 585 to 671 nm, and were covered using Rhodamine 590 and Sulforhodamine 640 dyes. The laser was a tuneable dye laser (Chromatix CMX-4) with ~1 μs pulse width and ~0.1 cm^{-1} resolution. Since the laser width is much larger than the RF period (~33 ns), it samples ~30 RF oscillations per laser pulse. Consequently, the laser triggering need not to be synchronous with the RF cycle and a time-averaged signal is generated.

The tuning of the resonant system and the separation of the IRC and PA signals are described in detail in a previous work.[10]

3.3 Results and Discussion

All IRC and PA optogalvanic signal profiles consist of only two peaks within the time scale that we investigated. For the sake of convenience, these are labeled IRC1, IRC2, PA1 and PA2.

A set of representative IRC signal profiles are shown in Fig. 3-4(a). They consist of a sharp, weak IRC1 peak and a sharp, strong IRC2 peak of opposite polarity. No shift of either of these peaks is observed when different $1s_j \rightarrow 2p_k$ excitations are excited (See Fig. 3-4(a)) or when the locus of laser excitation is varied (See Fig. 3-4(b)). The decay time for the IRC2 peak is ~3 μs in all cases, indicating that this peak is attributable to $1s_2 \rightarrow {}^1S_0$ trapping. No peak attributable to $1s_4 \rightarrow {}^1S_0$ trapping is observed. The IRC1

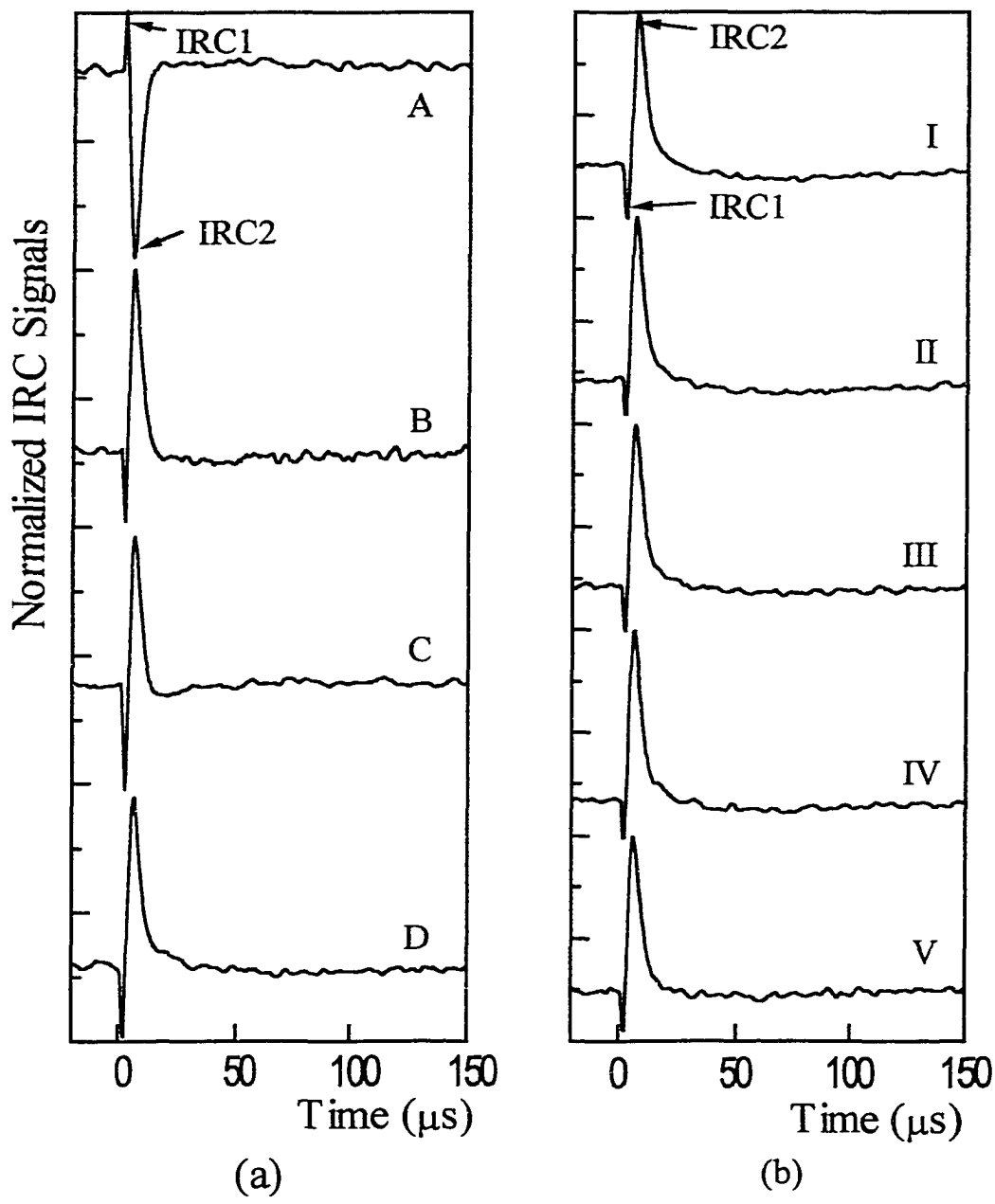

Fig. 3-4 IRC signals. The signals in (a) are for different $1s_j \rightarrow 2p_k$ excitations: A: $1s_2 \rightarrow 2p_2$; B: $1s_3 \rightarrow 2p_2$; C: $1s_4 \rightarrow 2p_2$; and D: $1s_5 \rightarrow 2p_2$. The signals in (b) refer solely to a $1s_5 \rightarrow 2p_5$ transition at the following plasma tube loci: I: d=0; II: d=3mm; III: d=6mm; IV: d=9mm; and V: d=12mm.

peak is attributable to population changes of the $1s_3$ and $1s_5$ metastable states that maintain the plasma.

The PA profiles are more complicated. However, all of them consist of two peaks: PA1 being temporally coincident with IRC2 and PA2 being much delayed, ~20 - 50 μs, relative to IRC1. The PA responses to different $1s_j \rightarrow 2p_k$ excitations are shown in Fig. 3-5(a). The PA1 peak exhibits decay time constants of 2-5 μs, indicative of $1s_2 \rightarrow {}^1S_0$ origination. The shape and signs of the PA1 peaks are identical to those of the IRC2 peak. When the site of laser excitation is altered, no obvious movement of the PA1 peak could be detected (See Fig. 3-5 (b)). All these observations cohere with a model of PA1 and IRC2 signals that originate in trapped $1s_2$ deexcitations.

The complexity of the PA profiles is totally vested in the behavior of the PA2 peaks. This complexity is a consequence of the fact that the ~20 μs decay time of the trapped $1s_4$ state causes the acoustic effects originating in $1s_4 \rightarrow {}^1S_0$ energy dumping to overlap temporally with those produced by the movement of the acoustic pulse associated with prompt energy dumping from the locus of excitation to regions of high carrier densities. Consequently, we will divide discussion of the behavior of the PA2 peaks into four categories:

3.3.1 The $1s_5 \rightarrow 2p_k$ Excitations

The $1s_5$ state is the most populous $1s$ state and excitation of it produces a very large negative change of ion densities. That is, it produces both an intense negative IRC1 peak, and launches an acoustic disturbance that is large enough to swamp any prompt acoustic signals associated with $1s_4$ trapping. In other words, the $1s_5 \rightarrow 2p_k$

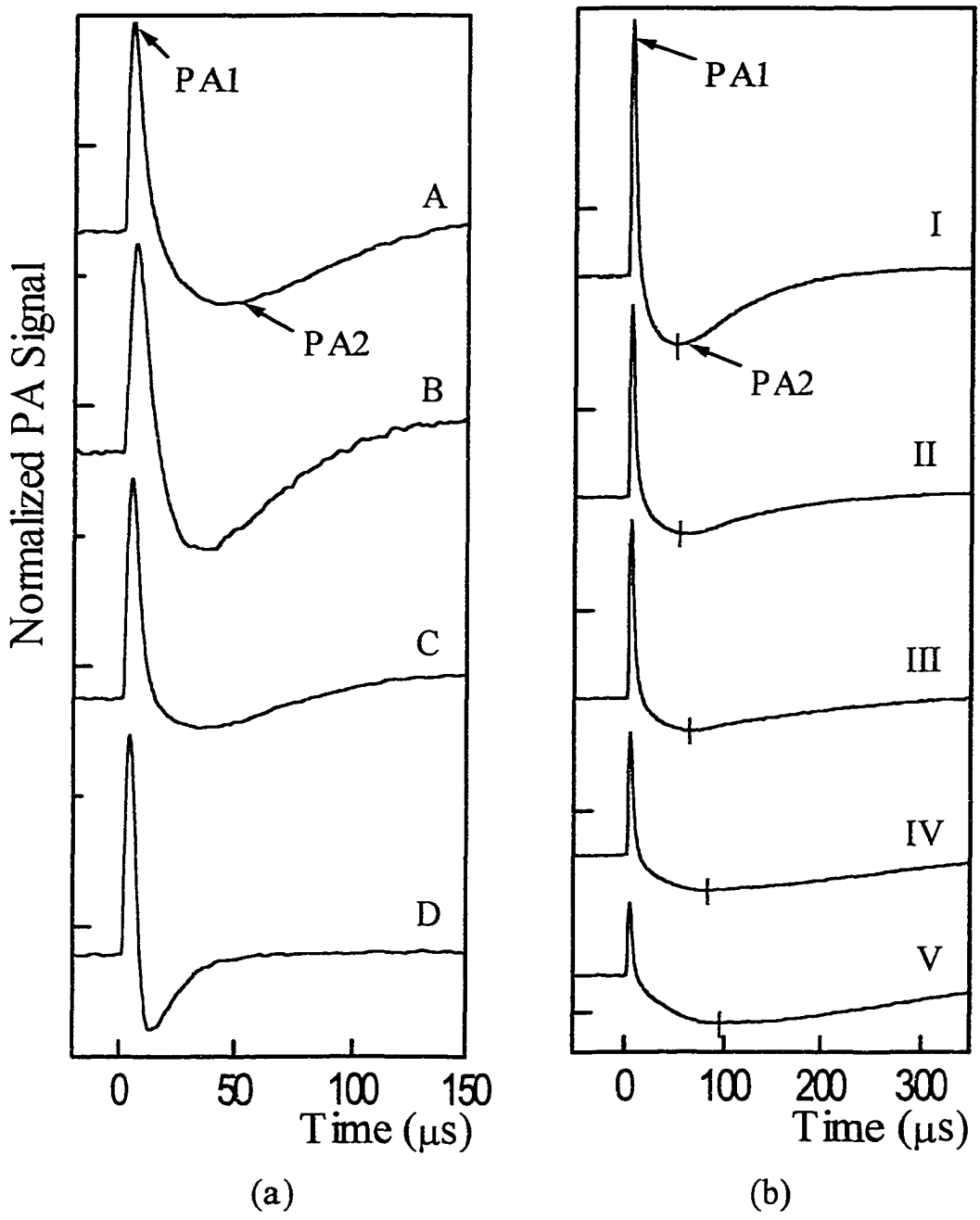

Fig. 3-5 PA signals. The signals in (a) are for different $1s_j \rightarrow 2p_k$ excitations: A: $1s_2 \rightarrow 2p_3$ (The actual signal is the inverse of that shown here); B: $1s_4 \rightarrow 2p_2$; C: $1s_3 \rightarrow 2p_7$; and D: $1s_5 \rightarrow 2p_5$. All of these signals have been normalized so that the PA1 peaks are of the same intensity. The signals in (b) refer to the $1s_5 \rightarrow 2p_5$ transitions excited at the following plasma tube loci: I: d=0; II:d=3mm; III: d=6mm; IV: d=9mm; and V: d=12mm. Approximate minima are indicated by a short vertical slash. The movement of PA2 as d increases is evident.

excitation is an extreme case in which the movement of the acoustic pulse, being largely devoid of any contamination by $1s_4$ trapping, should be most readily detected.

A typical behavior for $1s_5$ excitation is shown in Fig. 3-5 (b). The location of the PA2 peak is a clear function of the site of the laser excitation, as shown in Fig. 3-6. Since the correlation coefficient of the least square linear regression (R = 0.811) is greater than the correlation coefficient for a 0.01 level of significance ($R_{0.01}$ = 0.372), one can be 99% certain that the linear regression is reliable and a linear relation, $d = d_0 + \upsilon t$, exists. It also yields $\upsilon = 320\ ms^{-1}$, which is consonant with the velocity of sound in neon at 5 Torr and 60^0C. Therefore, the PA signal does indeed travel at the speed of sound. The value of d_0 is found to be 1.6 cm, suggesting that the primary high carrier densities occur in the vicinity of the upper electrode. The standard error of estimation (SD) is 0.0016. If one draws two lines $d = d_0 + \upsilon t - SD$ and $d = d_0 + \upsilon t + SD$, as shown by the two dotted lines in Fig. 4-7, the probability that a given experimental datum falls in the region between these two lines is 68.3%.

3.3.2 The $1s_4 \rightarrow 2p_k$ Excitations

These excitations produce the maximal change of $1s_4$ state densities and, hence, a large change of radiatively trapped $1s_4 \rightarrow {}^1S_0$ events. The acoustic signal produced by non-radiative $1s_4 \rightarrow {}^1S_0$ dumping is expected to dominate the long-time region and totally obscure that associated with pulse movement. In other words, this is another extreme case, one in which no movement of the PA2 peak should be detectable .

A typical $1s_4 \rightarrow 2p_k$ signal is shown in Fig. 3-5 (a) (profile B). The location of the PA2 peak is not a function of d and its decay time constant is ~20μs, all of which are consistent with expectation.

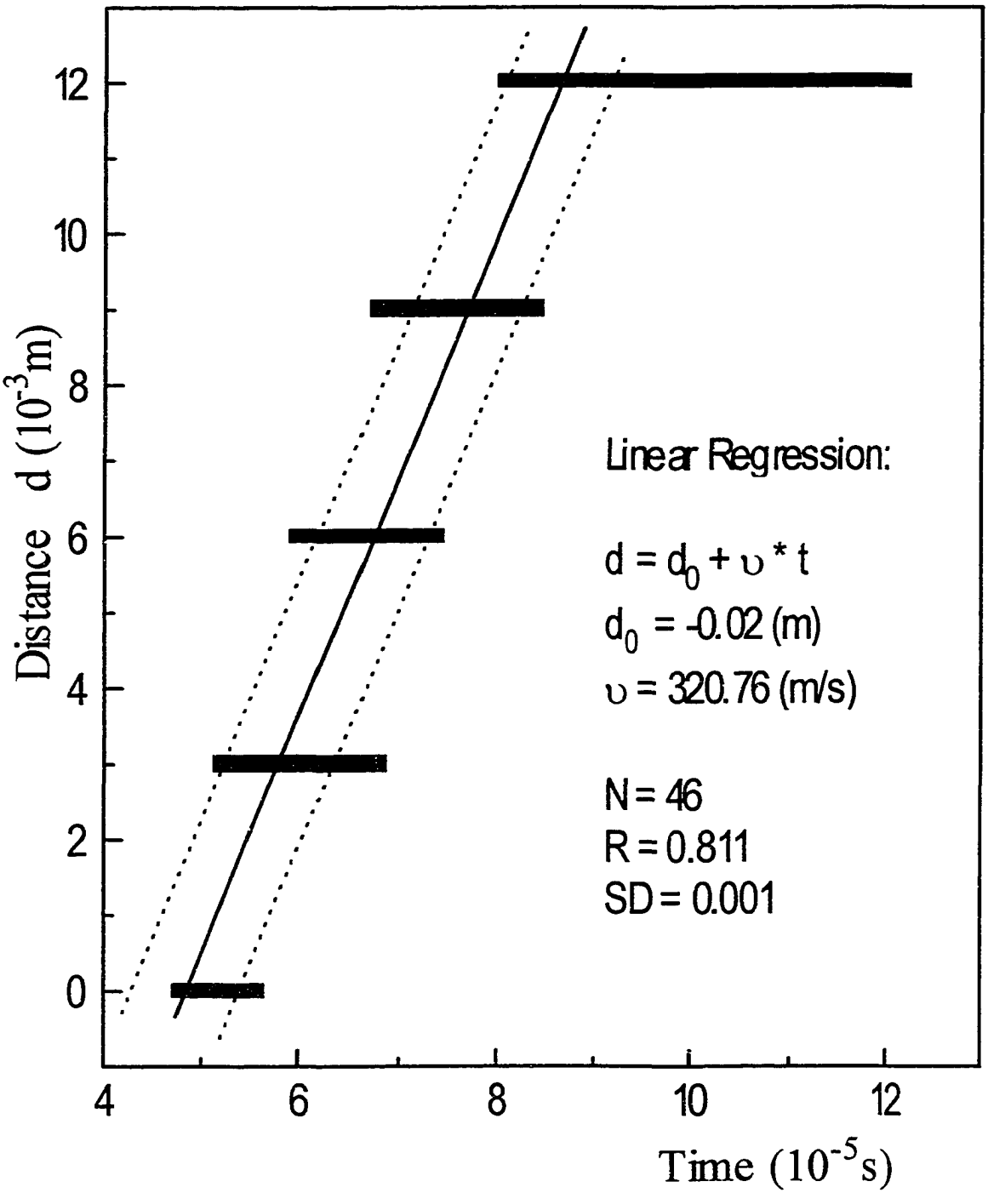

Fig. 3-6 Distance versus time for the PA2 band of the $1s_5 \rightarrow 2p_5$ neon excitation. The distance is determined by the site of the laser excitation. The time is that at the minimum of the PA2 peak. The error bar is the width of the band at a height 0.01V above the minimum. The solid line represents $d = d_0 + \upsilon t$, and the dotted lines represent $d = d_0 + \upsilon t + SD$ and $d = d_0 + \upsilon t - SD$. R is the correlation coefficient. N is the number of samples. SD is the standard error of estimation.

3.3.3 The $1s_2 \rightarrow 2p_k$ Excitations

These excitations produce a maximal change of $1s_2$ populations, which suggests a strong PA1 peak. The $1s_4$ and the metastable $1s_{3,5}$ populations are altered only by the decay branching of the $2p_k$ states. Thus, one expects a mixed situation in which the long-time region (i.e., the PA2 peak) is a convolution of the signal from $1s_4 \rightarrow {}^1S_0$ decay and a delayed signal of comparable intensity associated with the movement of an acoustic wave from the site of laser excitation. That is, the $1s_2 \rightarrow 2p_k$ excitations do not represent an extreme situation.

All observations agree with these deduction: the PA2 peak occurs at ~40 μs, which is longer than that for the $1s_4 \rightarrow 2p_k$ excitations; the decay times are greater than 20 μs; and the movement of the site of laser excitation produces effects on PA2 that are more shape alterations than time variations.

3.3.4 The $1s_3 \rightarrow 2p_k$ Excitations

The $1s_3$ populations are not as high as those of $1s_5$. Consequently, while excitations from the $1s_3$ state will produce a change of the metastable state populations, these may not be large enough to submerge the acoustic disturbances arising from $1s_4 \rightarrow {}^1S_0$ trapped radiation. That is, PA2 may represent a mixed situation (i.e., a convolution of two disturbances) rather than an extreme situation in which one disturbance dominates.

The experimental observations are much like those for the $1s_2 \rightarrow 2p_k$ excitations of item 3, above.

3.4 Modelling

The three critical ingredients of the OGE signal are ionizations, photoacoustic effects and collisional energy transfers.[7] The photoacoustic effect has been discussed in the Introduction.

There are three important ionization processes: direct photoionization, collision-assisted photoionization and Penning ionization. Direct photoionization and collision-assisted photoionization are fast processes whose rise time is coincident with that of the laser pulse, ~1 μs. Consequently, they will generate an immediate IRC response. Penning ionization dominates at low RF power and moderate pressure,[9,11] which is the case in this work. Penning ionization is

$$M^* + M \rightarrow M + M^+ + e^-$$

where M* is a metastable state (i.e., $1s_3$ or $1s_5$) and M is a ground state (i.e., $^1S_0$). Penning ionization will also be immediate. However recovery of the M* population will be a slow, collisionally dominated re-equilibration process that, in the present situation, may extend into the 0.1ms range. Depletion of the metastable states by direct, sub-ionization laser excitation of them will always produce a decrease of ionization rate.[9,11]

3.4.1 The IRC Signal

A typical IRC signal is modelled in Fig. 3-7. The rise time of IRC1, curve M, is determined by the rise time of the laser pulse and the response characteristics of the electronic circuit; its decay time (i.e., its return to equilibrium) is controlled by collisional events. The rise and decay of IRC2 is determined by the lifetime of the trapped $1s_2$ states. None of these kinetic occurrences is a function of either the particular $1s_j \rightarrow 2p_k$ excitations or the point of incidence of laser excitation. Therefore, neither excitation

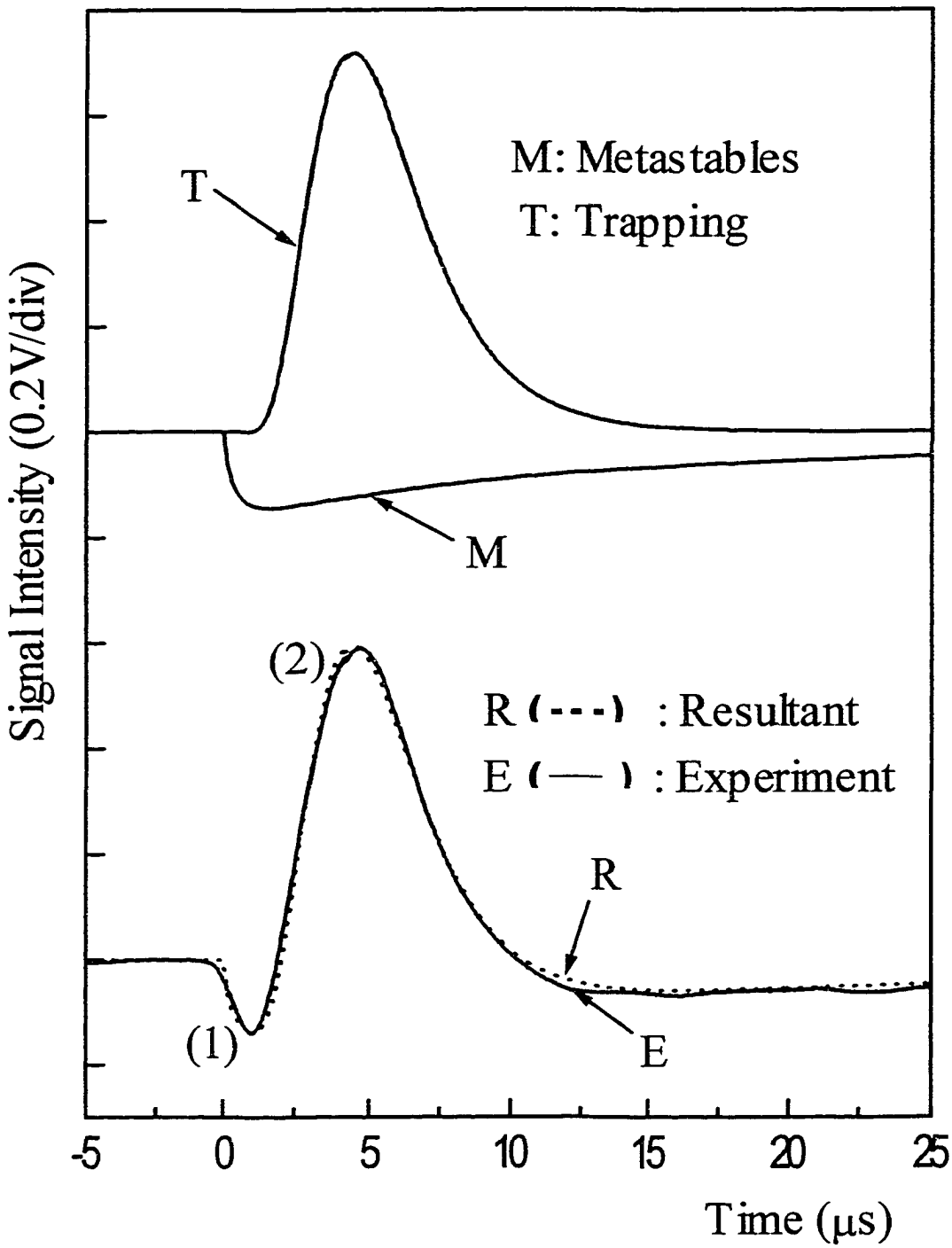

Fig. 3-7 Modelling of IRC signal formation (excitation $1s_4 \rightarrow 2p_3$). Log-normal functions are used to model the M and T components because they provide appropriate representations of the fast-rising, slow-decaying characteristics of OGE signals.

from different $1s_j$ states nor movement of the locus of laser excitation should alter either the IRC1 or IRC2 peaks. This assertion is verified by the sampling of experimental results shown in Fig. 3-4.

The $1s_4 \rightarrow {}^1S_0$ radiation trapping, in contrast to the $1s_2 \rightarrow {}^1S_0$ excitation trapping, is not found to be important in IRC signal generation, presumably because this trapping, because of its longer lifetime, is largely terminated by non-radiative degradation. For that very reason, however, $1s_4 \rightarrow {}^1S_0$ radiation trapping should be important in the generation of the PA signal.

3.4.2 The PA Signal

PA signal formation by $1s_4 \rightarrow 2p_2$ and $1s_5 \rightarrow 2p_5$ excitations is illustrated in Fig.3-8. As in the case of the IRC signal simulation, only two components, radiation trapping and metastable re-equilibration are used. The polarity and shape of the PA1 peak are determined by increases or decreases of populations. Regardless of the particular $1s_j$ state that is excited, a change of $1s_2$ populations will always occur, and a fast, sharp peak (T2) will be generated by the rapid diffusion of $1s_2 \rightarrow {}^1S_0$ trapped photons throughout the plasma. Thus, like its IRC counterpart (IRC2), the position of PA1 is independent of the particular $1s_j$ state that is excited and of the site of excitation.

The position and shape of PA2 is controlled by population changes in the trapped $1s_4$ and metastable $1s_{3,5}$ states. If the $1s_4$ population change is dominant, the shape of PA2 will be controlled by non-radiative $1s_4 \rightarrow {}^1S_0$ decay and, therefore, will peak at ~20 μs. If the metastable population changes dominate, the shape of PA2 will be controlled by recovery of the metastable populations and, particularly, by the travel requirements imposed on the shock wave; peaking, therefore, will depend on the

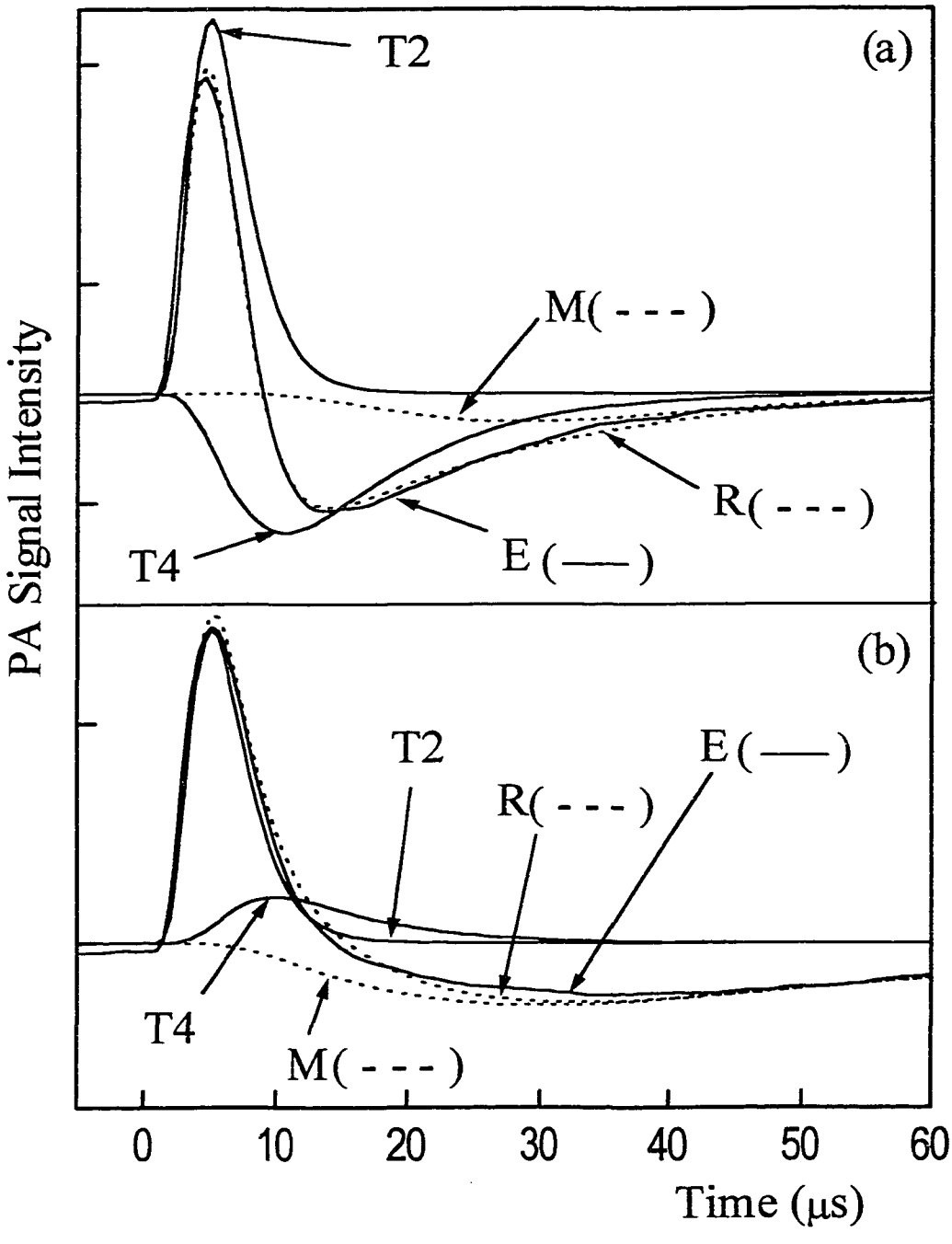

Fig. 3-8 Modelling of PA signal formation. The excitation $1s_4 \rightarrow 2p_2$ is shown in (a) and the excitation $1s_5 \rightarrow 2p_5$ is shown in (b). The symbols denote the following:

T2: Signal component attributed to $1s_2$ state trapping;
T4: Signal component attributed to $1s_4$ state trapping;
M: Signal component attributed to metastable state perturbation;
E: Experimental profile;
R: Convolution of T2, T4 and M resolvents.

excitation site and may occur anywhere from 40-100 μs. If the $1s_4$ and metastable population change are comparable, one will have a mixed situation for which the peak will occur at $t \leq 40$ μs and will exhibit no distinct dependence on time.

(a). The $1s_4 \rightarrow 2p_2$ PA signal: $1s_4 \rightarrow 2p_k$ excitations lead to an increase of $1s_2$ populations by decay of the $2p_k$ state, and to a sharp positive PA1 peak of decay time constant 2-5 μs (curve T2 of Fig. 3-8(a)). However, whereas $1s_2$ gains population, the $1s_4$ state suffers a loss. Recovery of the $1s_4$ populations will occur in ~20 μs. The signal component generated by depletion of $1s_4$ radiation trapping is modelled as the log-normal resolvent, curve T4 of Fig. 3-8(a). Curve M of Fig. 3-8(a) is the log-normal resolvent of the signal component generated by population re-equilibration of the metastable states. The resultant of these three components, curve R of Fig. 3-8(a), is an excellent match to the experimental profile, curve E of Fig. 3-8(a). Since the $1s_4 \rightarrow {}^1S_0$ trapping dominates the population re-equilibration of metastable states, which is relatively small in this case, PA2 of the $1s_4 \rightarrow 2p_2$ excitation will occur at shorter times and will be sharper than those of all other excitations (See Fig. 3-5 (a)).

(b). The $1s_5 \rightarrow 2p_5$ PA signal: The population re-equilibration of the metastable states plays the more important role in this case. Upon $1s_5 \rightarrow 2p_5$ excitation, decay of the $2p_5$ state occurs back to the $1s_2$ and $1s_4$ states, causing an increase of $1s_2$ and $1s_4$ trapped photons. The resulting signal components are represented by positive log-normal resolvents T2 and T4 in Fig. 3-8(b). The very significant metastable depletion generates a broad negative peak, represented by the log-normal resolvent M, which is delayed by acoustic travel requirements. The resultant of these three components (curve R), which

is an excellent match to the experimental profile (curve E), exhibits a broad PA2 peak that is delayed by ~50 μs.

(c). All other PA2 peaks, regardless of the $1s_j \rightarrow 2p_k$ excitation that produced them, can be deconvoluted in a similar way.

3.4.3 Predictor of PA Signal Profiles

The OGE PA profile is complex, and any simulation of it requires consideration of all the population changes wrought by the diversity of plasma processes alluded to throughout this paper. However, a simplified, qualitative approach, one based only on the initial depopulation caused by the laser excitation and the subsequent branching decay of the $2p_k$ excited populations seems to work quite well. While this approach will not be discussed here at any length, we will exemplify it in just one instance.[14]

In the $1s_5 \rightarrow 2p_2$ excitation, the $1s_5$ state is depleted by laser excitation. According to the $2p_2$ branching ratio,[12] however, there is a 48% return to the $1s_{3,5}$ metastable states, a 42% return to $1s_2$ and a 10% return to $1s_4$. Since the initial $1s_2$ populations are much smaller than $1s_4$, this redistribution produces a significant change of $1s_2$ and a rather small change of $1s_4$ populations. Therefore, $1s_2$ trapping will dominate $1s_4$ trapping, and a strong, fast, positive signal component (PA1) with decay time constant of 2-4 μs should be observed. The initial severe depletion of the $1s_5$ state and its re-equilibration by collision will generate a broad, delayed signal component (PA2. These simple deductions are fully in accord with experiment.

3.5 Conclusion

The OGE effect in a neon plasma has been interpreted on the basis of a redistribution of $1s_j$ populations caused by laser excitation. Radiatively trapped $1s_2$ and

$1s_4$ states produce an acoustic signal that differs from these produced by all other (i.e., non-radiatively trapped) states: a movement of the acoustic wave from the site of laser excitation to regions of high ion density is not required for a radiatively trapped state because such states permeate the entire plasma volume at an effective speed approaching that of light.

The $1s_2 \rightarrow {}^1S_0$ deexcitation is acoustically more effective in generating the PA1 peak than the $1s_4 \rightarrow {}^1S_0$ deexcitation. The longer lifetime of the latter, ~20 μs, relative to the former, ~2 μs, presumably ensures a higher degree of non-radiative deexcitations effect on the PA2 peak.

The optogalvanic ionization and acoustic components have been modelled. A demonstration is given for the IRC signal produced by all $1s_j \rightarrow 2p_k$ excitations and for the PA signals produced by the $1s_4 \rightarrow 2p_2$ and $1s_5 \rightarrow 2p_5$ excitations.

A qualitative model based on the branching decay of $2p_k$ to $1s_j$ states and on the initial depopulation of the $1s_j$ states has been broached but not discussed. It provides a correct specification of the signs of all signals. When the different time characteristics of the metastable ($1s_{3,5}$) and trapped ($1s_{2,4}$) states are added to this qualitative model, a correct prediction of the time course of the acoustic signal also results. This model will be discussed elsewhere.[13]

3.6 References

1. F. Paschen, *Ann. Phys.*, **60**(4), 405 (1919)
2. D. Kumar, R.R. Zinn and S. P. McGlynn, *J. Chem. Phys.*, **101**(3), 1959(1994)
3. A. E. Bulyshev, N. V. Denisova, and N. G. Preobrazhenskii, *Opt. Spectrosc.*, **64** (5), 590 (1988)

4. D. Kumar and S. P. McGlynn, *Chem. Phys. Lett.*, **176** (6), 536 (1991)

5. D. Kumar and S. P. McGlynn, *J. Chem. Phys.*, **93** (6), 3899 (1990)

6. D. Kumar, P.L. Clancy and S. P. McGlynn, *J. Chem. Phys.*, **90** (8),4008 (1989)

7. D. Kumar, R. R. Zinn, T. D. Armstrong, and S. P. McGlynn, *J. Phys. Chem.*, **99** (19), 7530 (1995)

8. In the case of an iodine discharge, these regions consist of ion sheaths in the vicinity of the electrodes. In the case of a neon discharge, these regions seem to be more diffuse and centered in the discharge.

9. Y. Uetani and T. Fujimoto, *Opt. Commun.*, **49** (4), 258 (1984)

10. Xuan Yao, D. Kumar and S. P. McGlynn, *J. App. Phys.*, **85** (6), (1999)

11. L. W. Schott, IEEE Transactions on Plasma Science, **19** (4), 612 (1991)

12. A. Ben-Amar, G. Erez and R. Shuker, *J. App. Phys.*, **54** (7), 3688 (1983)

13. X. Yao and S. P. McGlynn, unpublished material

CHAPTER 4: LASER OPTOGALVANIC ANALYSIS IN A RADIOFREQUENCY PLASMA: DETECTION OF IODINE ATOMS AND MOLECULES *

4.1 Introduction

Plasmas created by electrical discharges in gases have long been used in sensitive analytical instrumentation and pollution monitoring and control devices. The most significant series of events that occurred during the past two decades in the field of analytical atomic spectroscopy was the emergence of various atmospheric-pressure, flame-like plasma dissociation and excitation media, among them inductively-coupled plasma (ICP), capacitively-coupled plasma (CCP), direct-current plasma (DCP) and microwave-induced plasma (MIP). Of these, ICP has been most widely used (e.g., ICP-AES, ICP-MS) because of its remarkable selectivity and sensitivity. However, like any other analytical technique, ICP spectrometry has its limitations (e.g., sample introduction difficulties, interferences, noise, etc).

With most pneumatic nebulizers, only 1-5% of the sample solution can be injected into the discharge and, if solid sampling techniques are used, the reproducibility of the measurements deteriorates.[1] Stray light, matrix effects and spectral overlap are three groups of interferences in ICP-AES.[2] These interferences pose serious problems, even though much work has been done to minimize them.[3-9] The conventional ICP-AES

* Reproduced by permission from the *Microchemical Journal*. Copyright ©1999, *Academic Press*.

Minor changes have been made to the journal article in order to satisfy the format requirements of the Graduate School.

techniques also suffer background noise arising from the nebulizer and sample introduction.[10] Although the SICP (sealed inductively-coupled plasma) technique minimizes the low-frequency noise, the noise due to statistical variations of the RF (radio frequency) power input and to heat release to the environment still exists.

Radio-frequency laser optogalvanic spectroscopy (RFLOGS) is a new kind of spectrometry. It continues the use of plasma (ICP or CCP) as the source of excitation, atomization and ionization, as shown in Fig. 4-1. However, the RFLOGS technique has certain distinct advantages:

(1) In the RFLOGS system, the plasma can be either inductively or capacitively coupled to the system. The plasma can operate at lower pressures; it can be in either a continuous flow state or static (i.e., sealed tube) state; and the required sample sizes can be very small. Therefore, it demonstrates high flexibility and analytical merit. For example, one can use sealed, capacitively-coupled plasma (SCCP) to analyze toxic and reactive gases. Since no flow exists in this plasma, the contribution of flow variations to flicker noise is eliminated.

(2) In ICP-AES, ICP is used to excite atoms of the sample, and a photomultiplier is used to detect the resulting emission lines. Because photomultipliers exhibit dark current, even in the absence of illumination, there is always a background noise. The signal from the photomultiplier tube is also affected by shot noise and Johnson noise.[11] In the RFLOGS system, the LOGE signal consists of the change of electrical impedance of the plasma produced by resonant absorption of laser radiation by a plasma moiety. [12-15] This change is detected by a pick-up coil and treated by digital signal analysis. An external detector is not required in this system because the plasma, being an integral part

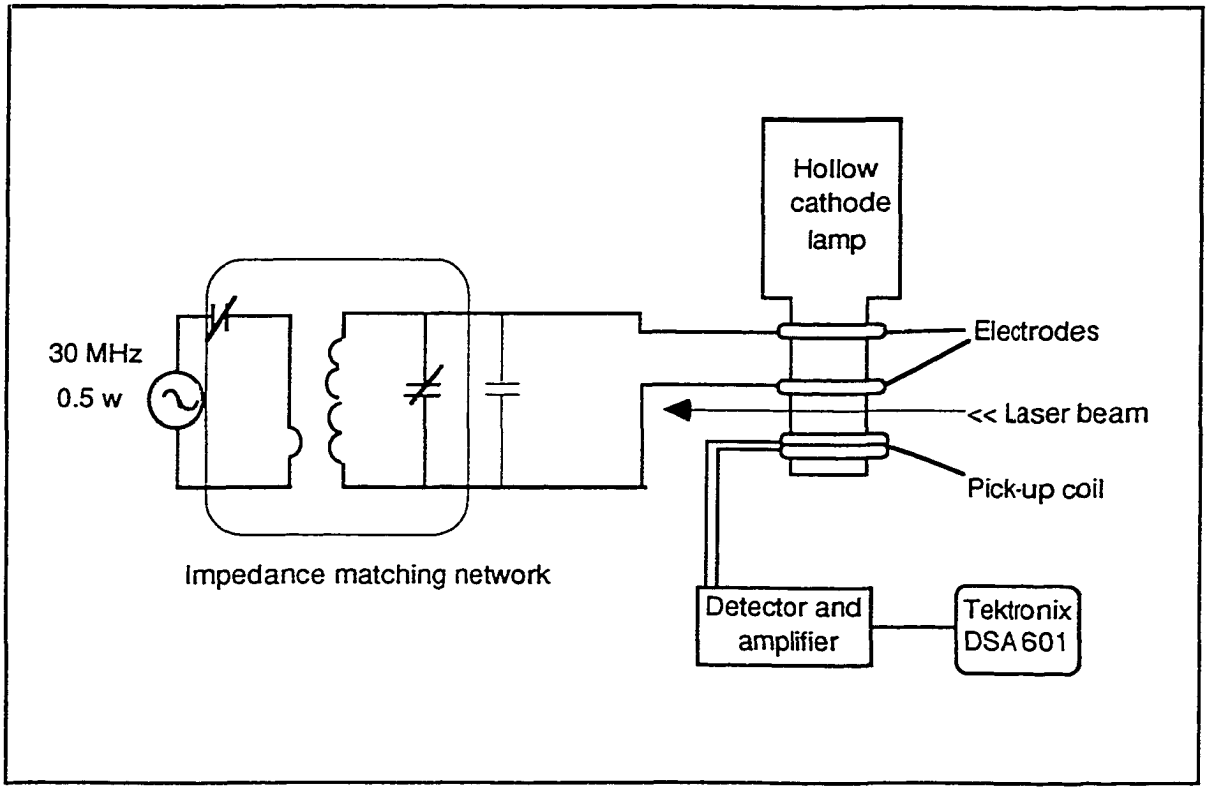

Fig. 4-1 Schematic of the experimental arrangement

of the detector circuit, acts as its own sensor. This makes the system less complicated and more reliable.

(3) Optogalvanic detection has the characteristics of zero background, selective excitation from metastable states, and the ability to pick up the very weak signals of the photoacoustic and photo-ionization effects from non-emitting species. Therefore, the RFLOGS technique has very high sensitivity. Finally, the overlap of emission lines, which so often occurs in ICP spectroscopy, is not pertinent to RFLOGS because it is not the emission that is monitored. Thus, the inter-element interferences that are so bothersome in ICP-AES, are totally eliminated. The resolution of RFLOGS spectrometry, indeed, is largely determined by the laser and can far exceed that of ICP.

Both DC and RF discharges may be used to generate the plasma. While DC discharges are simple to generate, they are, unfortunately, characterized by a non-uniform plasma (discrete discharge regions) and suffer the risk of electrode contamination by reactive gases or species present in the discharge. The RF discharge, on the other hand, has the advantages of spatial uniformity (except for a sheath that may sometimes occur in the vicinity of the electrodes), "contactless" nature (i.e., the metal electrodes need not be inside the discharge tube), and background noise levels that are not critically dependent on either the gas pressure or gas type.[16]

In the past ten years much work has been done on the application of optogalvanic spectroscopy. The species studied were:

Gases: Xe[17,20], N_2[18,19], CO_2[21,22], O_2[23], Ne[24,25] and Ar[26];

Metals: Cu, Au[27], Ca[28,29], U[30,31], Zr[32], Sr[33], Ag[34], As, Cd, Cr, Hg, Ni, Pb, and Sb[35];

Organics: CH_3Cl, CH_3OH, C_2H_5OH, C_2H_3Cl, C_2H_2, NH_3[36], and azulene[37].

However, most research has been focused on the mechanism and kinetics of optogalvanic signal generation, not on the conditions of analysis, the limits of detection or the working curves of analytes. This type of information is critical for chemical analysis, and we will attempt to emphasize it in this work.

4.2 The OGE Mechanism: Investigation in a Neon Plasma

The laser optogalvanic signal is the impedance change produced in plasma by laser irradiation. This signal contains two very different components:[38-40] one produced by ionization rate changes (IRC), the other by a change in the rate of radiationless energy dumping that leads to the photoacoustic (PA) effect. These two components, IRC and PA, can be separated experimentally.[39, 40] The method of separation is based on the fact that ionization alters the total concentration of charge carriers whereas acoustic effects do not; in the first case, this leads to frequency modulation and, in the latter case, to amplitude modulation of the resonance characteristics of the driver/plasma circuit. This topic has been discussed in previous works.[24, 41]

Using the signal separation technique, we have investigated the optogalvanic effects (OGE) induced by pulsed laser excitation of Ne $1s_{2,4} \rightarrow 2p_{1,3}$ transitions* in a low

* We use the Paschen notation for the neon energy states because papers in this field make extensive use of this traditional notation. However, for convenience we include a correspondence between the Paschen notation and the standard term symbols.

Paschen notation	Term symbols	Paschen notation	Term symbols	Paschen notation	Term symbols
$1s_2$	$(ns)\ ^1P_1$	$2p_1$	$(3p)\ ^1S_0$	$2p_6$	$(3p)\ ^1D_2$
$1s_3$	$(ns)\ ^3P_0$	$2p_2$	$(3p)\ ^3P_1$	$2p_7$	$(3p)\ ^3D_1$
$1s_4$	$(ns)\ ^3P_1$	$2p_3$	$(3p)\ ^3P_0$	$2p_8$	$(3p)\ ^3D_2$
$1s_5$	$(ns)\ ^3P_2$	$2p_4$	$(3p)\ ^3P_2$	$2p_9$	$(3p)\ ^3D_3$
		$2p_5$	$(3p)\ ^1P_1$	$2p_{10}$	$(3p)\ ^3S_1$

power, ~30 MHz, RF Ne discharge at ~5 Torr.[42] The effect of radiation trapping and collisional energy transfer on the generation of OGE signals, and the effect of different lower and upper states on the polarity and intensity of the OGE profiles were studied. It was found that:

- The polarity (sign) of the OGE signal is controlled by perturbations of the $1s_j$ populations, as shown in Fig. 4-2 and Fig. 4-3. No requirement for population inversion or laser action of the $2p_k \rightarrow 1s_j$ transition was needed.
- For a given upper $2p_k$ state, the OGE signals for excitations from the $1s_4$ state are much stronger than those from the $1s_2$ state. This is attributed to higher $1s_4$ populations: the data suggest that the relative populations are $N(1s_4)/N(1s_2) \approx 10$ and that the plasma temperature is $T \approx 10^3$ K.
- Population changes of the $1s_3$ and $1s_5$ metastable states, which changes the rates of Penning ionization, and $1s_{2,4} \rightarrow {}^1S_0$ radiation trapping, which leads to direct photon ionization of the $1s_{3,5}$ states, control the nature of the OGE signals. IRC profiles are readily modeled as a resultant of these Penning and trapped-photon ionizations, as shown in Fig. 4-4.
- The OGE signals are consequences of: (1) perturbation and reequilibration of the metastable $1s_3$ and $1s_5$ populations; (2) radiatively-trapped $1s_2 \rightarrow {}^1S_0$ photons; and (3) collisionally-induced energy transfer among all of the $1s_j$ states.

Ionization alters the charge carrier concentrations and, hence, the plasma impedance. Since the plasma is an integral part of a resonant circuit, this impedance alteration causes a change of the resonant frequency (i.e., a frequency modulation), a

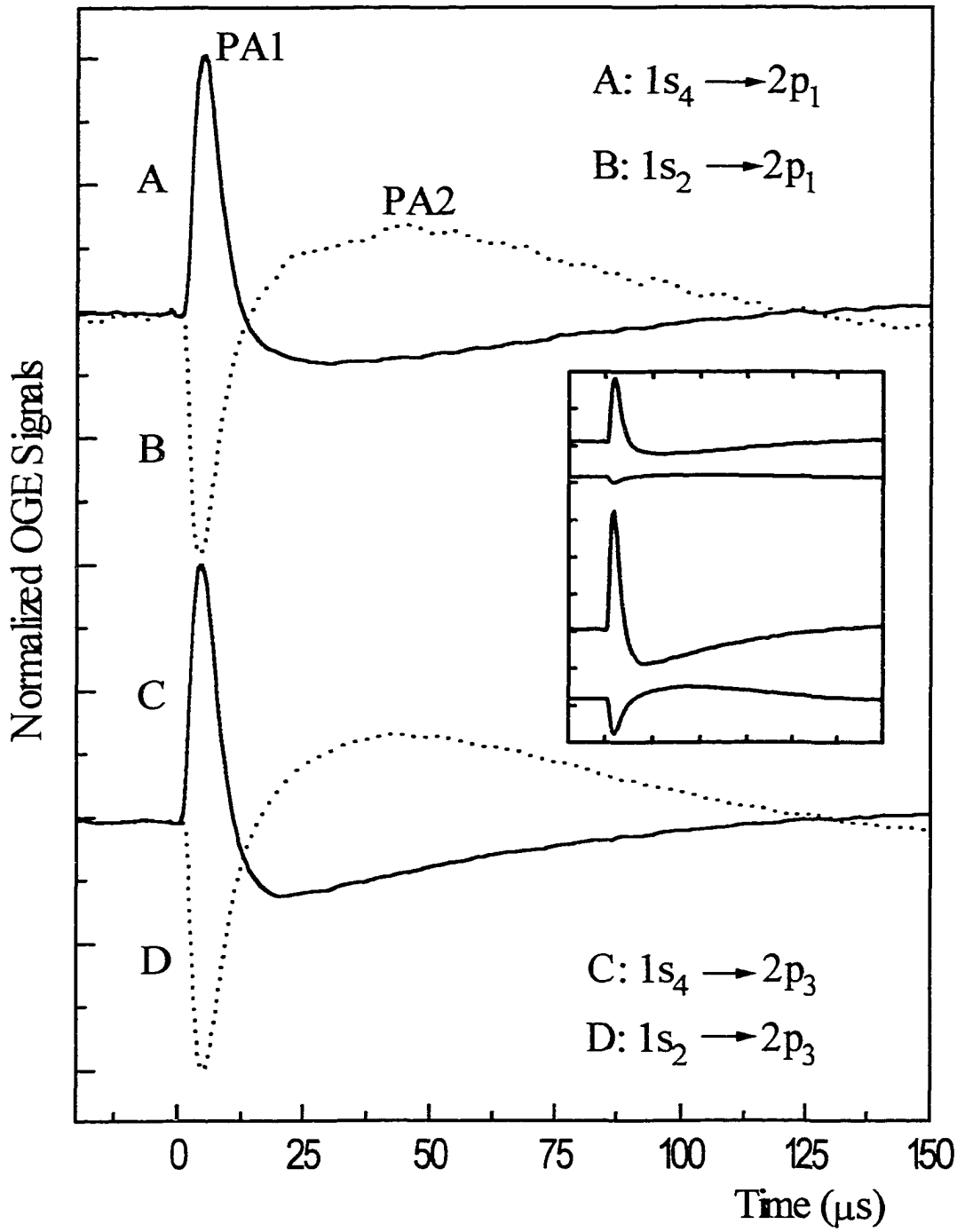

Fig. 4-2 The normalized PA components of the OGE signals for the $1s_{2,4} \rightarrow 2p_{1,3}$ excitations of neon. Normalization is used to emphasize the symmetry of the signals. The unnormalized signals, in similar top-to-bottom order, are shown in the insert, in which the y and x axes are scaled 0.5V/div and 25μs/div, respectively. In addition, the zero voltage positions in the insert have been arbitrarily separated to avoid crowding.

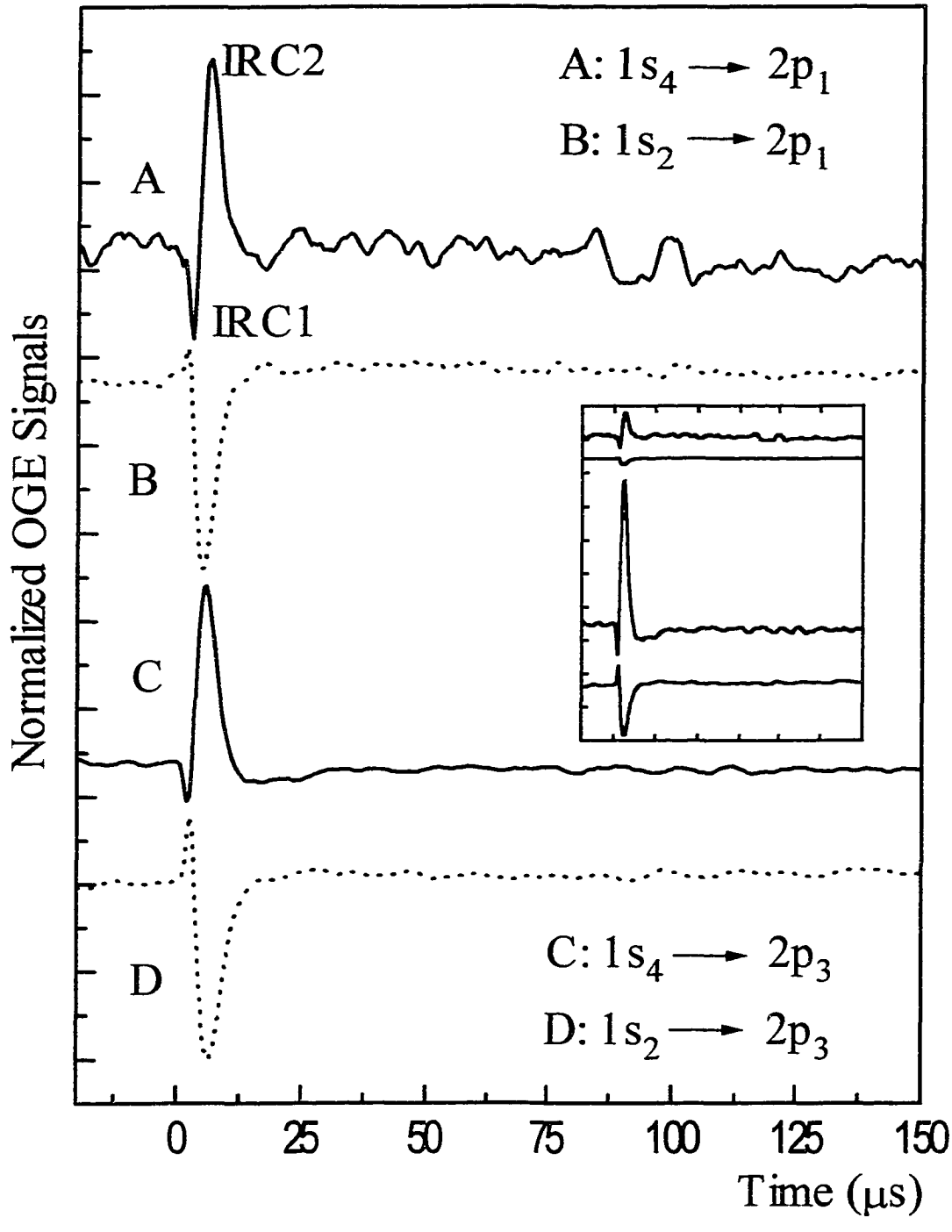

Fig. 4-3 The normalized IRC components of the OGE signals for the $1s_{2,4} \rightarrow 2p_{1,3}$ excitations of neon. Normalization is used to emphasize the symmetry of the signals. The unnormalized signals, in similar top-to-bottom order, are shown in the insert, in which the y and x axes are scaled 0.13V/div and 25μs/div, respectively. In addition, the zero voltage positions in the insert have been arbitrarily separated to avoid crowding.

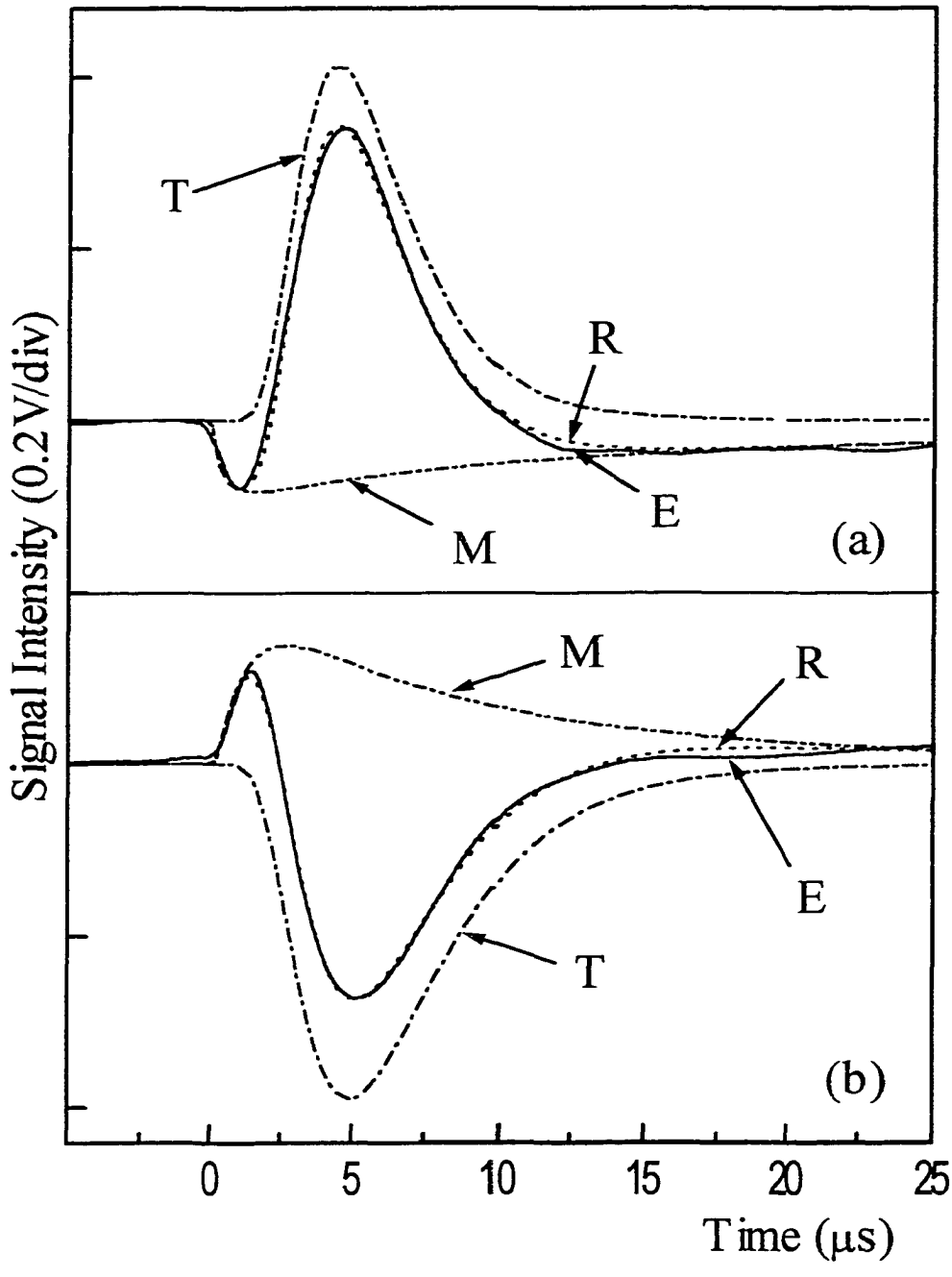

Fig. 4-4 Illustration of IRC signal formation produced by $1s_4 \rightarrow 2p_3$ (Fig. 4-4(a)) and $1s_2 \rightarrow 2p_3$ (Fig. 4-4(b)) excitations of neon. Log-normal functions are used to model the Penning collisional ionization of metastable states (M) and the $1s_2 \rightarrow {}^1S_0$ trapped radiation ionization (T). Curve denotations are:

Penning ionization of metastable states (M): —·—·—·—

Trapped radiation ionization (T): — — ———

Resultant of M and T (R): ----------

Experimental curve (E): ——————

change which, on the μs time scale of these experiments, is instantaneous. However, the acoustic disturbance must first travel to a region of large carrier concentrations, where the movement of these carriers by the decompression/compression pulse produces a detectable change of impedance. Thus, the acoustic effect is delayed by the time of travel from the site of laser excitation to the region of high carrier densities, as shown in Fig. 4-5.[43] To verify this model we used the experimental setup shown in Fig. 4-6 to study the relation between the delay of the signal (t) and the distance travelled by the acoustic wave (d). The results are shown in Fig. 4-7. Since the correlation coefficient of the least square linear regression (R=0.811) is greater than the correlation coefficient for a 0.01 level of significance ($R_{0.01}$=0.372), one can be 99% certain that the linear regression is reliable and a linear relation, $d = d_0 + \upsilon t$, exists. It also yields $\upsilon = 320\ ms^{-1}$, which is consonant with the velocity of sound in neon at 5 Torr and 60°C. Therefore, the PA signal does indeed travel at the speed of sound. The value of d_0 is found to be 1.6 cm, suggesting that the primary high carrier densities occur in the vicinity of the upper electrode. The standard error of estimation (SD) is 0.0016. If one draws two lines $d = d_0 + \upsilon t - SD$ and $d = d_0 + \upsilon t + SD$, as shown by the two dotted lines in Fig. 4-7, the probability that a given experimental datum falls in the region between these two lines is 68.3%.

4.3 Analytical Prospects: OGE in Iodine-containing Plasmas

4.3.1 Background Information

Iodine is the heaviest naturally-occurring halogen. It is a solid, melting at 113.6 °C. The solid sublimes at temperatures well below the melting point[44] to give a significant vapor pressure (e.g., ~178 mTorr at 22 °C). Iodine vapor is irritating to the

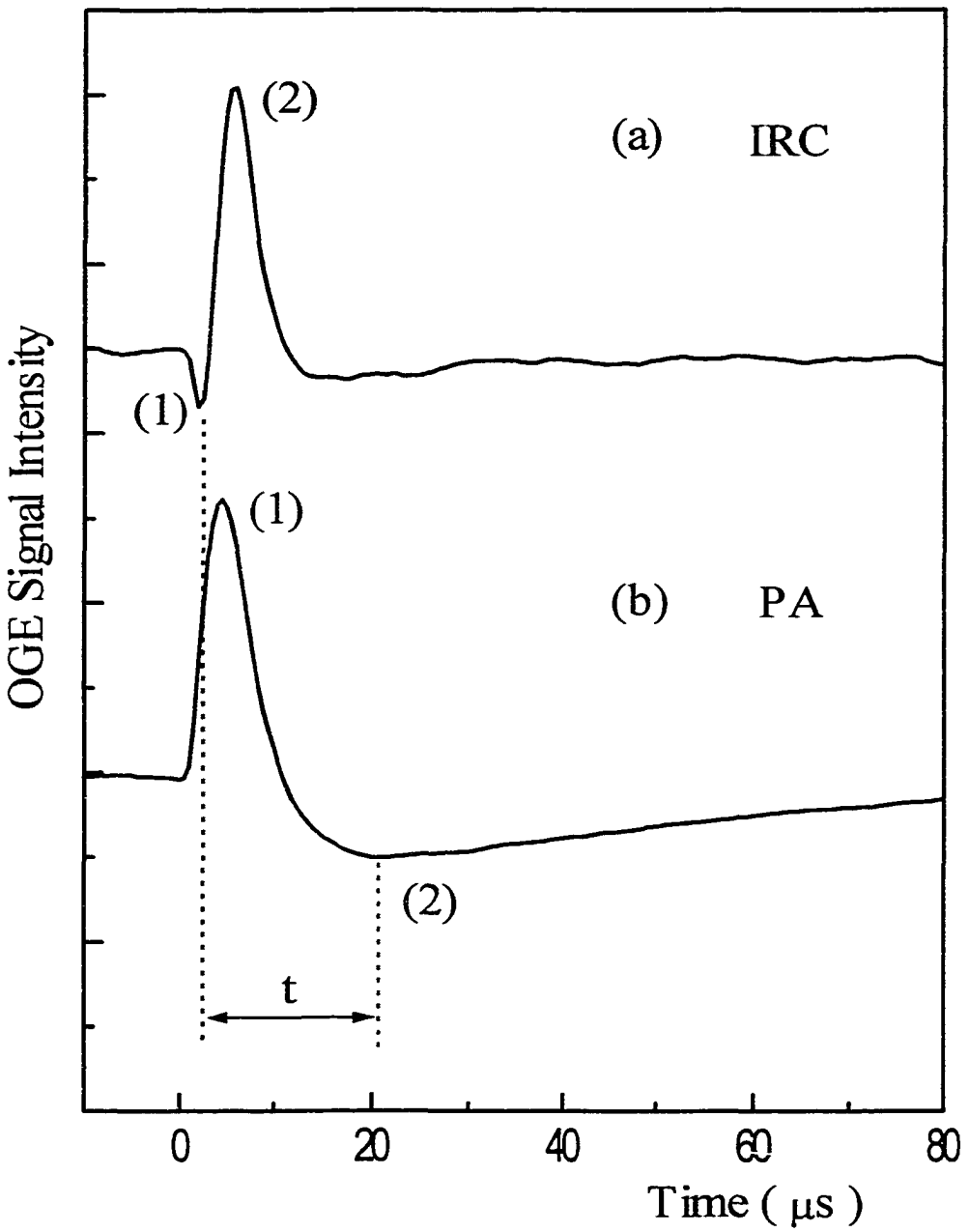

Fig. 4-5 IRC and PA signals illustrative of the model advanced in the text. Peaks are labelled sequentially and are referred to as IRC2, PA1, etc. IRC2 and PA1 are produced by the deexcitation of radiatively-trapped states; IRC1 and PA2 are generated by population changes of metastable states. The time t is that required for movement of an acoustic pulse from the site of excitation to a plasma region of high ion densities.

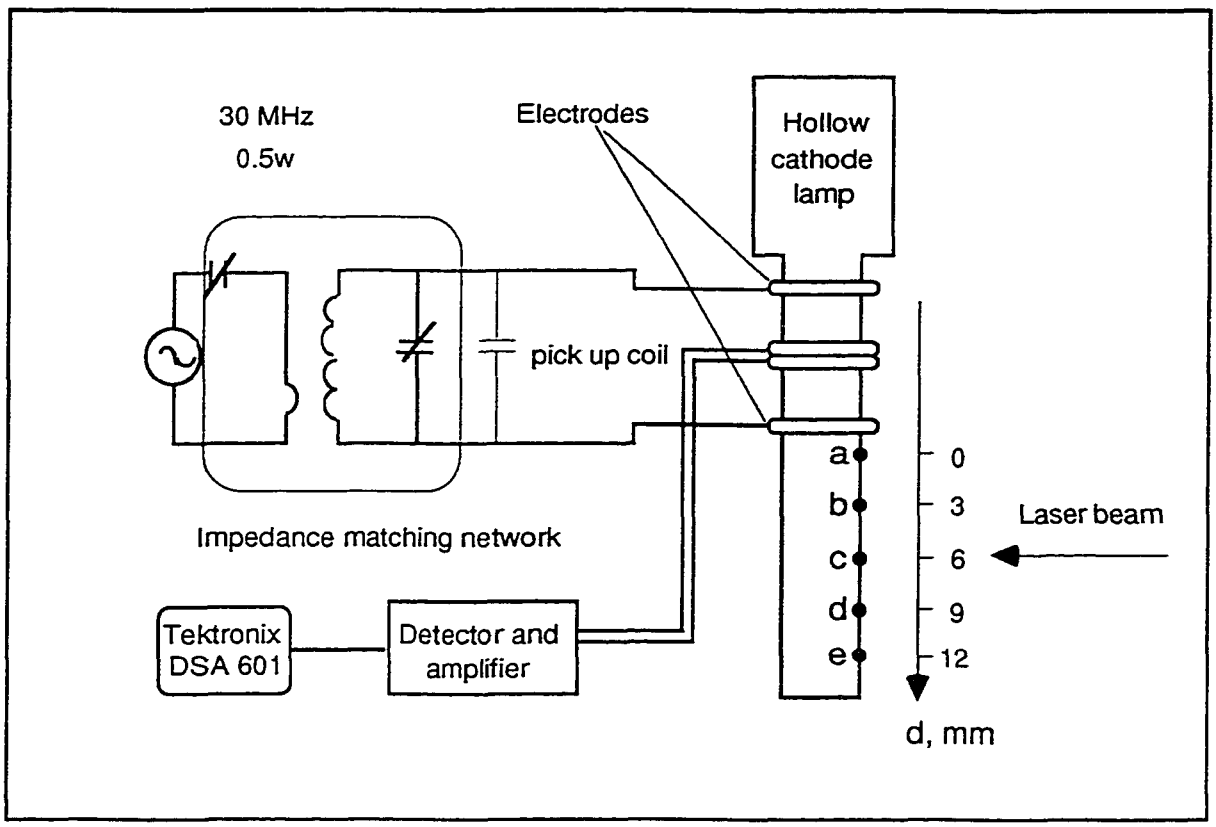

Fig. 4-6 Schematic of the experimental arrangement in a hollow cathode lamp. The two electrodes are ~30 mm apart. The laser excites the plasma at five sites, each separated by 3 mm. The first site, site a, lies 1-2 mm below the lower electrode.

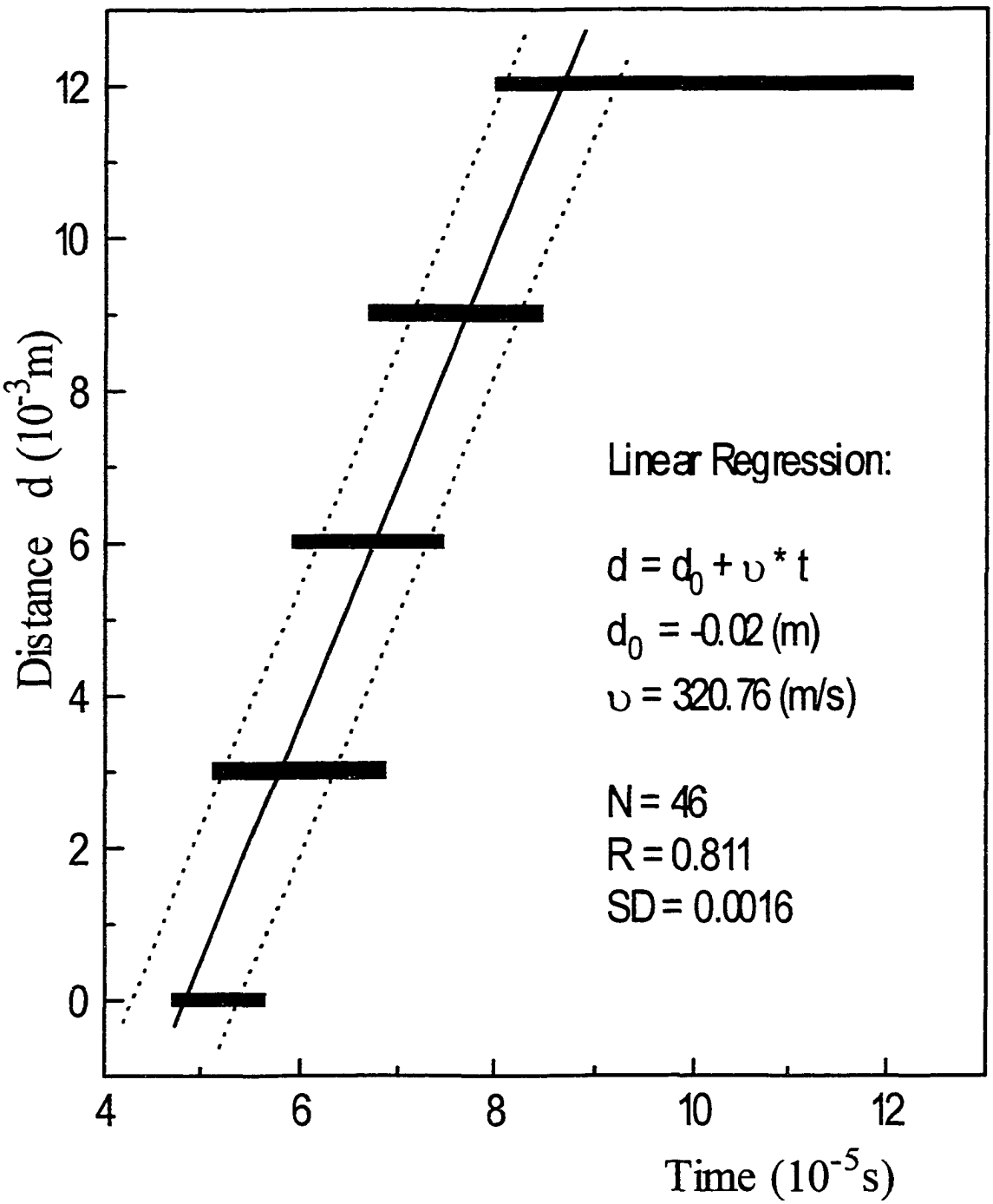

Fig. 4-7 Distance versus time for the PA2 band of the $1s_5 \rightarrow 2p_5$ neon excitation. The distance is determined by the site of the laser excitation. The time is that at the minimum of the PA2 peak. The error bar is the width of the band at a height 0.01V above the minimum. The solid line represents $d = d_0 + \upsilon t$, and the dotted lines represent $d = d_0 + \upsilon t + SD$ and $d = d_0 + \upsilon t + SD$. R is the correlation coefficient. N is the number of samples. SD is the standard error of estimation.

eyes, lungs and skin. The maximum safe concentration for repeated 8hr/day exposures is 0.1 ppm.[44]

The radioactive iodine (I^{129}) vapours, which may be released from nuclear reactor wastes, are extremely harmful. An initial by-product of the nuclear reaction in these wastes is atomic iodine that eventually produces molecular iodine. Consequently, monitoring of both radioactive atomic and molecular iodine (I^{129}) vapors is important to safe radioactive-waste storage.

The quantitative determination of iodine was formerly done by direct titration in neutral or dilute acidic solution. Now, most of this work is done by faster and more versatile instrumental analyses, such as colorimetry/catalysis, ion selective electrodes, gas chromatography, neutron activation analysis, cathodic stripping voltammetry,[45] ICP optical emission spectroscopy[46] or laser-induced fluorescence.[47, 48] However, the reliable determination of iodine in foods remains difficult because of the very low levels (less than 0.1 ppm) of iodine and its compounds that are present. Besides, very few methods can successfully analyse both solid and gas samples. Therefore, an analysis technique that is precise, simple, sensitive and versatile, and that is suitable to a simultaneous trace element detection mode, needs to be developed. Radio frequency laser optogalvanic spectroscopy (RFLOGS) is an attractive technique that suggests itself for this purpose.

The time-resolved laser optogalvanic spectroscopy of iodine in a radio frequency discharge has been studied in our Laboratories.[38] It has been shown that the OGE signal of iodine consists of two components, fast and slow. The fast component was believed to originate in direct laser and/or enhanced collisional ionization following laser

excitation. The slow component was thought to be generated by an actual physical movement of the charge carriers in a sensitive region of the plasma. It was also found that atomic excitations of iodine produce only the fast component whereas the molecular excitations of iodine produce only the slow component. In a recent preliminary work,[35] the PA and IRC components in the iodine OGE signals were identified and disentangled. The influence of iodine gas pressure, the type of carrier gas, the laser energy, the RF discharge power and the tuning of the operative RF circuit on signal intensity were studied. However, the limits of detection being preliminary, were imprecise. Furthermore, the influence of the wavelength of laser excitation on the OGE signal intensity was not investigated; nor were any working curves, the relationship between iodine concentration and OGE signal intensity, studied. The aim of this work is removal of these deficiences.

4.3.2 Experimental

The typical experimental arrangements are shown in Fig. 4-8. The iodine sample is housed (in static detection, Fig. 4-8(a)) or flows (in flowing detection, Fig. 4-8(b)) at different pressures in a quartz cell which is ~30 cm in length and ~8 mm in diameter. Two electrodes, ~25 mm apart, are wound around the exterior of the cell. RF power of 0.5 to ~3 W, ~32 MHz, is applied at very high voltage to the cell in order to generate a stable, low-noise, capacitively-coupled discharge. A resonantly-tuned pick-up coil is also wrapped around the exterior of the cell, ~6 mm below the bottom electrode. A pulsed dye laser (Chromatix CMX-4, ~1 μs pulse width, ~0.1 cm^{-1} resolution) whose wavelength is tuned to a desired atomic or molecular iodine transition excites the plasma transversely at a point between the lower electrode and the pick-up coil.

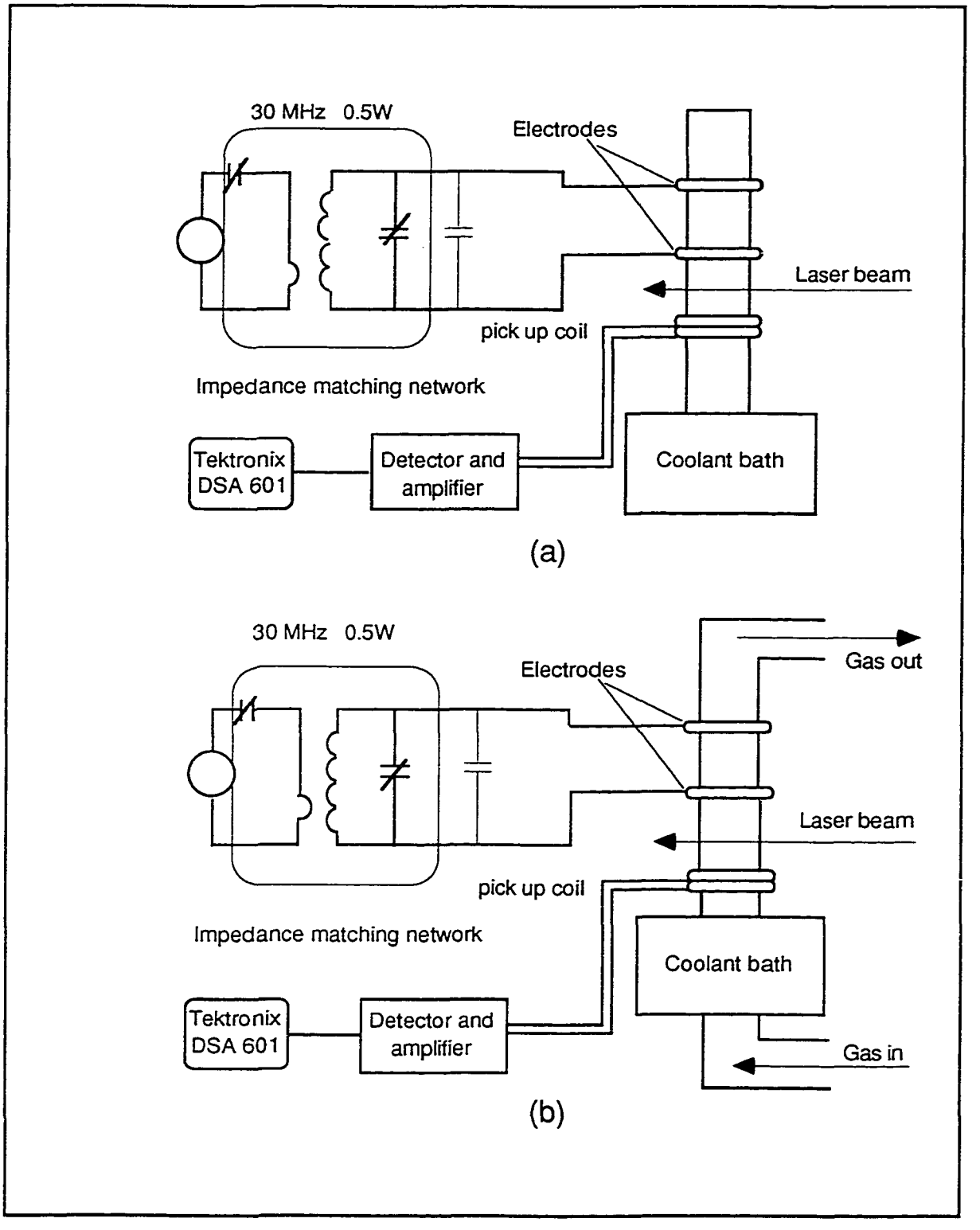

Fig. 4-8 Schematic of the experimental arrangements for detection of iodine

The concentration of the iodine gas sample can be adjusted by changing the partial pressure of iodine in the gas mixture (in flowing condition) or by changing the temperature (in static condition). For detection under flow conditions, the iodine vapours are fed into the carrier gas by metering valve. The pressure at the inlet of the discharge tube is measured first with only the carrier gas present and again after seeding with iodine vapor. The increase in pressure gives the pressure of the iodine vapor. For static, non-flow detection, a small piece of solid iodine is placed on the bottom of the discharge tube. The tube is degassed and evacuated by several freeze (liquid nitrogen)-pump-thaw cycles, then filled with nitrogen or air at appropriate pressures. The vapor pressure of iodine can be controlled by cooling the bottom of the tube either in a circulating coolant bath or by dry ice-solvent slurry. If the volume of a sample cell is V and the coolant temperature is T, the concentration of sample C can be calculated by

$$C = n/V = P/RT \text{ (mol/L)} = kP/RT \text{ (}\mu g/cm^3\text{)}$$

where n is the number of moles of I_2 in the gas phase, P is the partial vapor pressure of I_2 at T(K), and k is a constant that converts concentration from mol/L to $\mu g/cm^3$. For example, at -45°C, the vapor pressure of I_2 is 0.000108 Torr, and the concentration of the I_2 (gas) in the sample tube is 0.001934 $\mu g/cm^3$.

4.3.3 Results and Discussion

In view of the accessible laser wavelength available to us, we selected the excitations $^3P_1 6s[1]_{3/2} \rightarrow {}^3P_2 8p[2]_{5/2}$ (16912 cm^{-1}) and $X\ ^1\Sigma_g^+ \rightarrow B\ ^3\Pi(O_u^+)$ (16980 cm^{-1}) for study of the atomic and molecular iodine OGE signals, respectively. Signal strengths were measured in both static (non-flowing) and flowing conditions. Two gases, air and

nitrogen, were used as filler (non-flowing) and carrier gases (flowing). The limits of detection are shown in Table 4-1.

Table 4-1 Limits of Detection of Iodine Samples

Signal	Laser Wavelength	Detection Condition	Type of Filler or Carrier Gas	Limit of Detection* ($\mu g/cm^3$)
atomic	16912 cm^{-1}	non-flowing	air	$4.17*10^{-4}$
atomic	16912 cm^{-1}	non-flowing	nitrogen	$7.73*10^{-5}$
atomic	16912 cm^{-1}	flowing	air	$1.98*10^{-4}$
atomic	16912 cm^{-1}	flowing	nitrogen	$3.65*10^{-5}$
molecular	16980 cm^{-1}	non-flowing	air	$2.66*10^{-3}$
molecular	16980 cm^{-1}	non-flowing	nitrogen	$4.92*10^{-4}$
molecular	16980 cm^{-1}	flowing	air	$3.91*10^{-4}$
molecular	16980 cm^{-1}	flowing	nitrogen	$1.15*10^{-4}$

* The limit of detection is defined as:

$$C(P_{laser}/P_{std})(SN_{min}/SN)(N/N_{std})^{1/2}$$

where C is the concentration of sample, $\mu g/cm^3$; P_{laser} is the laser power used, mJ/pulse; P_{std} is the standard laser power in our experiment, 5 mJ/pulse; SN_{min} is the minimum signal to noise ratio, 2; SN is the obtained signal to noise ratio; N is the number of measurements averaged; N_{std} is the standard number of measurements, 3000.

4.3.3.1 Detection of Iodine in Non-flowing System

We varied the RF power and filler gas (air, in this case) pressures within specified ranges in order to study their effects on the iodine signal. Given the geometry of our experimental set-up (diameter of discharge tube ~8 mm, electrode spacing 2-3 cm), the

optimum RF power lies between 0.5 and 3.0 W. If the RF power is too low, the discharge tends to oscillate (low frequency relaxation oscillations) or to extinguish. On the other hand, if the RF power is too high, random noise in the plasma can become significant. For detection of atomic iodine, the signal intensity improves as the RF power increases from 0.5 to 1.0 W because, at higher RF power, more iodine molecules dissociate into atoms. However, no significant improvement of the molecular iodine signal occurs with increase of the RF power, presumably because the nature/shape of the plasma as well as the excited state population distributions change in adverse ways. Therefore, a linear correlation between RF power and the magnitude of the LOGE signal, whether for I_2 or I detection is not a given.

Both gases, air and nitrogen, are excellent diluents. Neither interferes with the LOGE signal of iodine nor do they introduce any background noise. The limit of detection is approximately one order of magnitude worse in air ($\sim 10^{-4}$ $\mu g/cm^3$) than that in nitrogen ($\sim 10^{-5}$ $\mu g/cm^3$). Another disadvantage of air is that it may lead to deposits on the interior of the discharge tube, and a consequent decrease of signal intensity.

4.3.3.2. Detection of Iodine in Flowing System

There should be no difference between the detection limits for iodine in non-flowing or flowing air. However, because the sample tube differs from one experiment to the other, the laser spot must be adjusted, the electronic circuit re-tuned and the operational conditions optimized, especially carrier gas pressure and RF power.

When using air as the carrier gas, it was found that RF power levels of 1 to 3 W and carrier gas pressures of 0.1 to 1.0 Torr generate the optimum atomic iodine signals. The detection limit for iodine atoms under these experimental conditions is $1.98*10^{-4}$

$\mu g/cm^3$, which is measured at P(air) = 0.147 Torr and RF power = 1.0 W. Further improvement to 10^{-5}-10^{-7} $\mu g/cm^3$ appears entirely reasonable. An RF power of ~1 W was found to generate optimum signals for iodine molecules. The detection limit of $3.91*10^{-4}$ $\mu g/cm^3$, impressive as it is, can be improved further.

When using nitrogen as the carrier gas, an RF power less than ~1.3 W caused plasma instability (low-frequency relaxation oscillations), while an RF power higher than 4.0W caused poor signal response. Therefore, the RF power was maintained within 1.3 to 4.0W. The detection limit under these experimental conditions is ~$10^{-5}$$\mu g/cm^3$ for both atomic and molecular iodine.

Iodine detectivity is ~10 times better in flowing nitrogen than in flowing air. Therefore, nitrogen is the preferable filler and carrier gas. On the other hand, unlike air, the detection of iodine atoms and molecules in nitrogen shows less variation. This may be explained by a smaller tendency to form deposits of iodine oxides on the inner wall of the discharge tube in the former case.

4.3.3.3. Identification of Atomic and Molecular Iodine Signals

Under certain experimental conditions both the slow (I) and fast (I_2) components are represented in both the PA and IRC profiles of the 16912 and 16980 cm^{-1} excitations, as is shown in Fig. 4-9. However, the signals at 16980 cm^{-1} have a stronger slow component and the signals at 16912 cm^{-1} have a stronger fast component. By carefully selecting the experimental conditions (i.e., the RF power, the air pressure, the position of the laser spot and the tuning of the equipment circuit), we can separate and identify the two signal components. Indeed, with the appropriate conditions, a strong, pure, slow I_2 component constitutes the PA profile of the 16980 cm^{-1} excitation whereas a strong,

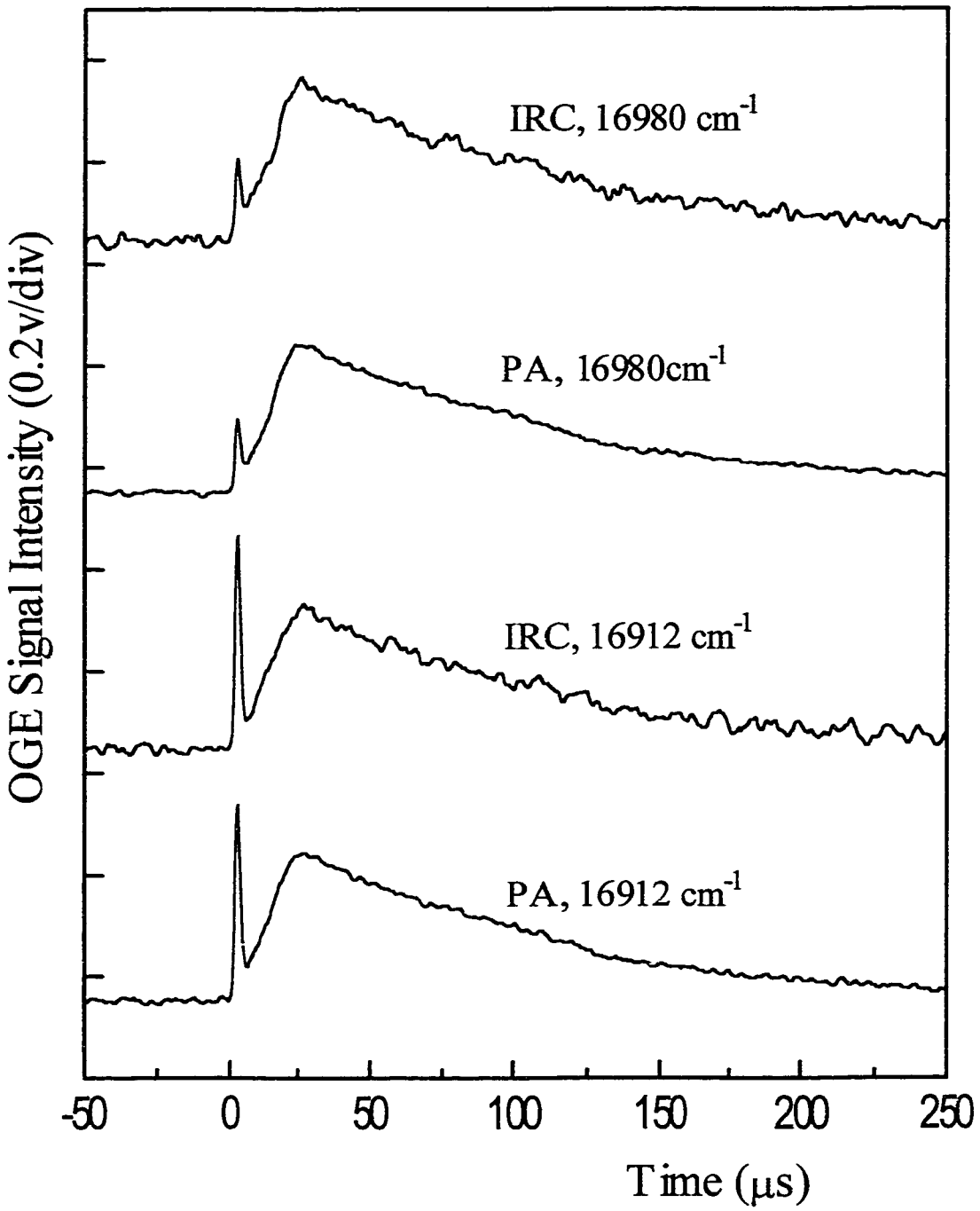

Fig. 4-9 Iodine OGE signals containing both fast and slow components. All profiles are recorded at P(filler gas) = 0.5 Torr and RF power = 2 W.

pure, fast I component constitutes the IRC profile of the 16912 cm^{-1} excitation, as shown in Fig. 4-10. Thus, the PA signal at 16980 cm^{-1} can be used to analyze iodine molecules and the IRC signal at 16912 cm^{-1} to analyze iodine atoms. On the other hand, those LOGE profiles that contain two signal components, slow and fast, provide a useful tool for determination of the relative concentrations of iodine molecules and atoms in a single measurement.

4.3.3.4. Detection at the Laser Wavelength of 533nm

As discussed previously, many factors influence signal intensity. Of these, the laser wavelength is critical. Now, the LOGE signal is actually the change of electrical impedance of the plasma produced by resonant absorption of laser radiation by a plasma moiety. Therefore, at a given laser power, the LOGE signal intensity will depend on the plasma absorptivity at that wavelength. Indeed, we can expect a stronger LOGE signal to be associated with strong absorption lines. To investigate the effect of laser absorptivity on the LOGE signal, we selected an $X \rightarrow B$ excitation at 533nm(i.e., 18762 cm^{-1}) which has an absorbance three times that at 16980 cm^{-1}.

The measurements were conducted under the same experimental conditions, nitrogen being the filler gas in a non-flowing system. The 18762 cm^{-1} signal was found to be a mixture of molecular and atomic signals. The molecular signal was 3 to 6 times stronger than that at 16980 cm^{-1}, as was also the atomic signal. The limits of detection were $4.16*10^{-7}\mu g/cm^3$ for iodine molecules and $2.32*10^{-7}\mu g/cm^3$ for iodine atoms, respectively. These results are superior to those obtained using most commercial ICP instruments.

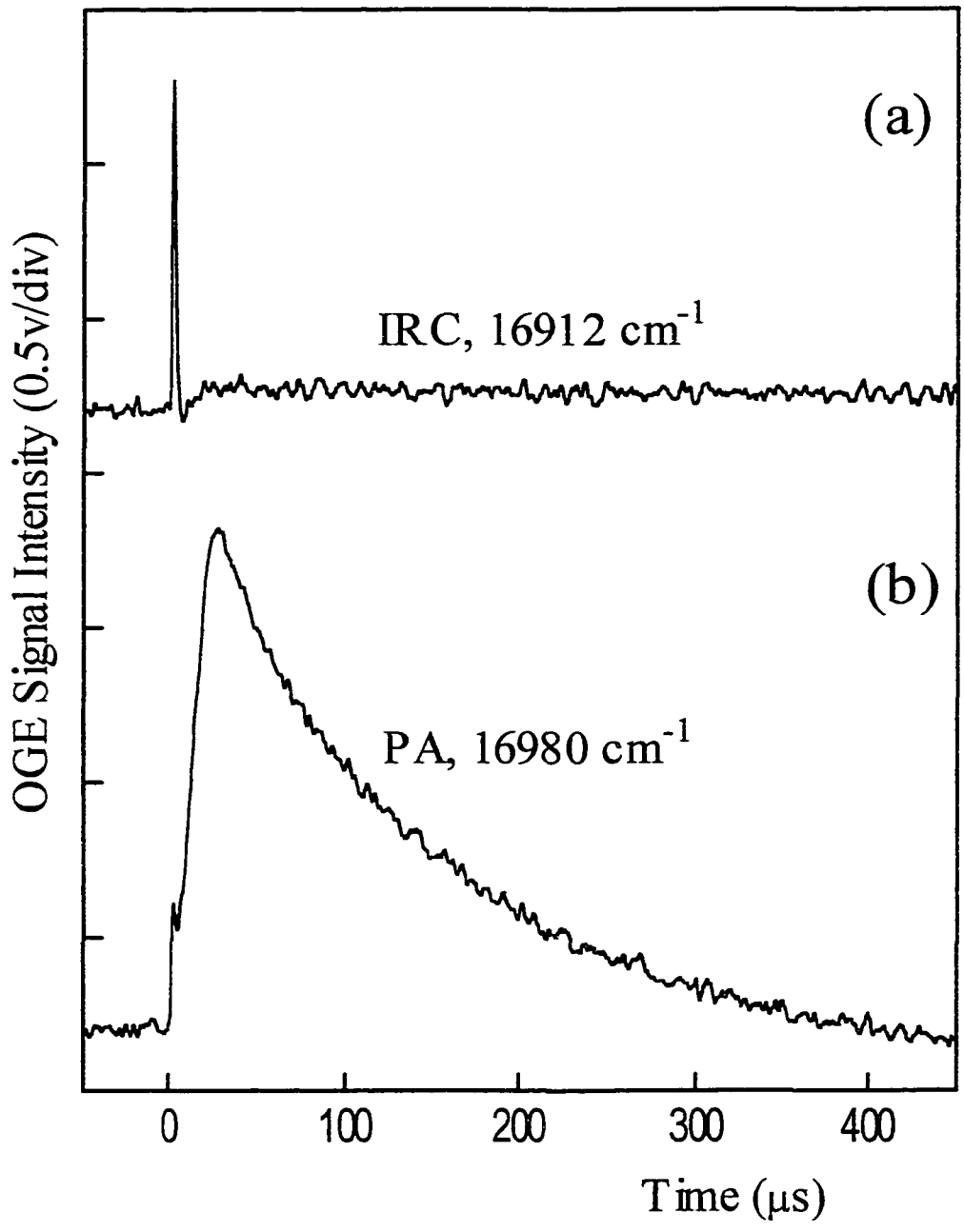

Fig. 4-10 Iodine OGE signals dominated by fast or slow components.
(a) was recorded at P(filler gas) = 1 Torr and RF power = 1 W;
(b) was recorded at P(filler gas) = 1 Torr and RF power = 0.5 W

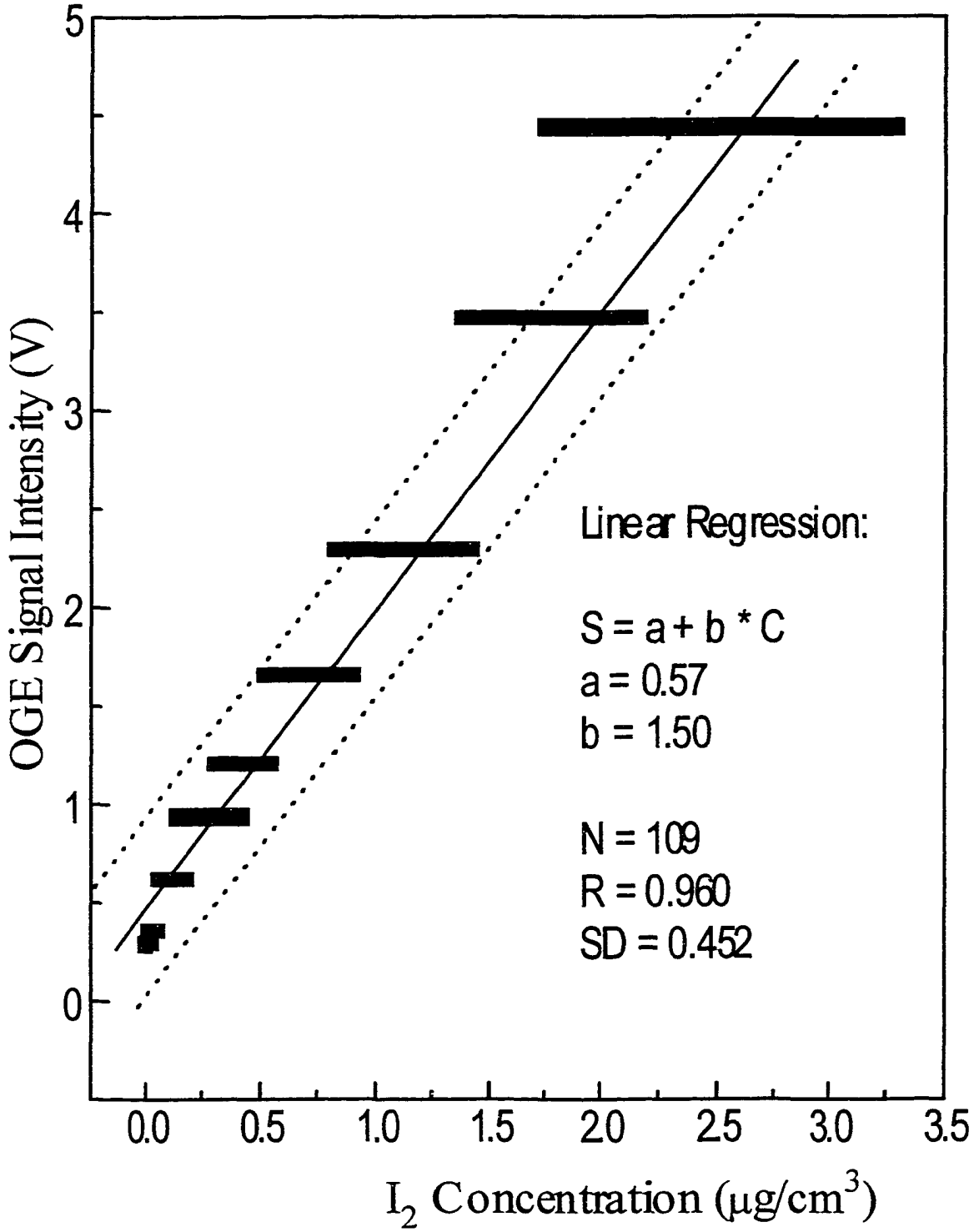

Fig. 4-11 The relationship between sample concentration and OGE signal intensity. The solid line represents S = a + b*C, and the dotted lines represent S = a + b*C + SD and S = a + b*C – SD. R is the correlation coefficient. N is the number of samples. SD is the standard error of estimation.

The relationship between sample concentration and LOGE signal intensity (working curve) was also studied. The results are shown in Fig. 4-11. Since the correlation coefficient of the least square linear regression (R = 0.960) is greater than the correlation coefficient for a 0.01 level of significance ($R_{0.01}$ = 0.254), one can be 99% certain that the linear regression is reliable. The standard error of estimation (SD) is 0.452. If one draws two lines S = a + b*C – SD and S = a + b*C + SD, as shown by the two dotted lines in Fig. 4-11, the probability that a given experimental datum falls in the region between these two lines is 68.3%. Therefore, the signal-concentration response is linear over a wide range, at least 3 orders of magnitude. Thus, one of the primary conditions for a successful quantitative analytical technique is fulfilled.

4.4 Summary

- The polarity (sign) of the LOGE signal is controlled by perturbations of the $1s_j$ populations. Population changes of the $1s_3$ and $1s_5$ metastable states, which changes the rates of Penning ionizations, and $1s_{2,4} \rightarrow {}^1S_0$ radiation trapping, which leads to direct ionization of the $1s_{3,5}$ states, control the nature of the LOGE signals. IRC profiles are readily modeled as a resultant of these Penning and trapped-photon ionizations. The LOGE signals are consequences of: (1) perturbation and reequilibration of the metastable $1s_3$ and $1s_5$ populations; (2) radiatively-trapped $1s_2 \rightarrow {}^1S_0$ photons; and (3) collisionally-induced energy transfer among the $1s_j$ states.
- The acoustic disturbance must first travel to a region of large carrier concentrations, at which time the movement of these carriers by the decompression/compression pulse produces a detectable change of impedance. Thus, the acoustic effect is

delayed by the time of travel from the site of laser excitation to the region of high carrier densities.

- The LOGS can be used to detect trace I atoms and I_2 molecules in both static and flowing conditions. By careful selection of the operating conditions (e.g., RF power, filler gas or carrier gas pressures, discharge tube geometry), a pure atomic iodine signal excited at 16912 cm^{-1} constitutes the IRC LOGE profile and a pure molecular iodine signal excited at 16980 cm^{-1} constitutes the PA LOGE profile.
- Both air and nitrogen can be used as the filler or carrier gas for LOGE iodine detection. No interferences or background noise from the filler or carrier gas were observed. The detection limits of iodine in nitrogen are about one order of magnitude better than that in air.
- The signal intensity, and therefore the detection limit, is affected by the experimental arrangement as well as the laser wavelength. An excitation that produces higher absorption in iodine is more likely to generate a stronger LOGE signal.
- The response of signal intensity-sample concentration is linear in a wide range. The detection limits achieved in our experiments are ~10^{-7} $\mu g/cm^3$ for both iodine atoms and molecules. We believe that optimization of the equipment and the experimental conditions can improve the detection limit by 2 to 3 orders of magnitude.

4.5 References

1. A. Montaser and D. W. Golightly, *Inductively Coupled Plasmas in Analytical Atomic Spectrometry,* p3, VCH Publishers, Inc., New York (1987)
2. M. Thompson and J. N. Walsh, *A Handbook of Inductively Coupled Plasma Spectroscopy,* p25, Blackie & Son Ltd., New York (1983)

3. S. S. Berman, J. W. McLaren and D. S. Russel, *Anal. Proc. Int. Winter Conf.*, Ed. R.M. Barnes, p586, Heyden, London (1981)

4. M. Thompson and J. N. Walsh, *A Handbook of Inductively Coupled Plasma Spectrometry,* p126, Blackie & Son Ltd., New York (1983)

5. G. M. Hieftje and S. W. Downey, *ICP Info. Newslett.*, 7, 560 (1982)

6. W. J. Crooks, G. R. Choppin and A. Saoto, *Anal. Lett.*, **27**(14), 2737 (1994)

7. J. Fucsko, S. H. Tan, H. La and M. K. Balazs, *Appl. Spec.*, **47**(2), 150 (1993)

8. M. Thompson and J. N. Walsh, *A Handbook of Inductively Coupled Plasma Spectrometry,* p29, Blackie & Son Ltd., New York (1983)

9. R. K. Winge, V. A. Fassel, V. J. Peterson and W. A. Floyd, *Inductively Coupled Plasma Atomic Emission Spectroscopy,* 1st edition, Elsevier, New York (1985)

10. T. Jacksier, M. J. Jahl and R. M. Barnes, *Spectrochimica Acta*, Part B, **47**(12), 1373 (1992)

11. Montaser and D. W. Golightly, *Inductively Coupled Plasmas in Analytical Atomic Spectrometry,* p103, VCH Publishers, Inc., New York (1987)

12. B. Barbieri, N. Boverini and A. Sasso, *Rev. Mod. Phys.*, **62**, 603 (1990)

13. C. R. Webster and C. T. Rettner, Laser Focus, **19**, 41 (1983)

14. J. E. M.Goldsmith and J. E. Lawler, *Contemp. Phys.*, **22**, 235 (1981)

15. R. A. Keller, B. E. Warner, E. F. Zalewski, P. Dyer, R. Engleman, Jr., and B. A. Palmer, *J. Phys. Colloq.*, **C7**, 23 (1983)

16. R. E. Muenchausen, R. D. May, and G. W. Hills, *Opt.Commun.*, **48**, 317 (1984)

17. D. Kumar, L. Klasinc, P.L. Clancy and S. P. McGlynn, *Int. J. Quantum Chem., Quantum Chem.Symp.*, **19**, 403 (1986)

18. D. Kumar, L. Klasinc, P.L. Clancy, R.V. Nauman and S. P. McGlynn, *Int. J.* Quantum *Chem., Quantum Chem. Symp.*, 1986, 20, 635

19. R. Djulgerova, V.Mihailov, *Spectroscopy Letters*, **26** (2), 347 (1993)

20. L. Klasinc, D. Kumar, P.L. Clancy and S. P. McGlynn, *Chem. Acta,* **59**, 643 (1986)

21. M. Tachikawa, T. Shimizu, *Japanese Journal of Applied Physics,* part 1, **30**(5), 1111 (1991)

22. L. Zink, F.S. Pavone, R. Meucci, *Optics Communications*, 77(1), 4123 (1990)

23. Y. Matsuda, K. Shuto, H. Fujiyama, *Surface & Coatings Technology*, **98** (1/3), 1420 (1998)

24. D. Kumar, R.R. Zinn and S. P. McGlynn, *J. Chem. Phys.,* **101**(3), 1959 (1994)

25. M. P. Scheer, F. Vermeersch and F. J. de Hoog, *Appl. Phys.,* **26**, 1700 (1993)

26. C.G.S. Costa, J.V.B. Gomide, A.A. Scalabrin, *Il Nuovo Cimento della Societa Italiana di Fisic,* **14**(6), 613 (1992)

27. Y. Zhang, L. Yin, Q. HU, G. Zhang, C. Jin and F. Lin, *Chinese Phys. Lett.*, **2**(9), 425 (1985)

28. S. Assimopoulos, A. Bolovinos, M. Aymar, *The European Physical Journal : d.,* **1**(3), 243 (1998)

29. S. Assimopoulos, A. Bolovinos, A. Jimoyiannis, *Journal of Physics,* **B27**(12), 2471 (1994)

30. S. Abhilasha, S. Qian, D.L. Monts, *Applied Physics b, Lasers and Optics*, **65**(4/5), 625 (1997)

31. C. M. Barshick, R.W. Shaw, J.M. Ramsey, *Analytical Chemistry,* **67**(20), 3814 (1995)

32. E.Langlois, J. Gagne, *J. Opt. Soc. of America,* **b11**(4), 552 (1994)

33. A.Jimoyiannis, A.Bolovinos, P. Tsekeris, *Zeitschrift fur Physik,* **d22** (3), 577 (1992)

34. D.L. Monts, M. Su, *Applied Spectroscopy*, **44**(4), 641 (1990)

35. D.L. Monts, S. Abhilasha, S. Qian, D. Kumar, X. Yao and S.P. McGlynn, *J. Thermophysics & Heat Transfer,* **12**(1), 66 (1998)

36. S. Zhou and G. Wang, *Acta Optica Sinica*, **3**(6), 495 (1983)

37. D. Kumar, R. V. Nauman, T. L. Mathers, R. Mohanty and S. P. McGlynn, *J. Indian Chem. Soc.,* **LXIII,** 10 (1986)

38. D. Kumar, P.L. Clancy and S. P. McGlynn, *J. Chem. Phys.*, **90**,4008 (1989)

39. D. Kumar and S. P. McGlynn, *J. Chem. Phys.*, **93**, 3899 (1990)

40. D. Kumar and S. P. McGlynn, *Chem. Phys. Lett.*, **176**, 536 (1991)

41. D. Kumar, R.R. Zinn, and S. P. McGlynn, *J. Phys. Chem.*, **99**, 7530 (1995)

42. Xuan Yao, D. Kumar, and S. P. McGlynn, *J. Appl. Phys.*, **85** (6), (1999)

43. X. Yao and S. P. McGlynn, *Int. J. Quantum Chem.*, Lionel Goodman 70th Birthday Dedicatory Volume (in press)

44. F. D. Snell and L. S. Ettre, *Encyclopaedia of Industrial Chemical Analysis*, **14**, p584, Interscience Publishers, New York (1971)

45. W. Holak, *Anal. Chem.*, **59**(17), 2218 (1987)

46. B. S. Sheppard, J. A. Caruso, and K. A. Wolnik, *Appl. Spectros.*, **44**(4) 712 (1990)

47. Qian Lin, Xiannian Liu, and Qike Zheng, *J. Radioanal. & Nuclear Chem.*, **212**(4), 313 (1996)

48. S. V, Kireev, A. V. Pit'ko and S. L. Shnyrev, *Optics & Spectros.*, **78** (6), 803 (1995)

CHAPTER 5: SUMMARY

1. The laser optogalvanic effects (LOGE) induced by pulsed laser excitation of Ne $1s_{2,4}\rightarrow 2p_{1,3}$ transitions in a low power, ~30 MHz radio frequency Ne discharge at ~5 Torr are described. The polarity (sign) of the LOGE signal is controlled by perturbations of the $1s_j$ populations. The steady state $1s_4$ population is $\sim 10^1$ times larger than the $1s_2$ population and the LOGE signals for $1s_4\rightarrow 2p_{1,3}$ excitations are correspondingly stronger than those for $1s_2\rightarrow 2p_{1,3}$ excitations. The plasma temperature is found to be ~1000 K. The excitations $1s_{2,4}\rightarrow 2p_3$ are more efficient at signal production than the $1s_{2,4}\rightarrow 2p_1$ excitations, which is contrary to prediction. The OGE signals are consequences of: (1) perturbation and reequilibration of the metastable $1s_3$ and $1s_5$ populations; (2) radiatively-trapped $1s_2\rightarrow {}^1S_0$ photons; and (3) collisionally-induced $1s_2$, $1s_4 \leftrightarrow 1s_3, 1s_5$ energy transfer. The LOGE signal components, both the ionization and photoacoustic constituents, are temporally coincident only when the immediate causative agents are trapped photons. When otherwise produced, the photoacoustic part is delayed relative to the ionization component by the time required for the acoustic wave to travel from the locus of excitation to the sensitive region(s) of the plasma.
2. The laser optogalvanic effect in low-power, low-temperature, radiofrequency plasma in neon has been studied by pulse excitation of various $\ldots 2p^5 3s \rightarrow \ldots 2p^5 3p$ (i.e., $1s_j\rightarrow 2p_k$ in Paschen notation) neon transitions and subsequent observation of the return to equilibrium of the separate ionization and acoustic LOGE components. Of

the four $1s_j$ states, the $1s_3$ and $1s_5$ metastables are responsible for plasma maintenance and the $1s_2$ and $1s_4$ states are radiatively trapped. The 10 $2p_k$ states merely serve as doorways for a laser-induced redistribution of the $1s_j$ populations. The ionization component, apart from signs, is identical for all excitations and is conditioned by two sets of kinetic events: the return to equilibrium of the $1s_3$ and $1s_5$ metastable populations and the radiative trapping of the $1s_2$ state. The acoustic components, while conditioned by the same events as well as by trapping of the $1s_4$ state, vary considerably from one $1s_j \rightarrow 2p_k$ excitation to another and from the ionization component. All differences are explicable on the basis of the following model:

(1) All non-radiative $2p_k \rightarrow 1s_j$ and $1s_{3,5} \rightarrow {}^1S_0$ deexcitations launch an acoustic wave at the site of laser excitation, but this wave must travel at the speed of sound to regions of high ion densities where, by a physical movement of the charge carriers, it registers an OGE effect.

(2) The $1s_{2,4} \rightarrow {}^1S_0$ non-radiative deexcitations also launch an acoustic wave but this wave produces an instantaneous LOGE signal because no travel requirement are imposed on it. A random walk of trapped states at the speed of light ensures that these states can dump their energy uniformly throughout the plasma and, specifically, that they can do so where the ion densities are high. That is, they do not have to travel at the speed of sound from the site of laser excitation to the region of high carrier densities.

3. The laser optogalvanic spectroscopy (LOGS) may be used to detect specific species in a plasma (ions, atoms, radicals or molecules) by selective laser excitation of the plasma. The plasma itself is merely the reservoir of electronically excited, ionized and

atomized species. Compared with conventional ICP-AES, OGE has many advantages: no external detector, zero background, no interferences, and greater versatility. Since the photoacoustic (PA) and ionization rate change (IRC) components of the LOGE signal can be separated, optogalvanic spectroscopy can exhibit a further selectivity based on this discriminatory ability. The LOGS method has been applied to iodine analysis. By careful selection of the operating conditions, pure atomic and pure molecular iodine signals constitute the PA and IRC profiles, respectively. The best detection limit, in a somewhat primitive experiment, is $\sim 10^{-7}$ μg/ml of I_2, which is comparable to laser-induced fluorescence. This detection limit can be improved by at least three orders of magnitude by optimizing the experimental conditions.

APPENDICES

A: Dry Ice -Solvent Slurries

To control the vapor pressure of iodine, dry ice-solvent slurry bath was used in the experiment to keep low temperatures (< 0 °C). Some dry ice-solvent slurries used in the experiment are shown in Table A.

Table A Dry Ice-Solvent Slurries

Solvent	Slurry Temp.(°C)
Aceton	-67.9
Chlorobenzene	-45
Bromobenzene	-30.8
Bromobenzene	-26
Carbon Tetrachloride	-23
Benzonitrile	-13
NaCl (+water)	-5

B: Transition Probability and Wavelength of Relevant Neon Transitions

The neon transitions studied in this work and their wavelengths, transition probabilities and branching ratios are shown in Table B. The energy levels are denoted in Paschen notations.

Table B Transition Probability and Wavelength of Relevant Neon Transitions

Transition	λ (nm)	A ($10^7 s^{-1}$)	A_{tot} ($10^7 s^{-1}$)	Branching ratio (%)
$1s_2 \rightarrow {}^1S_0$	73.589	66.40	66.40	
$1s_4 \rightarrow {}^1S_0$	74.370	4.96	4.76	
$2p_1 \rightarrow 1s_4$	540.056	0.09		1.3
$1s_2$	585.249	6.82	6.95	98.7
$2p_2 \rightarrow 1s_5$	588.190	1.15	5.31	20.9
$1s_4$	603.000	0.561		10.2
$1s_3$	616.359	1.46		26.6
$1s_2$	659.895	2.32		42.3
$2p_3 \rightarrow 1s_4$	607.434	6.03	6.06	99.5
$1s_2$	665.209	0.029		0.5
$2p_4 \rightarrow 1s_5$	594.483	1.13	5.23	21.4
$1s_4$	609.616	1.81		34.3
$1s_2$	667.828	2.33		44.2
$2p_5 \rightarrow 1s_5$	597.553	0.351	5.02	6.9
$1s_4$	612.845	0.067		1.3
$1s_3$	626.650	2.49		49.0
$1s_2$	671.704	2.17		42.7
$2p_6 \rightarrow 1s_5$	614.306	2.82	5.07	56.7
$1s_4$	630.479	0.416		8.4
$1s_2$	692.947	1.74		34.9
$2p_7 \rightarrow 1s_5$	621.728	0.637	5.03	12.5
$1s_4$	638.299	3.21		62.7
$1s_3$	653.288	1.08		21.1
$1s_2$	702.405	0.189		3.7
$2p_8 \rightarrow 1s_5$	633.443	1.61	5.04	32.9
$1s_4$	650.653	3.00		61.3
$1s_2$	717.397	0.287		6.9
$2p_9 \rightarrow 1s_j$	640.225	5.14	5.14	
$2p_{10} \rightarrow 1s_5$	703.241	2.53	4.04	
$1s_4$	724.517	0.935		
$1s_3$	713.890	0.231		
$1s_2$	808.246	0.012		

C: Letters of Permission

LOUISIANA STATE UNIVERSITY
AND AGRICULTURAL AND MECHANICAL COLLEGE
Department of Chemistry, LSU, Baton Rouge, LA 70803, USA
phone: (504)388-2945 fax: (504)388-3458
e-mail: xyao@unix1.sncc.lsu.edu

January 14, 1999

Mr. Steven J. Rothman
Editor of Journal of Applied Physics
P.O. Box 8296
Argonne, IL 60439-8296

RE: Your permission for the use of my manuscript in my dissertation

Dear Mr. Steven J. Rothman,

My manuscript, #JR-0504 (AIP code #067906), entitled: "Optogalvanic Transients in the $1s_{2,4} \rightarrow 2p_{1,3}$ Excitations of RF Neon Plasma", has been accepted for publication on your journal. This work is one part of my dissertation research. Since the copyright of this article has been transferred to your journal, I would like to get your permission to use this article, or one part of it, in my dissertation.

Please mail your letter to me at your earliest convenience or fax it to me at (225)388-3458.

Thanks.

Yours truly,

Xuan Yao

AMERICAN INSTITUTE OF PHYSICS

500 Sunnyside Boulevard
Woodbury, NY 11797-2999

Tel. 516-576-2268
Fax 516-576-2499

E-mail: rights@aip.org
http://www.aip.org

VIA FAX: 225-388-3458

19 January 1999

Xuan Yao
232 Choppin Hall, B12
Department of Chemistry
Louisiana State University
Baton Rouge, LA 70803

Dear Sir,

This is further to your request for permission to use material from American Institute of Physics publications.

Permission is hereby granted for one time reproduction – in print only, as per the requirements indicated below – of the following article(s):

Xuan Yao, "Optogalvanic Transients in the 1s2,4->2p1,3 Excitations of Radio Frequency Neon Plasma", accepted for publication in *Journal of Applied Physics* manuscript #JR-0504
to be reproduced in your dissertation.

[X] 1. The following credit line must appear in all copies (please fill in the information indicated by CAPITAL LETTERS): Reprinted with permission from FULL CITATION. Copyright YEAR American Institute of Physics.

[X] 2. NOTE: This permission does not apply to figures, tables or other materials credited to sources other than the copyright holder.

[X] 3. Obtain the authors' permission to use the material. The author's address can be obtained from the article.

[ ] 4. An invoice for permissions fee (net 30 days) of $0 will follow. Please make check payable to American Institute of Physics. Please note: Permission is not valid until payment is received.

Thank you for requesting permission to use materials copyrighted by American Institute of Physics. Please do not hesitate to contact us should you have any further questions.

Sincerely,

Ann C. Perlman

LOUISIANA STATE UNIVERSITY
AND AGRICULTURAL AND MECHANICAL COLLEGE
Department of Chemistry, LSU, Baton Rouge, LA 70803, USA
phone: (504)388-2945 fax: (504)388-3458
e-mail: xyao@unix1.sncc.lsu.edu

January 22, 1999

Mr. N. Yngye Öhrn
Editor of Int. J. Quantum Chem.
P.O. Box 118435
Gainsville, FL 32611-8435

RE: Your permission for the use of my manuscript in my dissertation

Dear Mr. N. Yngye Öhrn,

My manuscript, 2954-F, G 97-20, IJQC, entitled: "Optogalvanism in a Neon Plasma", has been accepted for publication on your journal. This work is one part of my dissertation research. Since the copyright of this article has been transferred to your journal, I would like to get your permission to use this article, or one part of it, in my dissertation.

Please mail your letter to me at your earliest convenience or fax it to me at (225)388-3458.

Thanks.

Yours truly,

Xuan Yao

INTERNATIONAL JOURNAL OF QUANTUM CHEMISTRY

P O. Box : 84.35. 2301 NEW PHYSICS BUILDING, UNIVERSITY OF FLORIDA, GAINESVILLE. FLORIDA 32511 8435
Telephone. (352)392-1597. FAX. (352)392-8722. E-Mail: ijqc@qtp ufl edu

January 29, 1999

Mr. Xuan Yao
Louisiana State University
Department of Chemistry
232 Choppin Hall B12
Baton Rouge LA 70803

Dear Mr. Yao,

You may certainly use parts of your paper entitled, "Optogalvanism in a Neon Plasma", with Dr. McGlynn for your thesis if he thinks this is appropriate.

What you cannot do is submit this paper, nor parts of it to another journal, that is considered "in the open-literature".

Good luck with your thesis and my best regards to Professor McGlynn.

Sincerely,

Michael C. Zerner
Associate Editor

MCZ/slw

LOUISIANA STATE UNIVERSITY
AND AGRICULTURAL AND MECHANICAL COLLEGE
Department of Chemistry, LSU, Baton Rouge, LA 70803, USA
phone: (225)388-2945 fax: (225)388-3458
e-mail: xyao@unix1.sncc.lsu.edu

January 25, 1999

Copyright Transfer
Academic Press
Microchemical Journal
525 B Street, Suite 1900
San Diego
CA 92101

RE: Your permission for the use of my manuscript in my dissertation

Dear Sir or Madam:

My manuscript, MSL 126, entitled: "Laser Optogalvanic Analysis in a Radio Frequency Plasma – Detection of Iodine Atoms and Molecules", has been accepted for publication on *Microchemical journal*. This work is one part of my dissertation research. Since the copyright of this article has been transferred to you, I would like to get your permission to use this article, or one part of it, in my dissertation.

Please mail your letter to me at your earliest convenience or fax it to me at (225)388-3458.

Thanks.

Yours truly,

Xuan Yao

Academic Press
525 B Street, Suite 1900
San Diego, CA 92101-4495

ACADEMIC
PRESS

February 2, 1999

Xuan Yao
Louisiana State University
and Agricultural & Mechanical College
Department of Chemistry, LSU
Baton Rouge, LA 70803
Fax: (225)388-3458

Dear Dr. Yao:

RE: Microchemical Journal

Thank you for your request to use material from your work published in an Academic Press publication.

It is now the policy of Academic Press that authors need not obtain permission in the following cases: (1) to use their original figures or tables in their future works; (2) to make copies of their papers for their classroom teaching; and (3) to include their Papers as part of their dissertations.

Sincerely,

Denise Blake for

Cindy MacDonald
Editorial Manager

attachment

VITA

Xuan Yao was born February 22, 1957, in Nanchang, Jiangxi, the People's Republic of China. He was graduated in 1974 from Nanchang No. 1 Middle School in Nanchang, China. He attended the Central-South University of Technology in Changsha, China, from 1978 to1981, where he received his bachelor of science degree in Materials Science and Engineering. The topic of his bachelor of science degree thesis was "Hypereutectic Al-Si Alloy Powder Preparation by Atomization". He then attended the Graduate School of the Central-South University of Technology in Changsha, China, from 1982 to1984, where he received his master of science degree in Materials Science and Engineering. The topic of his master of science degree thesis was "A Study of the Effect of Rare Earth Oxides on Cobalt".

Xuan Yao was employed as a Lecturer in the Department of Chemical Engineering, Hefei University of Technology, Hefei, Anhui, the People's Republic of China, from 1985 to 1993. He worked on the recycling of heavy metal wastes by chemical methods and research on ceramics, hard metals and ferrous powder metallurgy. He also worked on the establishment of the "Powder Metallurgy Laboratory" and cooperated with powder metallurgy companies in the development of powder metallurgy products and the design and maintenance of production lines. He taught various courses to college students and trained workers and technicians from factories

Since the fall 1993, Xuan Yao has been enrolled as a full-time graduate student in the Department of Chemistry, Louisiana State University, Louisiana. The topic of his doctoral dissertation is "The Laser Optogalvanic Effect in Radio Frequency Plasma:

Applications in Analytical Chemistry". He has worked on the mechanism of the laser optogalvanic effect and its application in instrumental analysis. He studied the plasma processes induced by laser excitations and the improvement of analytical instrumentation. In addition, he worked as a teaching assistant, teaching chemistry labs and tutoring students.

His publications include "Optogalvanism in a Neon Plasma", X. Yao and S. P. McGlynn, *Int. J. Quantum Chem.,* Lionel Goodman 70th Birthday Dedicatory Volume (in press); "Comparison of Atomization Sources for a Field-Deployable Laser Optogalvanic System", D. L. Monts, Abhilasha, S. Qian, D. Kumar, X. Yao, and S. P. McGlynn. *J. Thermophysics and Heat Transfer,* **12** (1), 66(1998); "Optogalvanic Transients in the $1s_{2,4} \rightarrow 2p_{1,3}$ Excitations of RF Neon Plasma", X. Yao, D. Kumar, and S. P. McGlynn, *J. Appl. Phys.,* **85**(6), (1999); "The Laser Optogalvanic Effect and Its Applications in Analytical Chemistry", X. Yao and S. P. McGlynn, presented at 54th Southwest ACS Meeting, Nov. 1-3, 1998, Baton Rouge, Louisiana; "Laser Optogalvanic Analysis in a Radio Frequency Plasma: Detection of Iodine Atoms and Molecules", X. Yao, R. C. Mohanty and S. P. McGlynn, accepted by the *Microchemical Journal;* "The Necessity of Developing the Database of P/M Mechanical Parts", X. Yao and Q. Luo, Proceedings of 1991 National P/M Academic Conference, China; "Electrolytic Erosion Process for Recycling Tungsten Wastes", X. Yao and Q. Luo, *Rare Metals and Cemented Carbide,* 1990, No. 1, p14; "Application of Computers in P/M Industry", X. Yao and Q. Luo, *Computer Technology and Application,* 1989, No. 4, p105; "Effect of Rare Earth Oxides on Martensitic Transformation and Mechanical Properties of Cobalt", X. Yao, H. Lu, and P. Huang,

Powder Metall. Tech., 5(3), 200, 1987; "The Cemented Carbide", X. Yao, HUT Textbook Publishing House, Hefei, Anhui, 1988.

The honors that he received include Outstanding Research Award, awarded by Louisiana State University, Baton Rouge, Louisiana, in 1997; Excellent Community Service, awarded by Chinese Consulate General in Houston, Texas, in 1995; Outstanding Teaching Award, awarded by the Hefei University of Technology, Hefei, Anhui, China, in 1990; scholarships during undergraduate and graduate studies at the Central-South University of Technology, China, from 1978 to 1984.

Xuan Yao has done much volunteer work in cultural exchange and community service since 1993. He has been the President of L.S.U. International Student Association (1995-1996), a Board member of the L.S.U. International Cultural Center (1995-1996), a member of the L.S.U. Student Advisory Committee (1995-1996) and President of the L.S.U. Chinese Student and Scholar's Association (1994-1995)

Xuan Yao is currently a candidate for the degree of Doctor of Philosophy in Chemistry which, he hopes, will be awarded to him in May 1999.

DOCTORAL EXAMINATION AND DISSERTATION REPORT

Candidate: Xuan Yao

Major Field: Chemistry

Title of Dissertation: The Laser Optogalvanic Effect in Radio Frequency Plasma: Applications in Analytical Chemistry

Approved:

Sean P. McGlynn
Major Professor and Chairman

Dean of the Graduate School

EXAMINING COMMITTEE:

Kalyat T. Valsaraj

Steven A Soper

Robert P. Hammer

Date of Examination:

02/18/1999

IMAGE EVALUATION TEST TARGET (QA-3)

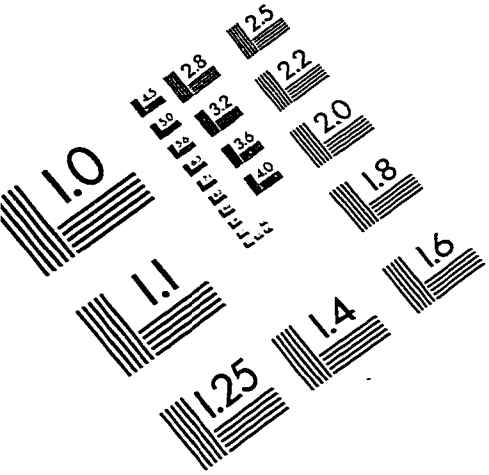

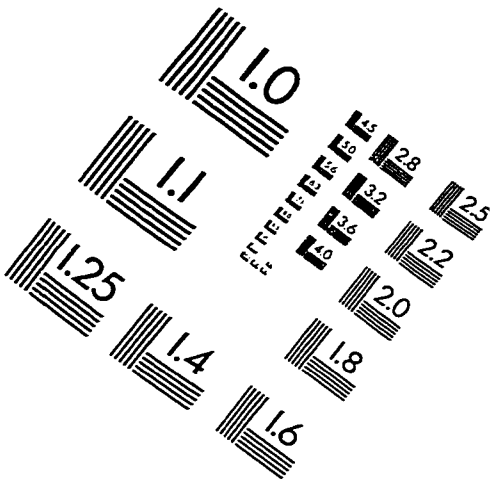

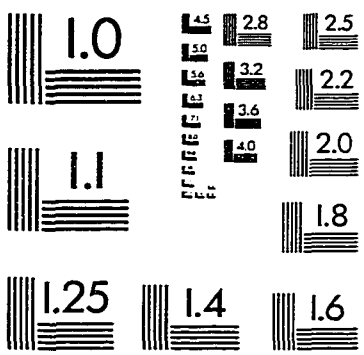

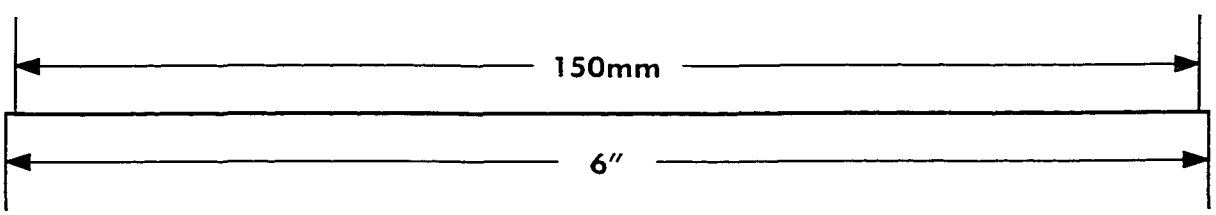

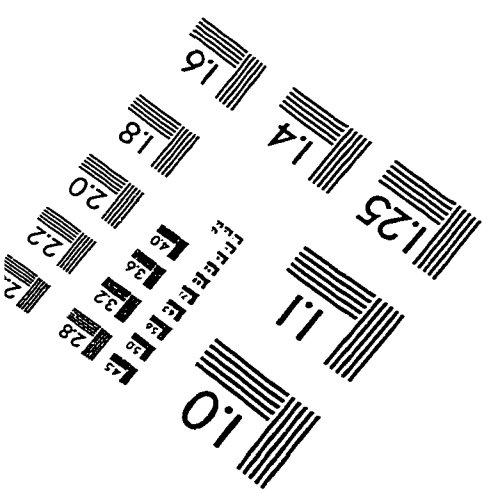

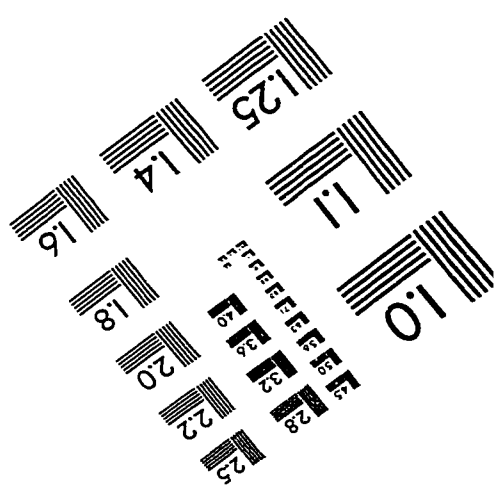

APPLIED IMAGE, Inc
1653 East Main Street
Rochester, NY 14609 USA
Phone: 716/482-0300
Fax: 716/288-5989